Developing High-performance Thin-film Composite Membranes for Water Recycling and Reuse

Liuqing Yang

A Thesis

in the Department

of

Chemical and Materials Engineering

Presented in Partial Fulfillment of the Requirements

For the Degree of

Doctor of Philosophy (Chemical Engineering) at

Concordia University

Montréal, Québec, Canada

October 2022

CONCORDIA UNIVERSITY
SCHOOL OF GRADUATE STUDIES

This is to certify that the thesis prepared

By: Liuqing Yang

Entitled: Developing High-performance Thin-film Composite Membranes for Water Recycling and Reuse

and submitted in partial fulfillment of the requirements for the degree of

DOCTOR OF PHILOSOPHY (Chemical Engineering)

complies with the regulations of the University and meets the accepted standards with respect to originality and quality.

Signed by the final examining committee:

_____ Chair
Dr. Andrea Schiffauerova

_____ External Examiner
Dr. Xianshe Feng

_____ Examiner
Dr. Chunjiang An

_____ Examiner
Dr. Pantcho P. Stoyanow

_____ Examiner
Dr. Xianming Zhang

_____ Thesis Supervisor
Dr. Zhibin Ye

Approved by   _____
                       Dr. Alex De Visscher, Graduate Program Director

December 05, 2022   _____
                       Dr. Mourad Debbabi, Dean

        Gina Cody School of Engineering and Computer Science

Abstract

Developing High-performance Thin-film Composite Membranes for Water Recycling and Reuse

Liuqing Yang, Ph.D.

Concordia University, 2022

Membrane-based separation technologies, as versatile platforms, have attracted considerable attention for water recycling and reuse, due to their ease of operation, high separation efficiency, excellent sustainability, relatively low energy consumption, and industrial viability. Among them, thin-film composite (TFC) membranes have been widely employed for the desalination of seawater and separation of small organic compounds. However, the state-of-the-art polyamide TFC membranes still suffer from the severe fouling and limited water permeability, which are mainly ascribed to their intrinsic surface hydrophobicity and uncontrollable interfacial polymerization process. To address the current challenges and limitations in TFC membranes, it is essential to develop new methodologies and design new functional materials for the fabrication of TFC membranes.

In this research, a new strategy based on the bioinspired chemistry has been explored for the fabrication of TFC membranes. In the strategy, polydopamine-modified cellulose nanocrystals (CNCs) with substantial quinonoid active sties have been prepared through oxidative auto-polymerization of dopamine, which enable the subsequent crosslinking with polyethylenimine (PEI). Electrospun nanofiber mats (ENMs) produced from electrospinning has been employed as the supporting layer in order to enhance the membrane permeability. TFC membranes are fabricated with the modified CNCs as the active layer via facile vacuum filtration on ENMs followed by further cross-linking with PEI. The achieved ultrahigh pure water permeability (PWP), superior dye rejection, and remarkable salt permeation demonstrate its great potential for the effective separation of dye/salt mixtures and recovery of these valuable components.

To expand the application of bioinspired chemistry in TFC membranes, a rapid co-deposition of dopamine with zwitterions (Z-DNMA) via covalent polymerization triggered by $CuSO_4/H_2O_2$ has

been further proposed to construct the thin film selective layer. The fabricated TFC membranes with the incorporated zwitterionic structure from Z-DNMA show enhanced surface hydrophilicity and superior fouling-resistant performance towards both typical hydrophobic contaminants (e.g., proteins) and organic molecules (e.g., organic dyes).

In addition to the development of new strategies, a new diamine monomer featured with trimethylamine *N*-oxide (TMAO) structure, *N,N*-bis (3-aminopropyl)methylamine *N*-oxide (DNMAO), has been designed for the fabrication of polyamide TFC membranes via interfacial polymerization. Its charged group (N^+-O^-) is directly connected without extra atoms and has the typical characteristics of zwitterions. The fabricated TFC membranes show high water permeability, high dye/salt selectivity, and improved antifouling ability. Apart from the polyamide TFC membranes, zwitterionic triethanolamine-based (Z-TEOA) polyester TFC membranes have been also fabricated via interfacial polymerization in this research. Z-TEOA endows a typical sulfonbetaine (SB) -based zwitterionic structure, which is one of the most widely used zwitterions in the fabrication of membranes. The performance of the polyester TFC membranes has been systematically investigated on the purification of dye- and antibiotic-contaminated wastewaters.

The results in this thesis demonstrate the promising application of bioinspired chemistry in the fabrication of TFC membranes for the treatment of organic compounds-contaminated wastewaters. Meanwhile, the new generation of zwitterions based on TMAO-derived structure shows a great potential for the modification of the conventional polyamide TFC membranes to alleviate fouling propensity. Furthermore, this research also highlights the promising application of zwitterionic-modified polyhydroxyl monomers in the fabrication of polyester TFC membranes to enhance fouling-resistant performance.

Keywords: thin-film composite membranes, zwitterion, dopamine, dye separation

Acknowledgements

Table of Contents

List of Figures

x

xiv

List of Tables

List of Abbreviations

AEP	N-aminoethyl piperazine
AFM	Atomic force microscope
ATRP	Atom transfer radical polymerization
((Boc)$_2$O	Di-ter-butyl dicarbonate
BSA	Bovine serum albumin
CB	Carboxybetaine
CHMA	1, 3-cyclohexanebis (methylamine)
CNCs	Cellulose nanocrystals
CNFs	Cellulose nanofibers
CNTs	Carbon nanotubes
COFs	Covalent organic frameworks
CP	Concentration polarization
CR	Congo red
DCM	Dichloromethane
DI	Deionized
DLS	Dynamic light scattering
DNMA	*N,N*-bis(3-aminopropyl)methylamine
DNMAO	*N,N*-bis (3-aminopropyl)methylamine *N*-oxide
EB	Evans blue
ENMs	Electrospun nanofiber mats
FAO	Food and Agriculture Organization

FDR	Flux decline ratio
FE-ESEM	FEI Quanta 450 environmental scanning electron microscope
FRR	Flux recovery ratio
FTIR	Fourier transform infrared
GO	Graphene oxide
GOQDs	Graphene oxide quantum dots
HCl	Hydrochloric acid
^{1}H NMR	^{1}H nuclear magnetic resonance
H_2O_2	Hydrogen peroxide
HPLC	High performance liquid chromatography
HTC	Cyclohexane-1, 3, 5-tricarbonyl chloride
IPC	Isophthaloyl chloride
MB	Methyl blue
MF	Microfiltration
$MgSO_4$	Magnesium sulfate
$MgCl_2$	Magnesium chloride
mLbL	Molecular layer-by-layer
MPD	*m*-phenylene diamine
NaAlg	Sodium alginate
NaCl	Sodium chloride
NaClO	Sodium hypochlorite
NaOH	Sodium hydroxide

Na_2SO_4	Sodium sulfate
NF	Nanofiltration
NMP	1-methyl-2-pyrrolidinone
OG	Orange G
PC	Phosphobetiane
PEG	Polyethylene glycol
PEI	Polyethylenimine
PES	Polyethersulfone
PIP	Piperazine
PPD	p-phenylenediamine
1,3-PS	1,3-propane sultone
PSf	Polysulfone
PVP	Polyvinylpyrrolidone
PWP	Pure water permeability
R_{ir}	Irreversible fouling ratios
R_r	Reversible fouling ratios
RO	Reverse osmosis
SB	Sulfonbetaine
SiO_2	Silicon dioxide
TAEA	Tris(2-aminoethyl)amine
TC	Tetracycline
TEOA	Triethanolamine

TFC	Thin-film composite
TFN	Thin-film nanocomposite
TGA	Thermogravimetric analysis
TiO$_2$	Titanium dioxide
TMAO	Trimethylamine N-oxide
TMC	Trimesoyl chloride
Tris	Tris(hydroxymethyl)aminomethane
UF	Ultrafiltration
VPBO	Victoria pure blue BO
WCA	Water contact angle
XPS	X-ray photoelectron spectroscopy
ZNF	Zwitterionic polyester NF membranes
Z-NF	Zwitterionic nanofiltration
Z-TEOA	Zwitterionic triethanolamine

Chapter 1. Introduction

1.1 Problem statement

The scarcity of global fresh water caused by water pollution and climate change is one of leading challenges nowadays encountered by mankind, which is expected to significantly restrict the economic and social development of the world.[1] The Food and Agriculture Organization (FAO) of the United Nations has estimated that over 2 billion people are suffering from water scarcity due to the climate change, urbanization, and industrialization.[2] Thus, to meet the increasing demands in clean water for sustainable human activities, it is crucial to develop reliable, efficient, environmental-friendly, and sustainable technologies for water recycling and reuse.

Textile industries with enormous water consumption are intensifying water scarcity.[3] Meanwhile, industrial wastewater from textile industries, as one of significant pollutants, are causing severe environmental and health issue.[4] Therefore, direct discharge of them into environment without proper treatments is strictly prohibited due to the special chemical properties of these organic dyes existing in the effluent from textile industries. To date, numerous methods, including oxidation, biological, and physical methods, have been developed to treat industrial wastewater and alleviate the impact on our ecological system.[5] The drawbacks of oxidation methods include the need of oxidants and the production of byproducts from the degradation of contaminants during the oxidation processes. For biological methods, the low efficiency and complicated operation system are main limitations for their application in the treatment of textile wastewater. Membrane separation technologies, as one physical method, have drawn immense attention owing to their distinctive properties.

Pressure-driven membrane separation technologies, including microfiltration (MF), ultrafiltration (UF), nanofiltration (NF), and reverse osmosis (RO) membranes, have currently emerged as the most attractive technologies for water recycling and reuse, due to their ease of operation, high separation efficiency, excellent sustainability, and industrial viability.[6] As shown in Figure 1.1, depending on the type of membrane technologies, suspended particles, oil emulsions, bacterial, viruses, proteins, small organic molecules, divalent ions, and even monovalent ions can be effectively removed from feed wastewaters.[7] In particular, membranes with thin-film composite

(TFC) structures are considered as the most effective and efficient separation processes for water purification and recycling in comparison with the conventional asymmetric membrane types.
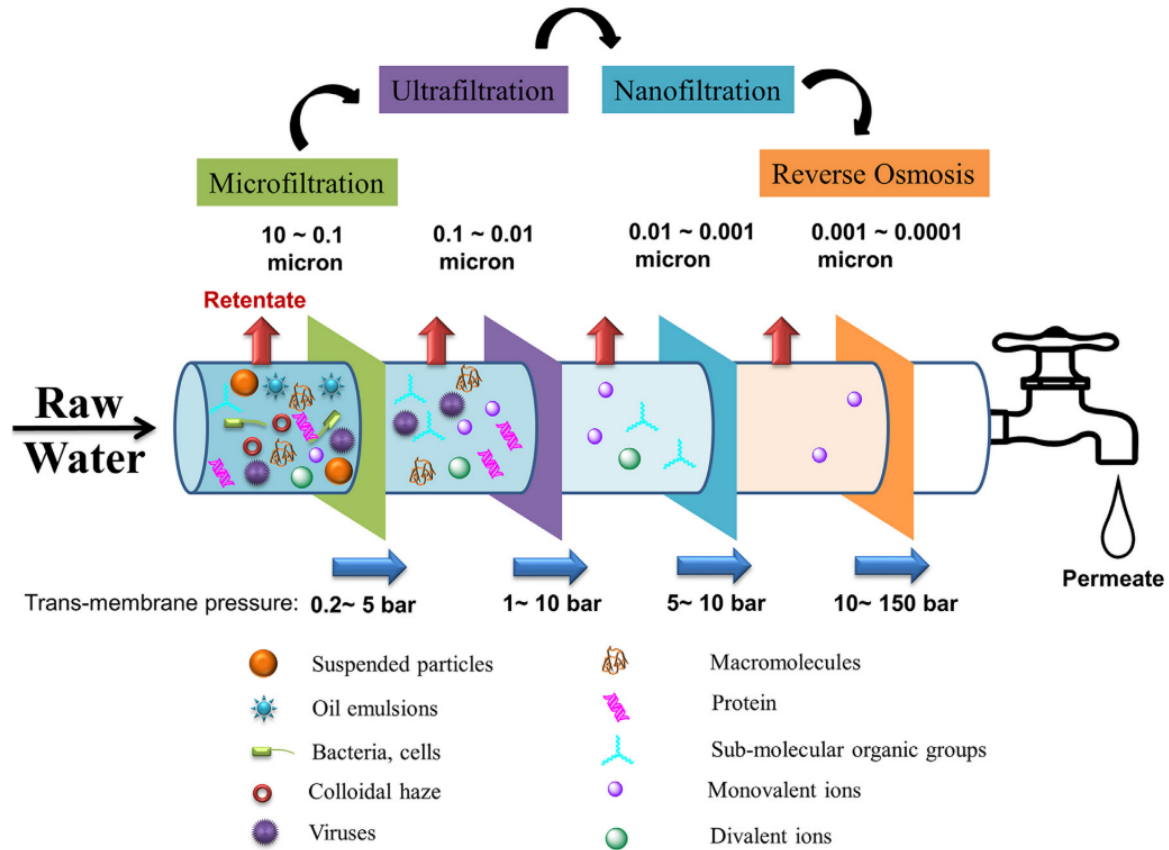
Figure 1.1 Schematic presentation of pressure-driven membrane separation technologies.[7]

To date, most commercial NF and RO membranes are TFC membranes in virtue of their distinctive advantages, including high water production ability, excellent separation efficiency/selectivity, and reduced energy consumption.[8] Its superior performance is inherently attributed to the two different contributing layers in TFC membranes, which are the thin film selective layer and the porous supporting layer.[9] However, One of the main challenges for TFC membranes is fouling, which is generally caused by the unwanted contaminants depositing on the membrane surface or inside of internal pores from the feed solution.[10] This consequently leads to a reduction in membrane permeability and selectivity, increases energy consumption, and thus damage the

2

membrane matrix during the water purification process, especially in long term operations. The fouling propensity of TFC membranes is mainly dependent on their surface properties such as surface hydrophilicity, roughness, pore size distribution, and charge density.[11,12] Despite various fabrication techniques have been developed to alleviate the fouling propensity via optimizing the membrane surface roughness and reducing the thickness of the TFC membranes, it is still a challenge to simultaneously achieve membrane fouling resistance while maintaining high membrane performance.[13] In addition to membrane fouling, the trade-off relationship between permeability and selectivity is another limitation that restricts the practical application of TFC membranes in water recycling and reuse. Despite various studies have been undertaken to improve TFC membrane performance, few of them can simultaneously achieve high water permeability, high removal efficiency, and effective fouling resistance. Therefore, it is imperative to develop new TFC membranes with high performance and fouling resistant ability for various wastewater treatments.

1.2 Research Objectives

On the basis of the above discussion, the growing crisis caused by water scarcity requires the development of highly efficient and sustainable water treatment technologies. Compared to the conventional methods, pressure-driven membrane separation technologies have shown great potential in the treatment of wastewaters from textile industries. However, some major limitations still restrict their widespread applications, such as low permeability and fouling propensity. Therefore, development of high-performance TFC membranes is urgently needed to satisfy the requirement for practical applications.

To achieve these objectives, this study proposes new methodologies to construct thin film selective layers of TFC membranes instead of the conventional interfacial polymerization. In addition, new functional materials have been proposed and synthesized to construct thin film selective layers in order to overcome the inherent limitations of TFC membranes fabricated from the interfacial polymerization. The specific research tasks are listed as follows:

- To overcome the limitations of TFC membranes fabricated from the interfacial polymerization, a bioinspired methodology based on dopamine has been proposed to construct thin film selective layers. In addition, electrospun nanofibers mats (ENMs)

3

prepared from electrospinning has been employed as the porous supporting layer to further improve membrane performance.

- The main obstacle to realize the practical application of bioinspired chemistry in the membrane fabrication is the time-consuming polymerization process. Therefore, a rapid covalent co-deposition of dopamine and diamine-zwitterion has been proposed to prepare the thin film selective layer on the polyethersulfone (PES) ultrafiltration membrane.

- In addition to the developed new methodology, a new generation of zwitterionic amine monomer derived from trimethylamine N-oxide (TMAO) is proposed for the fabrication of polyamide TFC membranes by the interfacial polymerization. The proposed zwitterionic amine monomer enables the fabricated TFC membranes with enhanced fouling resistant ability and water permeability.

- Apart from the polyamide TFC membranes, polyester TFC membranes have been investigated for the treatment of wastewaters from textile industries.

1.3 Thesis Outline

Chapter 1 is a concise introduction of problem statement and research objectives in this thesis.

Chapter 2 is a comprehensive literature review. It includes principles and applications of TFC membranes, their physiochemical properties, fabrication processes, functional materials, and major challenges. This literature review gives a comprehensive understanding and the latest developments of TFC membranes, as well as the current limitations.

Chapter 3 proposes an alternative methodology to construct thin film selective layer of thin film nanocomposite (TFN) membranes via crosslinking of PEI with polydopamine-modified CNCs. ENMs produced from electrospinning have been employed as the supporting layer to enhance the TFN membrane permeability due to their high porosity. The crosslinking structures are tuned by varying the molecular weight and concentration of PEI for optimum membrane performances. The optimum TFN membrane can achieve high water permeability, excellent organic dye rejection, and inorganic slat permeation.

Chapter 4 demonstrates a rapid covalent co-deposition of dopamine and diamine-zwitterion to fabricate TFC NF membranes via $CuSO_4/H_2O_2$-induced rapid polymerization. The diamine-

zwitterion (Z-DNMA) has a typical SB-based zwitterionic structure and two primary amine groups, which enable the formation of covalent bonds with polydopamine. The optimum NF membrane shows superior fouling-resistant performance towards both typical hydrophobic contaminants (e.g., proteins) and organic molecules (e.g., organic dyes). The promising results obtained in this study, including pure water permeability (PWP), dye rejection, and fouling-resistant performance, indicate its potential application in the treatment of wastewater from textile industries.

Chapter 5 presents a new diamine monomer featured with TMAO structure, *N,N*-bis (3-aminopropyl)methylamine *N*-oxide (DNMAO), for the fabrication of polyamide TFC membranes via interfacial polymerization. DNMAO is conveniently synthesized by the facile oxidation of tertiary amine group of *N,N*-bis(3-aminopropyl)methylamine (DNMA) with hydrogen peroxide. Its charged group (N^+-O^-) is directly connected without extra atoms and has the typical characteristics of zwitterions. The fabricated membranes show enhanced hydrophilicity and fouling resistance to organic dyes.

Chapter 6 introduces a new zwitterionic triethanolamine-based (Z-TEOA) monomer for the fabrication of zwitterionic polyester TFC NF membranes via interfacial polymerization under alkaline conditions. Z-TEOA is successfully synthesized via the ring-open reaction between TEOA and 1,3-propane sultone (1,3-PS). All fabricated membranes exhibit enhanced hydrophilicity and permeability due to the introduction of the zwitterionic functionality in the thin film polyester layers.

Chapter 7 lists the main contributions and significance of this thesis research, as well as some recommendations for the future research directions.

Chapter 2 Literature Review

2.1 Principles and applications of TFC membranes

2.1.1 The role of TFC membranes in water treatment

The water scarcity caused by human activities has been considered as one of the most critical challenges all over the world. Though 71% of the surface area on the earth is covered by water, most of them are seawater with high salinity. The freshwater available for humankind accounts for only 2.5%. In addition, the intensive water consumption by agriculture and industries intensify the crisis of global fresh water. Furthermore, the discharge of wastewaters produced from human activities without proper treatments may cause severe pollution on the available fresh water and further exacerbate water scarcity.

The recycling and reuse of wastewaters by proper treatments have been considered as effective ways to reduce water pollution and thus alleviate water scarcity. Pressure-driven membrane-based separation technologies have drawn intensive attention in various fields, including water treatment and recycling, seawater desalination, pharmaceutical process, and battery recovery, owing to their virtue of high selectivity and efficiency, relatively low energy consumption, facile operation conditions, and environmental sustainability. Among them, TFC membranes are capable of removing small organic compounds from wastewaters produced from textile and pharmaceutical industries. In addition to the treatment of these wastewaters to produce clean water for the discharge, TFC membranes have also been widely investigated to recovery valuable contaminants in these wastewaters for reuse. Therefore, the development of high performance TFC membranes, including high permeability, high selectivity, and excellent fouling-resistance, is needed for the practical applications.

2.1.2 The fabrication processes and materials for TFC membranes

TFC membranes are pressure-driven membrane-based separation technologies. Conventional polyamide TFC membranes are generally constructed by two independent layers: a) an ultrathin polyamide thin film selective layer generated by the interfacial polymerization of trimesoyl chloride (TMC) with *m*-phenylene diamine (MPD) and b) a porous supporting layer.[14,15] The

selectivity of TFC membranes is ascribed to the dense cross-linked networks from condensation polymerization of TMC and MPD (Figure 2.1). Due to the uncontrollable interfacial polymerization process, the thickness of this thin polyamide selective layer can achieve to around 0.2 μm.[16] TFC membranes prepared from the interfacial polymerization of monomers have been widely used for a variety of water recycling and reuse applications, particularly in seawater desalination and wastewater treatment owing to the excellent selectivity.[17] In general, these two layers can be prepared from different polymers and controlled independently.[18] Therefore, they can be individually optimized to achieve, as a whole, the desired selectivity and permeability while still maintaining excellent mechanical strength.[19]
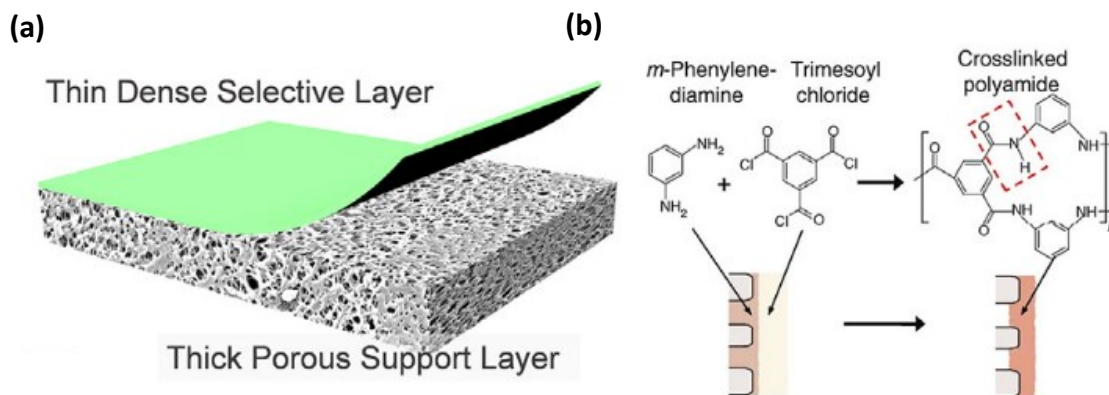
Figure 2.1 (a) Schematic illustration of the conventional polyamide TFC membrane structure; (b) the chemical structure of the polyamide TFC selective layer.[15]

The typical polyamide thin film selective layers can be employed for the fabrication of NF and RO membranes, depending on the solute size that they are able to remove from feed solutions. The pore size of TFC RO membranes are relatively small, ranging from 0.3 to 0.5 nm in diameter, while the pore size of TFC NF membrane ranges from 1 nm to 10 nm.[20] The pore size difference between these two types of membranes determines their practical applications in water treatment. TFC RO membranes are generally intended for the desalination of seawater and brine since they are able to remove monovalent salts, e.g., sodium chloride (NaCl), while TFC NF membrane can

be used for removal of macromolecular substances, such as carbohydrates, proteins, viruses, organic molecules, and even divalent salt ions. In addition, it is common to fabricate UF membranes via the construction of thin film selective layer on a porous supporting layer. Compared to the typical polyamide interfacial polymerization process for NF and RO membranes, the thin film selective layer of UF membranes are generally produced from loose cross-linked networks of functional materials with other polymers, e.g., crosslinking network of poly(vinyl alcohol) and glutaraldehyde.[21,22]

Generally, two different mechanisms have been proposed to illustrate pressure-driven membrane separation processes, which are molecular sieving model and solution-diffusion model, respectively (Figure 2.2). During separation processes, water molecules pass through the TFC selective layer while the solutes are retained in the feed solution side for both models. In the molecular sieving mode, only contaminants with smaller size than membrane pore size are able to pass through the thin film selective layer of TFC membranes. Therefore, the pore size and its distribution control in TFC UF membranes are crucial for improving membrane performance. On the contrary, in the solution-diffusion model, solutes permeate and dissolve into the thin film polymeric matrix of the membrane. Separation can be achieved with the difference in solubility and mobility of solutes within the thin film selective layer.[20] Thus, the thickness and crosslinking degree of thin film selective layer are dominant characteristics determining separation performance of TFC NF or RO membranes.
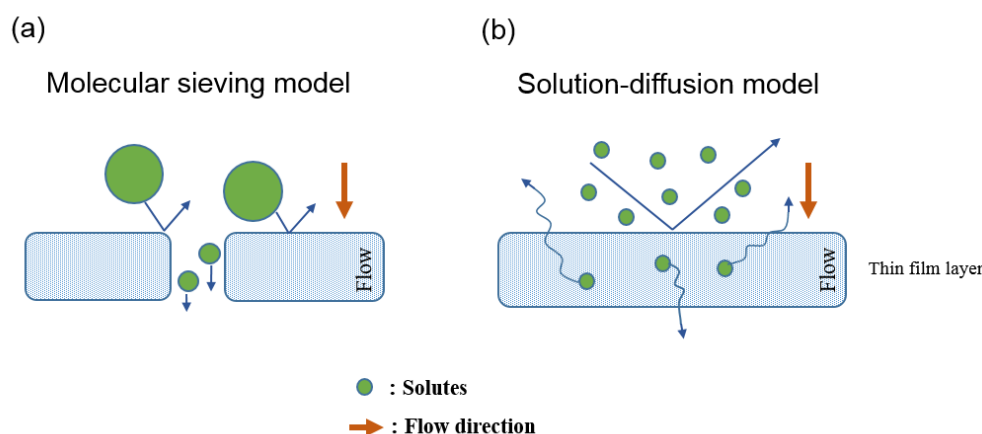
Figure 2.2 Solute transport process through thin film selective layer: (a) molecular sieving model; (b) solution-diffusion model.[20]

2.2 Challenges in TFC membranes

2.2.1 Membrane fouling

Despite TFC membranes have been extensively employed in the treatment of wastewaters various industries, one of the main challenges that prevents their further practical applications is the membrane fouling.[23-25] Fouling of TFC membranes can cause severe effects on the membrane performance, including the dramatic decrease of permeability, separation selectivity, long term operation stability, increased energy consumption, and shrinkage of the membrane lifespan. Membrane fouling is defined as the undesirable deposition and accumulation of solutes or attachment of contaminants on the membrane surface or inside the membrane pores.[26] Porous membranes such as MF and UF suffer from both external and internal fouling due to their porous structure,[25] while dense membranes like TFC membranes experience mainly external fouling.

In general, membrane fouling can be divided into inorganic fouling, organic fouling, and biofouling. Inorganic fouling, also termed as scaling, is ascribed to the accumulation of sparingly soluble inorganic compounds or mineral precipitates, while organic fouling is a result of the accumulation of colloids, particulate matters, and organic macromolecules. Biofouling is attributed to the adhesion, proliferation, and immigration of microorganisms onto the membrane surface, therefore leading to the formation of biofilm on the membrane surface.[27] In practice, membrane fouling is a systematic result caused by a combination of different types of contaminants.

The membrane fouling generally involves three stages, which are pore narrowing, pore blocking, and final cake layer formation. As shown in Figure 2.3, the virgin membrane firstly experiences the pore narrowing stage, which is caused by the attachment of small contaminants on the pore wall of membranes and subsequently lead to a reduced pore size distribution. With the continuing filtration, the contaminants with larger size can further deposit on the membrane pores and block all pores completely. Finally, the contaminants can fully deposit on the membrane surface and a dense cake layer is formed.
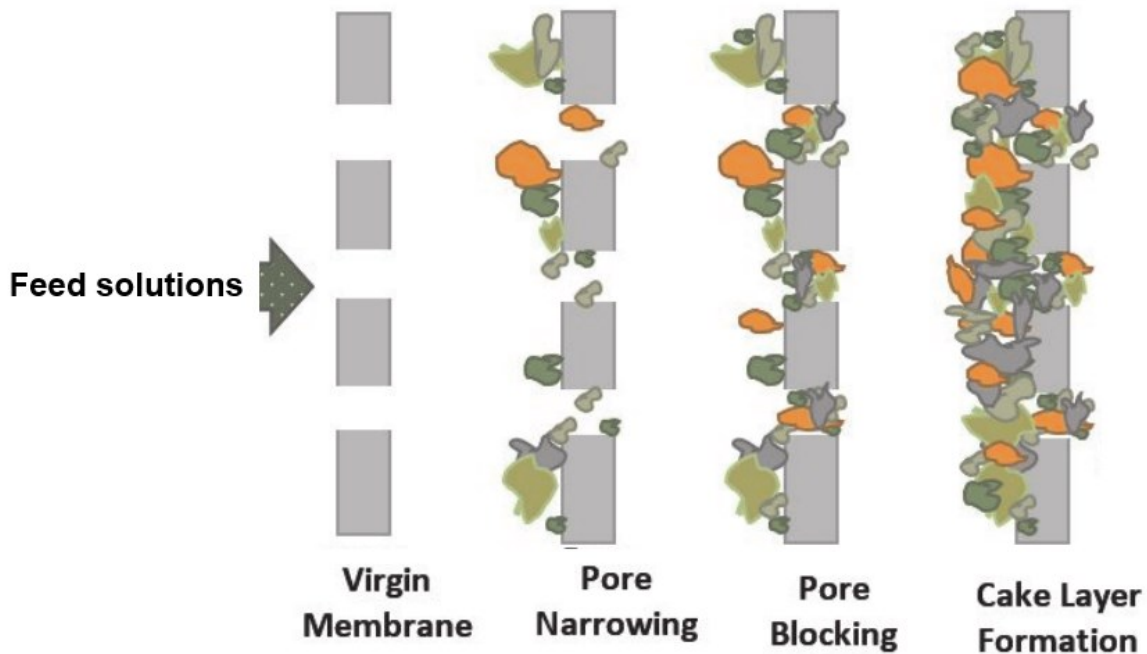
Figure 2.3 Schematic illustration of the membrane fouling.[28]

2.2.2 Consequences of fouling

On the basis of the above discussion, membrane fouling is mainly caused by the undesirable attachment and deposition of contaminants on the membrane surface or inside the membrane pores. The gradual growth of cake layer on the membrane surface may cause severe effects on the membrane performance, including permeability, selectivity, energy consumption, and membrane lifespan.

The membrane permeability depends on the pore size, pore size distribution, and porosity of membranes. Therefore, the initial pore narrowing and blocking stages will lead to a dramatic decrease of membrane permeability due to the reduced pore size and porosity of membranes. In addition, the formation of cake layer at the third stage on the membrane surface creates an additional obstacle, which can further reduce the permeability. Meanwhile, in order to compensate the lost permeability caused by the membrane fouling, a relatively higher external pressure is

required, which is accompanied by the increased energy consumption. In addition, the formed cake layer caused by the membrane fouling during the separation process can inevitably increase the trans-membrane pressure as well as the concentration polarization (CP).[29] Trans-membrane pressure is the lowest pressure required to allow water molecule pass through the membrane. CP refers to the concentration gradient of solutes on the membrane surface resulting from the accumulation of solutes retained by the membrane, which is one of the most important factors influencing the selectivity of membranes. Upon the formation of a fouling layer on the membrane surface, the back diffusion of solutes from membranes to the feed solution is hindered. The concentration of solutes (C_w) at the membrane surface can be significantly elevated (C_w*) due to the gradual formation of a fouling layer, where CP* > CP as illustrated in Figure 2.4. Therefore, with an increase in CP caused by the fouling on the membrane surface, the passage of solutes through the membrane can be significantly increased, resulting in a decreased selectivity.[30] Furthermore, the long-term accumulation of these contaminants on the membrane surface may damage membrane structures and reduce their lifespan.

$$\text{(a)} \ CP^* = \frac{C_W^* - C_P^*}{C_C - C_P^*}$$

$$\text{(b)} \ CP = \frac{C_W - C_P}{C_C - C_P}$$

$$CP^* \ > \ CP$$
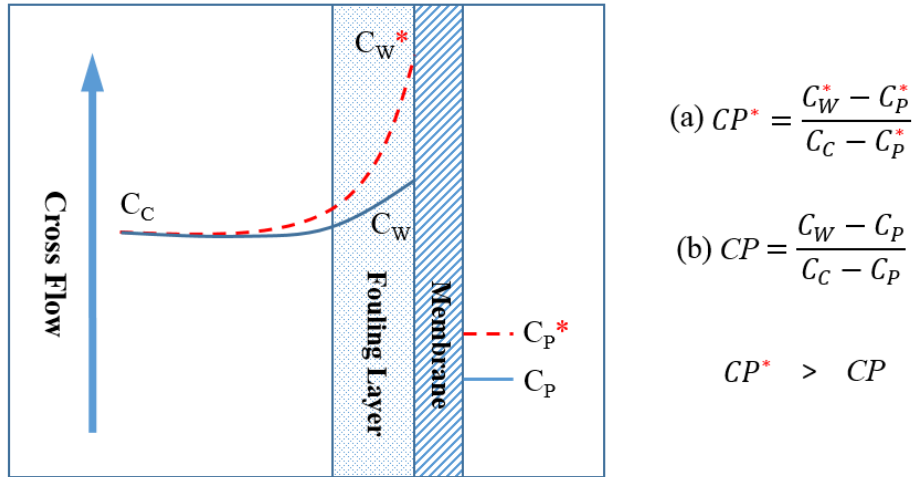
Figure 2.4 Comparison of concentration polarization in membrane separation process: (a) After membrane fouling; (b) before membrane fouling.

2.2.3 Prevention and mitigation of fouling

Membrane fouling as the main challenge during the separation process is inevitable. Therefore, prevention and mitigation of fouling is a reliable approach to maintain membrane performance. To date, various methods have been developed to prevent and mitigate the membrane fouling, including pretreatment of wastewaters, membrane surface cleaning, and development of fouling-resistant membranes.

Pretreatment has been widely used in the operation of TFC membranes. The main purpose of pretreatment is to prevent the pore blocking of TFC membranes caused by the contaminants with large size, such as suspended particles, oil emulsions, and nature organic matters. The most widely used pretreatment process is coagulation-flocculation-sedimentation. With the addition of coagulants into wastewaters, the charged particles or nature organic matters are aggregated, which can be effectively separated from the liquid phase by the following sedimentation or UF membrane filtration.[31] Another extensively employed pretreatment is disinfection by chlorine exposure to mitigate the biofouling of microorganisms. Chlorine species as strong oxidants are able to prevent the growth of these microorganisms in the wastewaters. However, the residual chlorine species in the wastewaters can cause severe damages to the polyamide thin film selective layer of polyamide TFC membranes by the chlorination reaction of polyamide chains, thus lead to a fatal effect on the selectivity of these membranes.

In addition to the pretreatment of wastewaters, membrane surface cleaning can also alleviate the effect of fouling on the membrane performance. The commonly used cleaning agents include surfactants, acid, alkali, and oxidizing sanitizers. After the surface cleaning, membrane permeability can be partially recovered due to the removal of formed cake layer on the TFC membrane surface. However, membrane surface cleaning can inevitably increase the operational cost of membrane separation processes.

Furthermore, development of fouling-resistant TFC membranes is another vital methodology to overcome the membrane fouling. Over past decades, various functional materials with improved properties have been developed for membrane applications. These polymeric materials, including polyvinylidene fluoride (PVDF), PES, nylon 6, and other polyamide polymers, have excellent mechanical strength, thermo-stability, and corrosion resistance. However, the intrinsic relatively

hydrophobic characteristics of these materials can lead to increased fouling propensity due to the hydrophobic interactions between membrane surface and contaminants on the feed side.[32] In addition, surface charge and roughness of membranes are also vital properties involved with membrane fouling. Membranes with strengthened negatively charged surface and smoother surfaces can significantly reduce the fouling propensity of TFC membranes.[12,33] Therefore, fabrication of TFC membranes with proper surface properties, especially suitable surface hydrophilicity, is a promising strategy to reduce the membrane fouling.

（1）Surface hydrophilicity

It has been demonstrated that TFC membranes with improved surface hydrophilicity exhibit enhanced fouling-resistant performance to organic fouling and biofouling. This is due to the formation of a hydration layer between the hydrophilic membrane surface and water via strong hydrogen bond interactions (Figure 2.5). This stable hydration layer can reduce or even prevent the contact of the membrane surface with hydrophobic foulants.
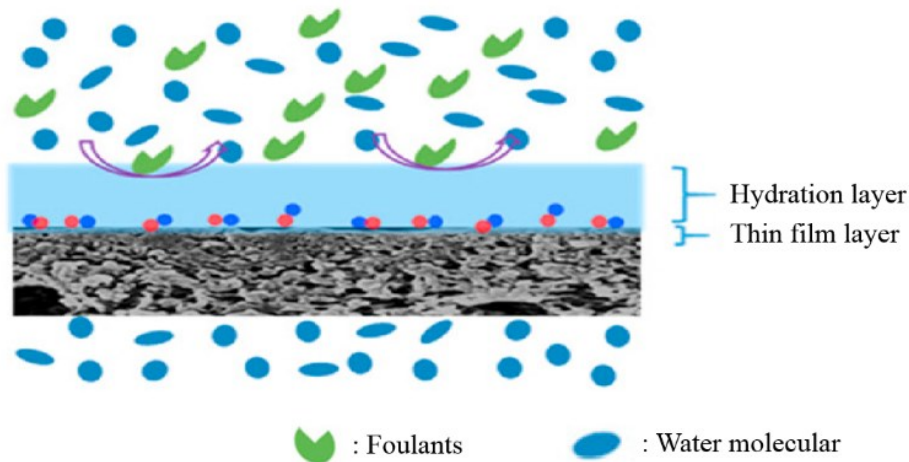
Figure 2.5 Hydration layer between hydrophilic membrane surface and water molecular.[34]

（2）Surface charge

Zeta potential is used to represent membrane surface charge degree. Contaminants such as microorganisms, proteins, polysaccharides, and macromolecules, usually have a negatively

charged surface. Increased negative charge density on the surface of TFC membrane can significantly reduce adsorption of negatively charged contaminants via electrostatic repulsion at the membrane-water interface.[35]

（3）Surface roughness

Despite increased surface roughness of the membrane can increase membrane permeability ascribed to the increased membrane surface area available for water transport, it can lead to severe membrane fouling due to enhanced interactions between the rough surface and foulants.[36] Polyamide TFC membranes have characteristic ridge-and-valley-like roughness features, which are induced by the release of nano-bubbles in the amine monomer aqueous solution during the interfacial polymerization.

2.2.3 Other challenges

In addition to the membrane surface fouling, insufficient water permeability is other main challenge, which restricts the practical applications of TFC membranes. The conventional TFC membrane fabricated via the interfacial polymerization often renders a dense thin film selective layer with a substantial thickness and a random network of pores, which is the main cause for the insufficient water permeability. Despite the production efficiency of clean water can be improved by increasing the external pressure, the concomitant consequence is the increased energy consumption. Furthermore, the high pressure employed in the membrane-based separation processes can intensify the effect of CP and reduce the membrane selectivity. Therefore, development of alternative methodologies for the fabrication of TFC membrane with high water permeability is urgently needed to satisfy the practical applications.

2.3 Development of high performance TFC membranes

The performances of TFC membranes, including permeability, selectivity, and fouling-resistant ability, are determined by the surface properties of the thin film selective layer. To achieve enhanced permeability, selectivity, as well as fouling resistance, various strategies have been developed, including: (a) development of new active monomers; (b) hydrophilic modification of monomers; (c) hydrophilic modification of the thin film selective layer; (d) roughness and thickness control of the thin film selective layer; (e) employment of nanomaterials as additives

during the interfacial polymerization; (f) other types of TFC membranes. In addition to the thin film selective layer, the porous structure of the supporting layer can also impact the membrane permeability. For instance, the supporting layer with higher porosity and larger pore size has a lower hydraulic resistance and trans-membrane pressure, thus produce a higher water permeability.
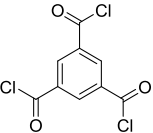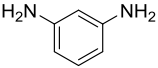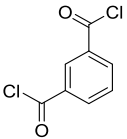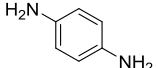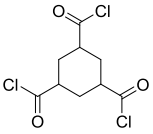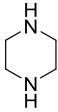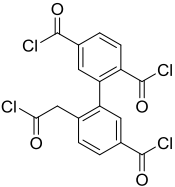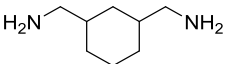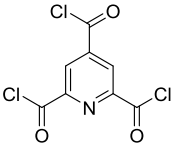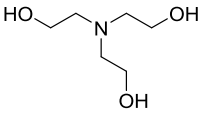
2.3.1 Thin film selective layer

a. Development of new active monomers

Chemical structures and properties of active monomers play a significant role in determining the characteristics of the thin film selective layer, such as pore dimension, thickness, roughness, and hydrophilicity. Therefore, the proper design of two types of active monomers is vital to enhance the performance of TFC membranes. Table 2.1 shows examples of well-developed monomers for the construction of thin film selective layer. TMC and MPD are the most commonly used monomers for the fabrication of polyamide TFC membranes, demonstrating more than 98% salt rejection and an acceptable level of permeability.[37] Therefore, it can be used for seawater desalination. In order to further improve the permeability of TFC membranes, isophthaloyl chloride (IPC) and cyclohexane-1, 3, 5-tricarbonyl chloride (HTC) have been developed to replace TMC, while MPD is replaced by piperazine (PIP) and 1, 3-cyclohexanebis (methylamine) (CHMA). Study results show that the permeability of TFC membranes can be improved with decreased salt rejection, which is ascribed to the decreased crosslinking degree of cross-linked polyamide networks (e.g. IPC) and increased pore size distribution (e.g. CHMA).[38]

Despite numerous active monomers have been developed for the fabrication of thin film selective layers via the interfacial polymerization, they still suffer from trade-off between permeability and selectivity, as well as fouling propensity due to the intrinsic hydrophobicity of crosslinked polyamide networks.

Table 2.1 List of monomers developed for the fabrication of TFC membranes.[38]

Acyl Chloride Monomer (abbreviation)	Chemical Structure	Amine Monomer (abbreviation)	Chemical Structure
Trimesoly chloride (TMC)		m-Phenylenediamine (MPD)	
Isophthaloyl chloride (IPC)		p-Phenylenediamine (PPD)	
Cyclohexane-1, 3, 5-tricarbonyl chloride (HTC)		Piperazine (PIP)	
Om-Biphenyl tetraacyl chloride (om-BTEC)		1, 3-Cyclohexanebis(methylamine) (CHMA)	
Pyridine-2,4,6-tricarbonyl trichloride (PTC)		Triethanolamine (TEOA)	

b. Hydrophilic modification of active monomer

To overcome the intrinsic hydrophobicity of TFC membranes, modifications on active monomers have been intensively investigated to improve the surface hydrophilicity of TFC membranes. The most commonly used methodology is to incorporate a zwitterionic structure into the active amine monomer. To date, zwitterionic polymers can be mainly divided into three categories: phosphobetiane (PC), sulfonbetaine (SB), and carboxybetaine (CB) (Figure 2.6).[24] Compared to other hydrophilic polymers (e.g. poly(vinyl alcohol) and chitosan), the equilibrium charge distribution and charge neutrality endow them remarkable ability to form a strong hydration layer at molecular level via hydrogen bonds.
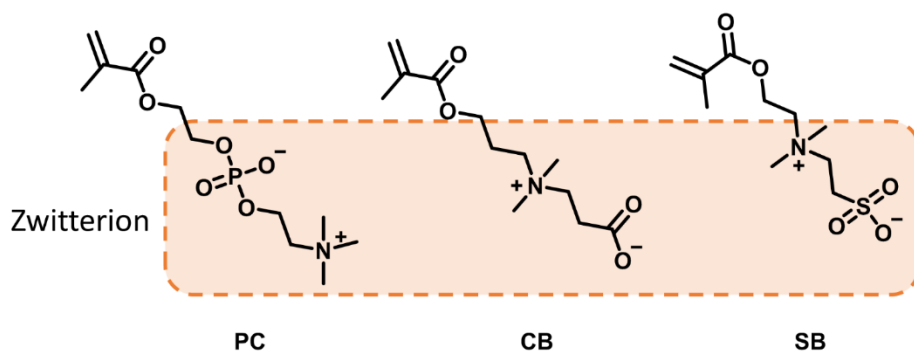
Figure 2.6 Chemical structures of typical zwitterionic polymers.

Despite their special structure properties favor the formation of hydration layer, zwitterionic polymers still suffer from challenges of poor solubility and processability.[39] Therefore, instead of incorporation of bulk zwitterionic polymers into thin film selective layers, zwitterion-modified active amine monomer is a relatively efficient strategy for constructing zwitterion-modified thin film selective layer. As shown in Figure 2.7, 1,3-PS has been widely used to modify active tertiary amine monomers, including tris(2-aminoethyl)amine (TAEA), DNMA, N-aminoethyl piperazine (AEP), p-phenylenediamine (PPD), to form zwitterionic tertiary amine monomers via ring-open

17

reaction.[34,40-44] Then, the synthesized zwitterionic amine monomers can react with acryl chloride monomers via the interfacial polymerization to form hydrophilic thin film selective layers.
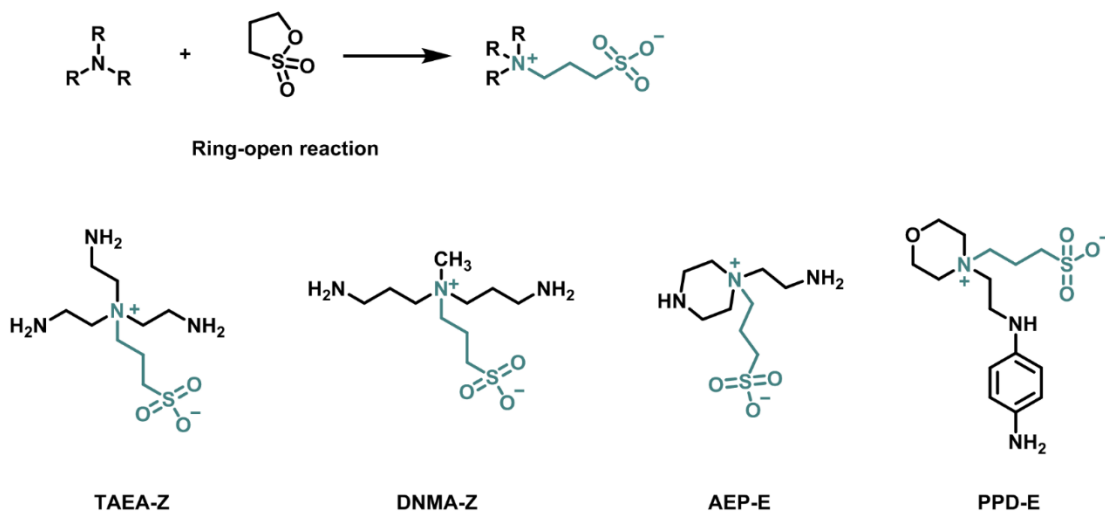
Figure 2.7 Zwitterionic modification of active amine monomers for improving hydrophilicity of TFC selective layer.[34,40-42,44,45]

In addition to direct modifications on active amine monomers, the surface modification of thin film selective layer is another alternative strategy for anchoring zwitterionic polymers. Based on the chemical properties of polyamide, zwitterionic monomers or polymers are able to be introduced via carboxyl groups derived from acryl chloride monomers during the interfacial polymerization. As shown in Figure 2.8a, the zwitterionic monomer (CB-based) reacts with carboxyl groups via condensation reaction on the top surface of thin film selective layer to form an extra hydrophilic layer for enhancing fouling-resistant performance.[46] In addition to the surface modification with zwitterions, in-situ construction of zwitterionic polymer via atom transfer radical polymerization (ATRP) technique can significantly improve fouling-resistant performance of TFC membranes, due to the formation of a thicker zwitterionic polymer layer compared to small molecular condensation polymerization (Figure 2.8b).[47,48]
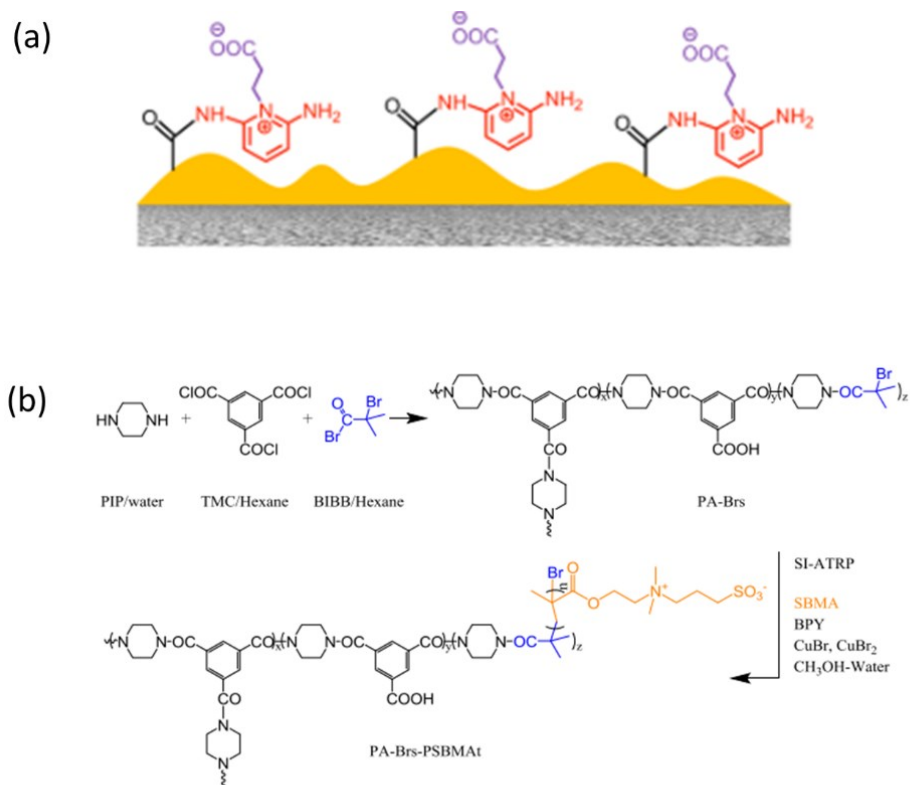
Figure 2.8 (a) Introduction of zwitterionic monomer on polyamide thin film selective layer via condensation reaction,[46] (b) introduction of initiator for ATRP during interfacial polymerization process.[47,48]

The selectivity of TFC membranes is mainly ascribed to the highly crosslinked thin film selective layer.[49] However, the formation of polyamide thin film selective layer is limited to the diffusion of amide monomer and acryl chloride monomer between the boundary of water and solvent liquid phase.[50,51] The rapid condensation polymerization between monomers is a self-terminated film growth process due to the restricted diffusion of monomers to another solvent phase upon the formation of dense polyamide thin film selective layer. Therefore, conventional TFC membranes fabricated via interfacial polymerization process still suffer from the limitation of uncontrollable

polymerization reaction between two monomers, in which a random cross-linked network of pores and dense selective layer with substantial thickness are produced.[52]

In order to reduce the thickness and roughness of thin film selective layer for improving its permeability and fouling-resistant performance, different strategies with controlled interfacial polymerization process have been developed, including electrospray technique,[53-55] molecular layer-by-layer deposition (mLbL),[56,57] and construction of a sacrificial layer before interfacial polymerization.[58] As shown in Figure 2.9a and b, electrospray technique allows the formation of active monomers as nanoscale droplets in the present of strong electrical field and subsequently deposit onto a porous substrate, where condensation polymerization happens between nanoscale droplets of active monomers.[50] The nanoscale droplets allow the sufficient contact and subsequent reaction between active monomers. As shown in Figure 2.9b, the thickness of thin film selective layer can be adjusted via controlling the scan number of the stage. This developed electrospray approach is able to fabricate TFC membranes with tunable thickness and roughness without compromising its selectivity. In addition to the electrospray technique, mLbL is another alternative approach to realize the thickness control of thin film selective layer.[59-62] Figure 2.9c shows that mLbL process involves the sequential reaction of amine monomer and acryl chloride monomer to construct molecular level selective layer with chemical robust, highly crosslinked, and dense cross-linked networks. This process is not restricted by the kinetic and mass transfer limitations between different solvent phases presented in the conventional interfacial polymerization.
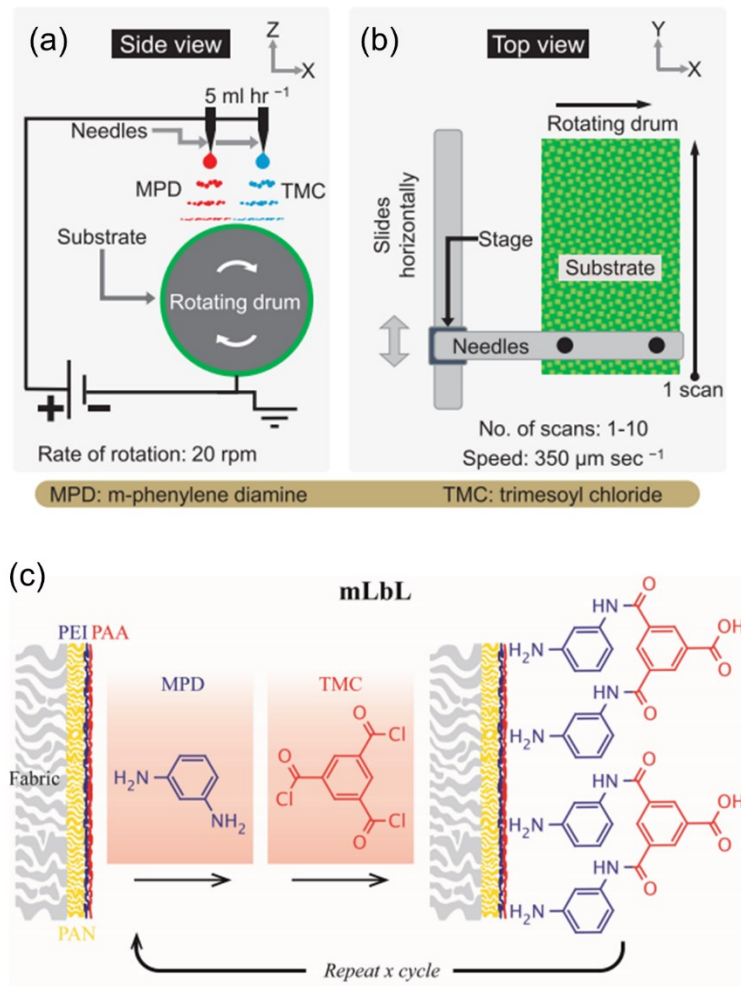
Figure 2.9 Schematic illustration of (a) side view of the electrospray technique, (b) top view of the electrospray technique,[50] and (c) the molecular layer-by-layer process (mLbL).[59]

 e. Nanomaterials as additives during interfacial polymerization

Despite the thickness of thin film selective layer has a substantial effect on the membrane permeability, the hydrophilicity or chemical properties of thin film selective layer are also crucial to the performance of TFC membranes, including permeability and fouling-resistant ability. Nanomaterials, as an emerging material category, have drawn extensive attention in various

industries due to their remarkable chemical and physical properties, such as high special surface area and abundant functional groups.[63,64] To date, in order to improve the performance of TFC membranes, various nanomaterials have been designed and employed as additives for the fabrication of TFC membranes.[65] The application of nanomaterials in the fabrication of TFC membranes can be divided into three directions: (a) introduction of nanomaterials into the polymer matrix of thin film selective layer during interfacial polymerization; (b) construction of an extra interlayer between the porous supporting layer and thin film selective layer before interfacial polymerization; (c) surface modification on the surface of thin film selective layer. In general, the TFC membranes with incorporation of nanomaterials are termed as thin film nanocomposite (TFN) membranes.

Carbon-based nanomaterials, including graphene oxide (GO),[37,66,67] graphene oxide quantum dots (GOQDs),[68,69] and carbon nanotubes (CNTs),[70,71] are the dominant categories for the fabrication of TFN membranes. The fabricated TFN membranes with incorporation of nanomaterials have exhibited significant potential to overcome the trade-off between permeability and selectivity. The enhanced performance is mainly ascribed to the optimized surface properties and morphology.[72,73] In general, carbon-based nanomaterials have a relatively higher hydrophilicity caused by the abundant functional groups, e.g., hydroxyl, amine, and carboxyl groups. Therefore, the well-established method used for the incorporation of nanomaterials is dispersing them into active amine monomer aqueous phase rather than organic acryl chloride solvent phase. However, over decades of development in application of nanomaterials, the TFN membranes still suffer from the limited surface hydrophilicity because of the intrinsic hydrophobicity of polyamide thin film selective layer and insufficient hydrophilicity of nanomaterials, as well as their poor dispersibility in active amide aqueous phase. To further improve the hydrophilicity of nanomaterials, the modifications on nanomaterials have been investigated, such as construction of zwitterionic polymers on the surface of these nanomaterials via ATRP.[74,75] Other nanomaterials, such as titanium dioxide (TiO$_2$),[76] silicon dioxide (SiO$_2$),[77] and zeolite[78] are also intensively employed for the fabrication of TFC selective layer. In addition, the incorporation of plant-derived hydrophilic cellulose nanocrystals (CNCs)[8,79-81] or cellulose nanofibers (CNFs) into the polymer matrix of thin film selective layer has also been investigated. The abundant hydroxyl groups on the surface of CNCs or CNFs endow the fabricated TFN membranes with enhanced hydrophilicity, even

improved chloride-resistant ability due to the formation of ester bonds between hydroxyl groups and acryl chloride.

In addition to the incorporation of nanomaterials into the thin film selective layer, pre-construction of a nanomaterial layer on the porous supporting layer is beneficial for the subsequent formation of polyamide thin film selective layer.[82-85] As shown in Figure 2.10, the pre-constructed CNT layer on the porous supporting layer can efficiently avoid penetration of cross-linked polyamide networks into the bottom porous supporting layer, thus, producing a thinner selective layer with enhanced permeabilit.
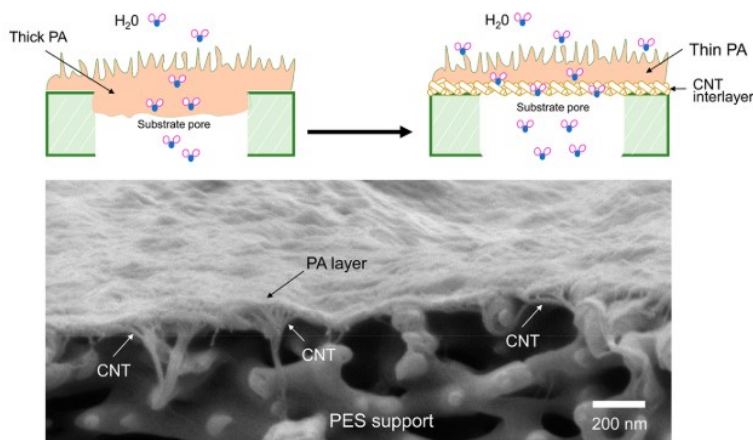
Figure 2.10 Schematic illustration of polyamide TFC membranes with a CNT interlayer between porous supporting layer and polyamide thin film selective layer.[82]

 f. Other types of TFC membranes

In addition to the conventional polyamide TFC membranes, bioinspired polymers, as a class of rapidly emerging functional materials, have been extensively implemented for the construction of thin film selective layer in order to achieve enhanced water permeability and rejection ability in the application of nanofiltration membranes. Dopamine, known as "bio-glue", is the most representative one due to its environmental friendliness and versatility.[86,87] The oxidative polymerization of dopamine endows with the strong adhesive property on various organic and inorganic surfaces. The dopamine polymerization process involves the formation of semi-quinone

and quinone from catechol and subsequent covalent bonding with amine groups. Therefore, numerous efforts have been dedicated to develop TFC membranes with employing materials with catechol structure and other functional materials containing abundant amine groups. To date, the developed catechol-derived structural materials including catechol, dopamine, tannic acid, gallic acid, and epigallocatechin gallate (as shown in Figure 2.11), have been widely adopted for constructing thin film selective layer via crosslinking with polyethylenimine (PEI).[88-91] The fabricated TFC membranes enable the removal of small organic molecules from wastewater or the fractionation of dye/salt mixtures from textile industries. However, it is still a challenge to simultaneously achieve high permeability, high rejection ratio of contaminants, and fouling-resistant performance.
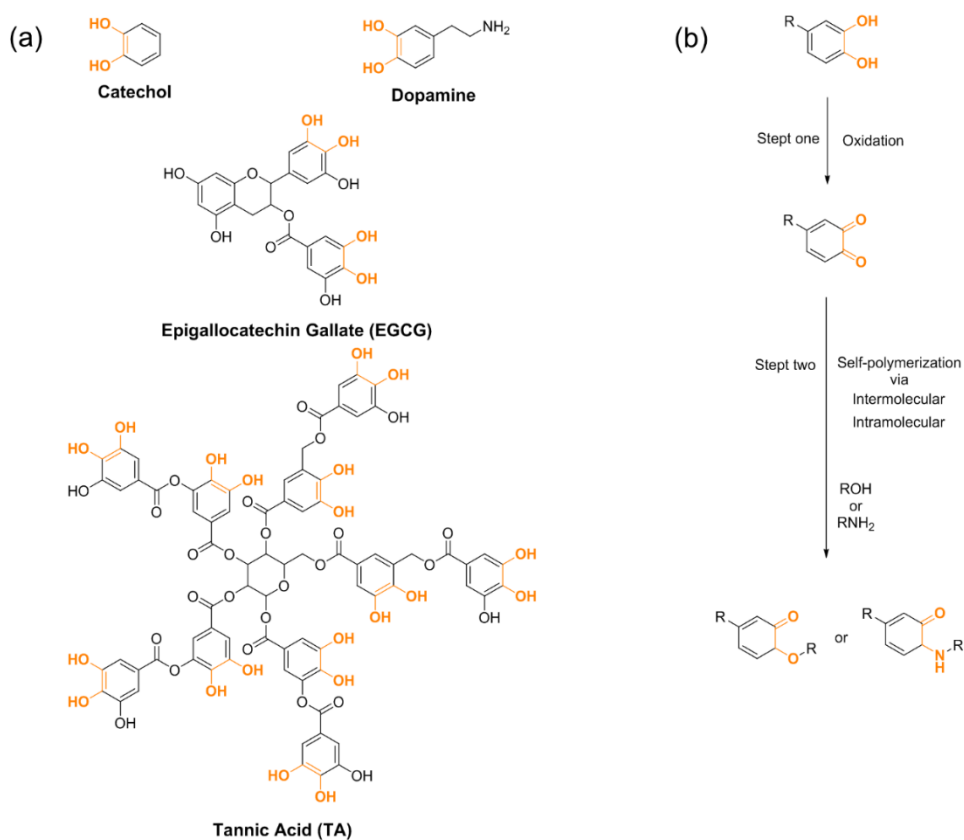
Figure 2.11 (a) Bio-inspired and plan-inspired phenolic materials,[92] (b) possible oxidative self-polymerization process of phenolic materials.[13,88]

Nanoporous materials, including mesoporous silica nanoparticles and covalent organic frameworks, have been recently employed for the construction of the active barrier for nanofiltration.[52,93,94] Despite these nanoporous materials endow the nanofiltration membranes with ultrahigh flux by virtue of their porous structure, tedious synthetic processes and insufficient rejection ability still restrict their applications. Membranes with combined high water permeability and high rejection ability are yet to be developed.

2.3.2 Porous supporting layer

Performance of TFC membranes can be largely determined by the characteristics of the porous supporting layer, including the surface hydrophilicity and porosity. In general, hydrophilic materials are preferred for the preparation of the porous supporting layers since they have less resistance to water molecules passing through the membrane, thus, enhancing water permeability. In addition, a porous supporting layer with a high porosity is also favorable for enhancing water permeability. Numerous works have been conducted by introducing hydrophilic additives into the polymeric solutions during preparation process of porous supporting layer, including polyvinylpyrrolidone (PVP), polyethylene glycol (PEG), SiO_2, and GO.[95-97] The addition of these hydrophilic materials enables to improve the hydrophilicity of the porous supporting layer as well as its porosity. In addition, the structure properties of the porous supporting layer can be optimized by increasing its porosity via other techniques (e.g. electrospinning). Electrospinning is a versatile membrane preparation method, which can produce nanofiber mats by applying a high voltage between a nozzle and drum collector.[98] Figure 2.12 shows the typical electrospinning process. Nanofiber mats formed by the electrospinning technique have an ultrahigh porosity (≥80%), which provides more channels for water to pass through TFC membranes.
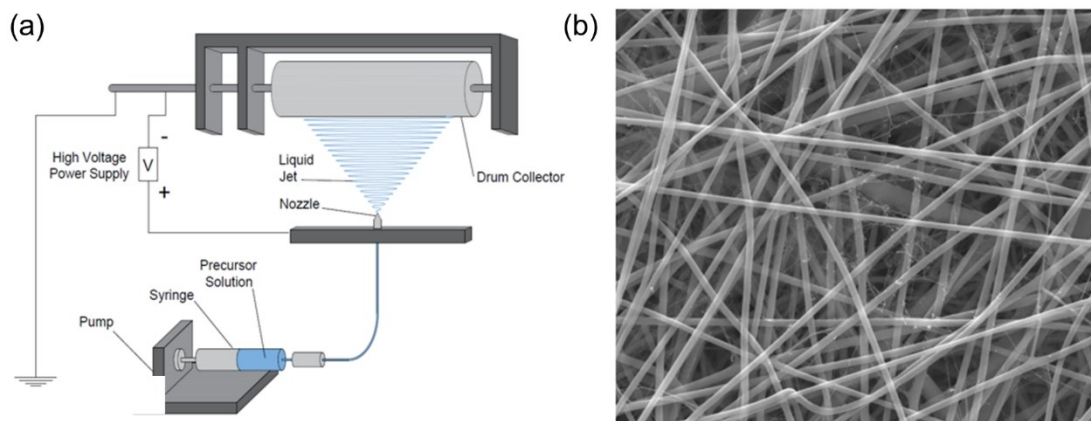
Figure 2.12 (a) Schematic illustration of a typical electrospinning process; (b) electrospun nanofiber mats produced from electrospinning process.

2.4 Research gap and limitations

To date, the state-of-the-art TFC membranes are polyamide TFC membranes fabricated from the conventional interfacial polymerization. Despite significant progress has been achieved via tuning fabrication processes and developing new monomers, some intrinsic drawbacks still restrict their widely applications, such as the substantial thickness of thin film selective layers produced from uncontrollable self-terminated polymerization and their fouling propensity. Other alternative methodologies for the construction of thin film selective layers have also been developed, including bio-inspired chemistry, direct surface coating of various nanosheets, and in-situ formation of nanoporous thin film layer on the supporting layer. However, they still suffer from some limitations. For instance, bio-inspired chemistry depends the oxidative self-polymerization, which is a time-consuming process. Meanwhile, the formed aggregates from bio-inspired monomers (e.g. dopamine and catechol) can adhere on the surface of supporting layer and block membrane pores, thus reduce the permeability of TFC membranes.

Therefore, for the application of bio-inspired chemistry in the fabrication of TFC membranes, to develop efficient methodologies avoiding the block of aggregates on the pores of supporting layer

should be considered. Meanwhile, in order to enhance the fouling-resistant ability of bio-inspired TFC membranes, the investigation of co-deposition of bio-inspired monomers with other zwitterions via stable covalent bonds should be undertaken.

Although the development of new methodologies for the construction of thin film selective layers is urgently needed, the conventional interfacial polymerization as the predominant methodology in the fabrication of TFC membranes is still undisputed at present. As summarized above, various zwitterionic monomers have already been designed to overcome the fouling propensity of these TFC membranes. However, the scope of zwitterionic structures in TFC membranes should be further explored to improve the hydrophilicity of TFC membranes, thus enhance their fouling-resistant performance. Apart from the zwitterion-modified polyamide TFC membranes to achieve enhanced fouling-resistant performance, polyester TFC membranes show relatively stronger hydrophilicity compared to the pristine polyamide TFC membranes due to the existence of abundant hydroxyl groups. However, there are few zwitterion-modified polyester TFC membranes reported so far in the investigation of their fouling-resistant performance.

In summary, new types of zwitterion should be explored for the fouling-resistant application in TFC membranes via interfacial polymerization, including polyamide and polyester TFC membranes. In addition, alternative methodologies are needed to overcome the drawbacks of typical TFC membranes fabricated from interfacial polymerization.

Chapter 3 Thin film nanocomposite membranes with polydopamine-modified cellulose nanocrystals

This chapter is adapted from a paper published in *Desalination* (**Yang, L.**; Liu, X.; Zhang, X.; Chen, T.; Ye, Z.; Rahaman, Md. S., High performance nanocomposite nanofiltration membranes with polydopamine-modified cellulose nanocrystals for efficient dye/salt separation. *Desalination* 2022, 521, 115385).

Abstract

CNCs, as a class of renewable and sustainable nanomaterials, are attracting increasing attention for membrane-based separation applications. In this study, hierarchical loose thin film TFN NF membranes are fabricated via the stacking of polydopamine-modified core-shell-structured CNCs on ENMs, followed by the crosslinking with PEI. Prepared by convenient oxidative self-polymerization of dopamine on CNCs, the polydopamine-modified CNCs contain abundant quinonoid active sites for the subsequent crosslinking with PEI. The crosslinking structures are tuned by varying the molecular weight and concentration of PEI for optimum membrane performances. With the loosely constructed crosslinking networks between modified CNCs and PEI, the optimum TFN membrane shows the outstanding performance in the filtration of Congo red (CR)/NaCl solution, with superior dye rejection (99.91%), salt permeation (98.86%), and ultrahigh PWP (128.4 LMH bar-1). Notably, the optimum TFN membrane also exhibits an impressive selectivity factor of 1098 for the separation of CR/NaCl. The PWP, dye rejection, and dye/salt selectivity are much higher than those of most reported NF membranes. The present work demonstrates the potential of our novel strategy incorporating polydopamine-modified CNCs for the fabrication of high performance NF membranes for various separation applications.

3.1 Introduction

Textile industries, which have experienced tremendous development thus far, produce highly toxic wastewaters containing organic dyes, inorganic salts, and other contaminants such as surfactants and auxiliary chemicals.[99,100] The discharge of textile effluents without proper treatment would

lead to irreversible destruction to aquatic environment and raise human health concerns due to the intrinsic chemical structural and non-biodegradable properties of the contaminants.[101] In efforts to minimize the severe impact of pollutants from textile industries on the ecosystem, conventional strategies developed to date mainly focus on the adsorption or degradation of these contaminants. However, extensive energy consumption coupled with the increasingly stringent environmental restrictions and losses of valuable dyes and inorganic salts seriously restrict their applicability.[102-104]

Membrane-based separation technologies have drawn intensive attention in various fields, including water treatment and recycling, seawater desalination, pharmaceutical process, and battery recovery, owing to their virtue of high selectivity and efficiency, relatively low energy consumption, facile operation conditions, and environmental sustainability.[105,106] In particular, NF with the use of membranes with molecular weight cut-off from 200-1000 Da is one of most viable separation technologies for dye recovery because of its relatively low capital/operating costs and high selectivity.[13,107-111] However, conventional polyamide TFC NF membranes fabricated via the interfacial polymerization technique still suffer from the limited control over the polymerization, which often renders a dense active layer with a substantial thickness and a random network of pores.[112] The dense active layer can retain dyes and salts simultaneously through steric hindrance and Donnan effect, rather than separating dyes and salts for reuse.[113] Meanwhile, an increased osmotic pressure in the feed solution caused by the low salt permeation compromises the permeability and selectivity of NF membranes.[88] All these challenges call for developing efficient NF membranes with a superior performance (e.g., high dye rejection and high salt permeation).

Apart from the conventional polyamide TFC NF membranes, extensive efforts have been undertaken to fabricate high-performance NF membranes with loose structures for the separation of dye/salt mixtures. Various strategies have been developed by improving the interfacial polymerization, including the process optimization of the interfacial polymerization by electrospray[53] and incorporation of nanomaterials into the membranes, such as GO/CNTs,[110] GOQDs,[69] TiO_2,[114] through the interfacial polymerization. In addition, the pre-construction of a nanoscaffold interlayer of CNTs,[82] CNCs,[115] or cadmium hydroxide nanostrands[116] on a porous supporting layer before interfacial polymerization has also been developed to further improve the membrane performance. Moreover, ENMs produced from electrospinning have also been reported

as porous supporting layers to fabricate membranes.[117-119] The prepared TFC membranes showed improved due to the ultrahigh porosity of ENMs.[120] Despite the enhanced permeability, the resulting membranes still suffer from the above-mentioned limitation of the inherent structural frame from the conventional interfacial polymerization. Relative to the optimization of conventional interfacial polymerization, other nanoporous materials, including covalent organic frameworks (COFs) and mesoporous silica nanoparticles, have also been recently employed for constructing the loose active barrier for NF membranes.[111,121-123] Though these nanoporous materials endowed the NF membranes with ultrahigh flux by virtue of their porous structures, tedious synthetic processes and insufficient rejection of dyes still restrict their applications. Membranes with combined high permeability and high selectivity of dyes/salts are yet to be developed.

Bioinspired polymers, as a class of rapidly emerging functional materials, have been extensively implemented for multifunctional solid surface coating. Among them, mussel-inspired chemistry has attracted considerable attention and achieved a substantial progress.[92] Based on the previous researches, the functionality of mussel-inspired chemistry is ascribed to the abundant 3,4-dihydroxy-L-phenylalanine in mussel foot proteins.[92,124] Dopamine with a similar molecular structure to the 3,4-dihydroxy-L-phenylalanine, also known as "bio-glue", is the most representative one due to its environmental friendliness and versatility.[125,126] To date, deposition or co-deposition of dopamine has been widely employed in the surface modification of different types of membranes,[127,128] interlayers for TFC membrane fabrications,[129,130] and the construction of selective layers in TFC membranes.[131,132] Xu et al. fabricated NF membranes by co-deposition of dopamine and branched PEI on the surface of polyphenylene sulfide membranes.[133] The resultant membranes showed high dye rejection (>99%), but with only moderate PWP. Other bio-inspired polymers with catechol-simulated structures, including catechol, tannic acid, gallic acid, and epigallocatechin gallate, have also been used to construct TFC membranes.[88-90,134] Despite improved dye rejection and enhanced permeation of multivalent salts, the oxidative self-polymerization process can proceed not only on the membrane surface but also inside pore walls, which inevitably blocks the water channels and thus compromises the membrane permeability. In addition, aggregated clusters formed by the uncontrollable oxidative self-polymerization of catechol-simulated materials can adhere on the surface of membrane active layer, which limits their applications for water purification.[125,135-137]

Tackling the challenge, we report here the fabrication of loose TFN membranes incorporating polydopamine-modified core-shell-structured CNCs cross-linked with branched PEI as an active layer, which is stacked on porous ENMs. The high porosity of ENMs is conducive to enhance the membrane permeability. CNCs, as a kind of natural and non-toxic nanomaterials, have been extensively used for membrane fabrications by surface coating or as additives due to their special properties, such as abundant functional groups on the surface, rod-like structure, and high surface area-to-volume ratio.[81,138,139] Herein, CNCs are employed uniquely as a substrate for the deposition of polydopamine onto the ENMs, with the aim of reducing the blocking of water channels and formation of aggregates on the surface of active layer. Meanwhile, the unique rode-like structure and high surface area-to-volume ratio of CNCs facilitates the formation of multiple quinonoid active sites on the modified CNCs for the subsequent construction of crosslinked networks with branched PEI via the formation of covalent bonds. The effects of molecular weight and concentration of branched PEI, as well as the coating density of the modified CNCs on the membrane performance have been systematically investigated. To the best of our knowledge, this is the first strategy on the construction of polymerized catechol-simulated membrane active layer while without blocking pores or reducing porosity. The resulting membranes show superior performance with the combined ultrahigh water permeability, high dye rejection, and high dye/salt selectivity, demonstrating the potential of this novel strategy for the fabrication of high-performance loose NF membranes for various separation applications.
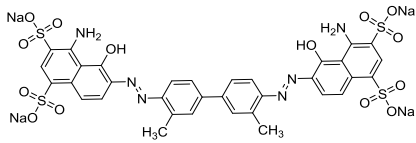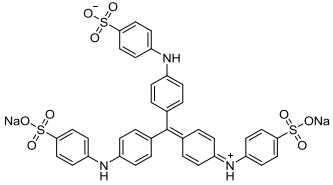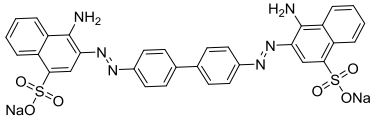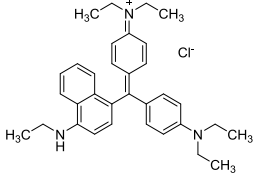
3.2 Experimental

3.2.1 Materials

Nylon 6 pellets, PEI (branched, M_w = 25,000 and 2000 Da), dopamine hydrochloride, tris(hydroxymethyl)aminomethane (Tris), Evans blue (EB), Methyl blue (MB), Congo red (CR), and Victoria pure blue BO (VPBO) were obtained from Aldrich (Oakville, ON, Canada). Properties of all organic dyes are listed on Table 3.1. Formic acid (88.0%), acetic acid (99.7%), hydrochloric acid (36.5%), sodium chloride (99.0%), sodium sulfate (98.0%), magnesium chloride (99.0%), and magnesium sulfate (99.0%) were provided by Thermo Fisher Scientific (St. Laurent, QC, Canada). Cellulose nanocrystals (-OSO_3^- functionalized) were supplied by Celluforce Co. Ltd

(Montreal, QC, Canada). Deionized (DI) water was prepared using a Milli-Q purification system (Millipore, Billerica, MA, USA). All the chemicals were used as received.

Table 3.1 Properties of the organic dyes used in this study.

Dyes	Chemical structure	Molecular weight (g mol^{-1})	$\lambda_{max}{}^a$ (nm)
Evans Blue (EB)		960.8	608
Methyl Blue (MB)		799.8	592
Congo Red (CR)		696.7	500
Victoria Pure Blue BO (VPBO)		514.1	614

^{a} Maximum absorption wavelength.

3.2.2 Preparation of Polydopamine-Modified CNCs

The polydopamine-modified core-shell CNCs were prepared by mixing the CNC dispersion in DI water with dopamine hydrochloride in Tris buffer solution at pH 8.5.[92] Figure 3.1a shows the preparation process. In detail, CNCs (0.1 wt%) were dispersed in DI water under sonication for 30 min, followed by the addition of dopamine hydrochloride (0.1 wt%) and Tris (50 mM) into the mixture. Then, the pH of as-prepared mixture solution was adjusted to 8.5 using 0.5 M HCl

solution. Subsequently, the freshly prepared solution was mixed under magnetic stirring for 24 h at ambient temperature. The mixture turned from the initially clear solution to the black, which is the characteristic color of polydopamine coatings. The resulting polydopamine-modified core-shell CNCs were obtained by filtration with at least three times of washing of DI water. The final black power was redispersed in DI water and stored at 4 °C before use and characterization.

3.2.3 Preparation of ENMs of Nylon 6

ENMs of Nylon 6 were fabricated using a Nanospinner (NE300, Inovenso, Turkey) as we reported before.[98,140] Nylon 6 solution (21 wt%) was prepared by dissolving Nylon 6 pallets in a mixture of formic acid and acetic acid (4/1, v/v) at ambient temperature under magnetic stirring for 12 h. Then, the prepared Nylon 6 solution was loaded into a 30 mL syringe connected to the nozzle. Electrospinning was undertaken at a constant flow rate of 0.18 mL h^{-1} and 25 kV voltage with a distance of 9 cm between the nozzle tip and collector. The detailed fabrication process of ENMs is described in Figure S3.1.

3.2.4 Fabrication of TFN Membranes

Briefly, TFN membranes were fabricated by the vacuum-assisted surface coating of polydopamine-modified CNCs on the ENM substrate followed by crosslinking with PEI in a Tris buffer solution. As shown in Figure 3.1b, a prescribed quantity of polydopamine-modified CNCs was deposited on an ENM by vacuum filtration. Subsequently, the coated membrane was immersed in the freshly prepared Tris buffer solution (50 mM, pH 8.5) containing PEI of different molecular weights and concentrations at ambient temperature for 6 h. Table 3.2 summarizes detailed fabrication conditions for the various TFN membranes. In particular, TFN0.1-Control was prepared as a control membrane without crosslinking with PEI in order to investigate the role of PEI in the TFN fabrication process. TFN membranes with three coating densities of modified CNCs varying from 0.1 g m^{-2}, 0.2 g m^{-2}, and 0.3 g m^{-2} have been fabricated. Here, the following examples are given to describe the designation of all as-prepared TFN membranes. For instance, in TFN0.1-0.5L and TFN0.1-0.5H, the first number (0.1) denotes the coating density of modified CNCs and the second number (0.5) denotes the PEI concentration (g L^{-1}) in the crosslinking solution, and the final capital letter (H or L) indicating the high molecular weight (25,000 g mol^{-1}) or low molecular weight (2,000 g mol^{-1}) PEI used for crosslinking.

Table 3.2 Summary of TFN membrane fabrication conditions.

Membrane	Coating density (g/m²)	PEI concentration (g/L)	Molecular weight of PEI (g/mol)
TFN0.1-Control	0.1	-	-
TFN0.1-0.5H	0.1	0.5	25000
TFN0.1-0.5L	0.1	0.5	2000
TFN0.1-0.1L	0.1	0.1	2000
TFN0.1-0.02L	0.1	0.02	2000
TFN0.1-0.005L	0.1	0.005	2000
TFN0.1-0.001L	0.1	0.001	2000
TFN0.2-0.02L	0.2	0.02	2000
TFN0.3-0.02L	0.3	0.02	2000

All TFN membranes were immersed in a Tris buffer (50 mM) solution with PEI at pH 8.5 except TFN 0.1-Control as the control (without immersion in the Tris buffer solution).

3.2.5 Characterizations and Measurements

The Fourier Transform Infrared (FTIR) spectra of the modified CNCs and TFN membranes were obtained on a Thermo Scientific Nicolet 6700 Analytical FTIR spectrometer. Particle size distributions of the pristine and modified CNCs were obtained with a Brookhaven NanoBrook Omni instrument by dynamic light scattering (DLS). Thermogravimetric analysis (TGA) of the pristine and modified CNCs were carried out on a TA instruments Q50 thermogravimetric analyzer. Zeta potential of the pristine and modified CNCs was obtained on a Malvern Zetasizer. Water contact angle measurements were performed on a contact angle system (VCA, AST Products, Inc.).

Membrane surface and cross-sectional morphologies were observed via a FEI Quanta 450 environmental scanning electron microscope (FE-ESEM) after platinum coating (~4 nm). X-ray photoelectron spectroscopy (XPS) was performed on a Thermo Scientific K-Alpha XPS spectrometer. The surface roughness of the TFN membranes was investigated with an atomic force microscope (AFM) (NanoINK Inc. Skokie, IL, USA) in the tapping mode.

2.6 TFN Membrane Performance Tests

All membrane performance tests were conducted at 2.0 bar using a stirred dead-end filtration cell with a stirring speed 350 rpm. The effective area of the filtration was 3.14 cm^2. The TFN membranes were compacted at 2.5 bar with DI water for 30 min to reach a steady state before testing. In this study, a series of solutions of dyes and inorganic salts at a concentration of 200 ppm and 1 g L^{-1}, respectively, were employed as feed solutions. The TFN membrane permeability (P, LMH bar^{-1}) was calculated using the following equation:

$$P = \frac{V}{A \times t \times \Delta P} \tag{3.1}$$

where V is the volume (L) of the permeate, A is the effective filtration area (m^2), t is the operation time (h) and ΔP is the trans-membrane pressure (bar). The solute rejection (R) was calculated using:

$$R = \left(1 - \frac{C_p}{C_f}\right) \times 100\% \tag{3.2}$$

where C_p and C_f are solute (dye or salt) concentrations of the permeate and feed solutions, respectively. Dye concentration was determined with a UV-vis spectrophotometer (Agilent Cary 8454), while salt concentration was measured using a conductivity meter (OAKTON conductivity meter, CON 11 series, Vernon Hills, IL USA).

The dye/salt selectivity factor (α) was calculated from the salt and dye permeability. This coefficient indicates the dye/salt separation ability of the fabricated TFN membranes. It was calculated according to:

$$\alpha = \frac{100 - R_{salt}}{100 - R_{dye}} \tag{3.3}$$

where R_{salt} and R_{dye} represent the rejection of inorganic salt and dye, respectively.
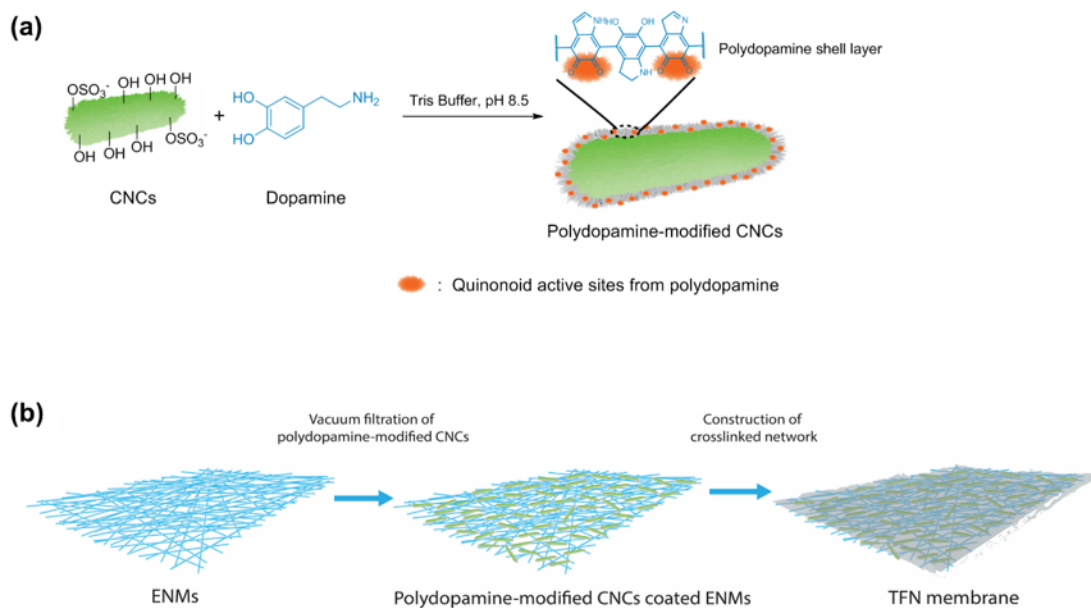
Figure 3.1 Schematic illustration of (a) the preparation process of polydopamine-modified CNCs and (b) the fabrication process of TFN membranes.

3.3 Results and discussion

3.3.1 Preparation and characterization of polydopamine-modified CNCs

In our strategy, polydopamine-modified core-shell-structured CNCs are prepared via the oxidative self-polymerization of dopamine in the presence of CNCs at a weak alkaline condition (pH 8.5). Dopamine, a dominant component of *M. edulis* foot protein, endows versatile adhesive property on both inorganic and organic surfaces. Though the exact adhesive mechanism is still unknown, the resulting polydopamine here is expected to form a coating layer on the surface of CNCs through hydrogen bonding, ionic bonding, as well as the subsequent intermolecular polydopamine network forming through covalent and noncovalent bonding.[124,136] As shown schematically in Figure 3.1a,

the thin polydopamine layer formed on the surface of CNCs is also expected to provide substantial quinonoid active sites for the subsequent formation of imine with amine in PEI to render cross-linking. FTIR spectra of the pristine CNCs and polydopamine-modified CNCs are presented in Figure 3.2a. Compared to the pristine CNCs, modified CNCs show a slight enhancement of the peak at 3340 cm^{-1} (O-H and N-H stretching), indicating the successful introduction of dopamine. Meanwhile, the intensified and broader characteristic peak at 1610 cm^{-1} is attributed to stretching vibrations of C=C in aromatic rings and bending vibrations of N-H in polydopamine, which also confirm the successful preparation of the modified CNCs. The core-shell structure of the modified CNCs is also confirmed with DLS (Figure 3.2b), which shows a significant increase in the hydrodynamic diameter from 117 to 193 nm as a result of the formation of the shell layer. In addition, the modified CNCs show an increased zeta potential (-34.7 mV vs. -14.7 mV; Figure 3.2c) compared to the pristine CNCs, which is ascribed to the coverage of the negative groups (-OSO$_3^{-1}$) on the pristine CNCs surface by the polydopamine shell layer. TG characterization was conducted under a nitrogen atmosphere to evaluate the thermal behavior of the pristine CNCs and modified CNCs. TG shows that the decomposition of the pristine CNCs occurs above 280 °C with a dramatic weight loss of 60% within 280-310 °C (Figure 3.2d), which is consistent with earlier reports.[141,142] Polydopamine, as a control, shows a lower thermal stability because of its complex and broad molecular weight distribution. Relative to the pristine CNCs, the decomposition of the modified CNCs starts at a much lower temperature of around 170 °C, which is ascribed to the lower thermal stability of the polydopamine coating layer. These characterization results confirm the successful formation of polydopamine-modified core-shell-structured CNCs.
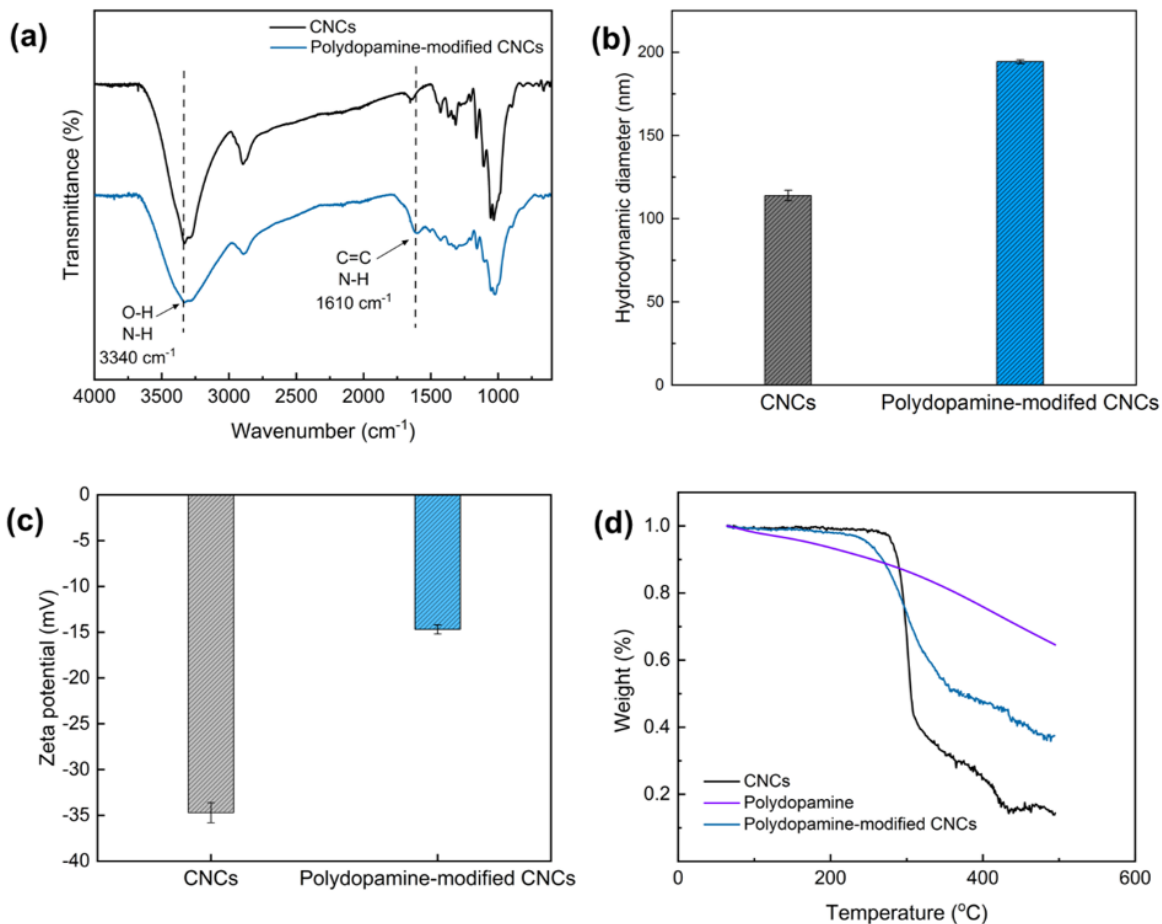
Figure 3.2 Characterizations of the pristine CNCs and polydopamine-modified CNCs: (a) FTIR spectra, (b) particle size distribution by DLS, (c) zeta potential at pH = 7, and (d) TGA curves (10 °C min^{-1} in a N$_2$ atmosphere).

3.3.2 Characterization of TFN membranes

The separation performance of TFN membranes is intrinsically determined by the thickness and pore size of the membrane surface active layer, as well as the properties of porous supporting layer. Herein, the ENM is adopted as the porous supporting layer due to their ultrahigh porosity, with multiple interconnected microporous channels facilitating rapid water transportation. As shown in Figure 3.3a and Figure S3.2a, the top view SEM image of the bare ENM displays stacked multi-

layered nanofibers with a uniformed diameter. The average pore size and porosity of ENMs are around 170 nm and 78%, respectively, based on our previous study.[98] The polydopamine-modified CNCs have been assembled on the ENM substrate at different coating densities with assistance of vacuum filtration, followed by cross-linking with PEI through the covalent bonding of the quinonoid active sites of polydopamine on the modified CNCs with amine groups of PEI (Figure 3.3a). The modified CNCs cross-linked with PEI form the active thin film layer on ENMs. Two PEIs of different molecular weights (2,000 and 25,000 g mol^{-1}) have been used to cross-link the polydopamine-modified CNCs. Meanwhile, different PEI concentrations have also been used to optimize the membrane performance as summarized in Table 3.2.

Figure 3.3b shows the top view surface morphologies of TFN membranes prepared with the modified CNCs at various coating densities (0.1 to 0.3 g m^{-2}). One can observe that the defect-free modified CNC layer is constructed on the ENM substrate in each membrane. In the case of TFN0.1-0.02L of the low coating density, the distinct interwoven fibrous structure of ENMs is visible. The TFN membranes with relatively higher coating densities (TFN0.2-0.02L and TFN0.3-0.02L) display smoother surfaces (Figure S3.3). Meanwhile, the individual rod-like CNCs can be observed within all TFN membranes (Figure 3.3b). In addition, small quantities of sphere-like nanoparticles (NPs) of polydopamine are also found on the TFN membrane surfaces, which should be produced in the preparation of the modified CNCs. Like the polydopamine coated on CNCs, these polydopamine NPs can also be cross-linked with PEI. Unlike micron-scale ploydopamine aggregates produced from the conventional surface coating methodology,[143,144] the effect of these polydopamine NPs at small quantities on the membrane performance should be negligible. From the cross-sectional views of the membranes (Figure 3.3c), the distinct hierarchical architectures can be observed, as well as the increasing coating layer thickness with the increase in coating density. As shown in Figure S3.4, the thickness of the coating layer increases almost linearly from 118 to 355 nm as coating density increases from 0.1 g m^{-2} for TFN0.1-0.02L to 0.3 g m^{-2} for TFN0.3-0.02L. This confirms that the coating of the polydopamine-modified CNCs on ENMs is controllable. All these results indicate that the strategy developed herein for TFN membrane fabrication is highly effective in restricting the formation of large scale polydopamine aggregates, thus efficiently preventing the blockage of water passage channels in both the active layer and the microporous supporting layer.
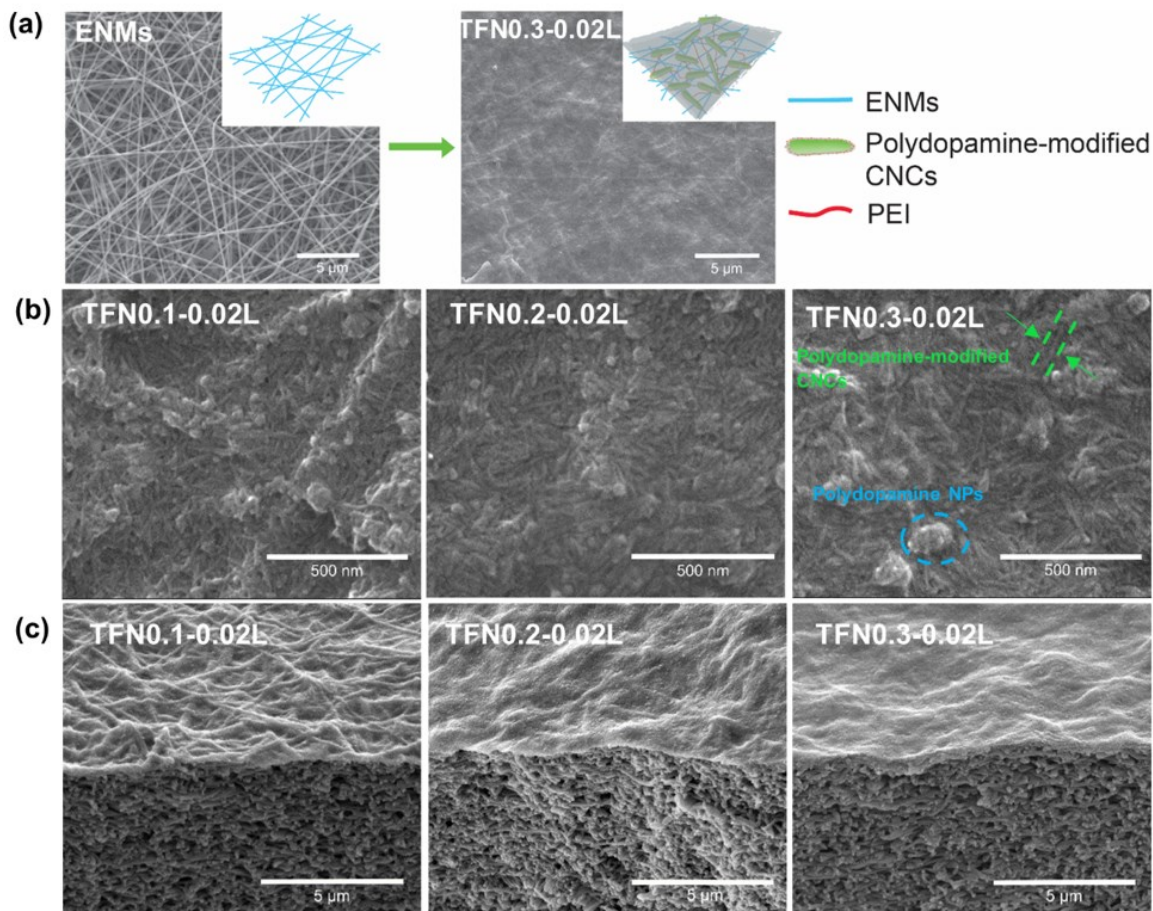
Figure 3.3 Surface and cross-sectional SEM images of TFN membranes: (a) schematic illustration of the morphological structure of TFN membranes, (b) surface SEM images (scale bar: 500 nm, magnification of 100000), and (c) cross-sectional SEM images (scale bar: 5 μm, magnification of 10000).

The functional groups present on the TFN membranes have been determined with ATR-FTIR. As shown in Figure 3.4a, the characteristic peaks at 1545 cm^{-1}, 1637 cm^{-1}, and 3294 cm^{-1} are ascribed to N-H deformation, C=O stretching, and N-H stretching vibrations, respectively, of the Nylon 6-based ENM substrate.[98] In comparison with the pristine ENMs, two new peaks are observed

with the TFN membranes at 3340 and 1060 cm^{-1}, respectively. The former corresponds to O-H and N-H stretching vibrations of CNCs and polydopamine, respectively. The latter is ascribed to C-O stretching vibrations of primary hydroxyl groups from CNCs. The intensities of the new peaks are enhanced with the increase of the coating density from 0.1 to 0.3 g m^{-2}. These FTIR results also demonstrate qualitatively the presence of the CNCs on ENMs.

To further verify the presence of PEI in the cross-linked thin film coating layer, surface elemental compositions of the fabricated TFN membranes have been quantified with XPS. As shown in Figure 3.4b and Table S3.1, the dominant elements on the TFN membrane surface include C 1s, O 1s, and N 1s, originating from CNCs, polydopamine, as well as PEI. Compared to TFN0.1-Control membrane without PEI, obvious increases in the relative intensity of N 1s are seen in other TFN membranes, demonstrating the incorporation of PEI as it has a higher N content than polydopamine. Among the TFN membranes, TFN0.1-0.5H has the highest atomic percentage of N 1s (7.61%). TFN0.1-0.5L, prepared under identical conditions as TFN0.1-0.5H except with the use of lower-molecular weight PEI, shows instead a lowered N 1s percentage of 5.58%, indicating that PEI with a higher molecular weight has an enhanced immobilization with a higher crosslinking degree. With the set of membranes fabricated at different PEI concentration (TFN0.1-0.5L, TFN0.1-0.02L, and TFN0.1-0.001L), the N 1s percentage decreases gradually from 5.58% to 4.46%, suggestive of the reduced cross-linking with the decrease of PEI concentration. The same trend of change is also noticed with the N/O ratio as PEI does not contain O. Among another set (TFN0.1-0.02L, TFN0.2-0.02L, and TFN0.3-0.02L) prepared with different coating densities of the modified CNCs while at identical PEI deposition conditions, the N/O ratio decreases from 0.14 to 0.1 with the increase in the coating density. This should result from the reduced penetration of PEI into the CNC thin film layer with the increase of coating density. On basis of all above spectroscopic results, it can be concluded that the molecular weight and concentration of PEI in the deposition solution have significant effects on the crosslinking degree of thin film coating layer, thus impacting the comprehensive performance of the fabricated TFN membranes.
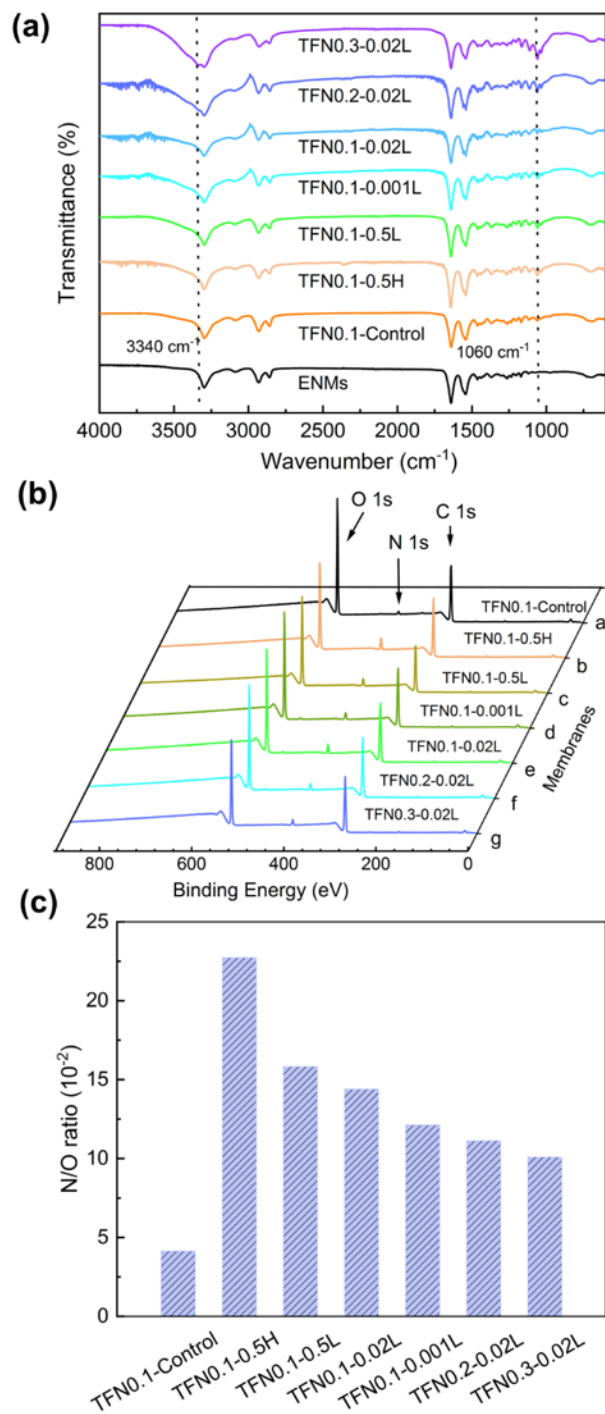
Figure 3.4 Surface chemical composition analysis of the TFN membranes: (a) ATR-FTIR spectra, (b) XPS spectra, and (c) N/O ratio from XPS spectra.

3.3.3 Membrane separation performance

The effects of membrane fabrication parameters, including the molecular weight and concentration of PEI, and the coating density of the modified CNCs, on the separation performance (PWP and dye rejection) of the resulting membranes have been systematically investigated for their optimization. As shown in Figure 3.5a, the control membrane, TFN0.1-Control, has a high PWP of 448.3 LMH bar^{-1} while with the MB rejection of only 66.31%. The high PWP and low MB rejection result from the loose non-cross-linked thin film layer without the treatment of PEI. Upon the treatment with PEI, a dramatic increase in MB rejection (99.49% and 99.83% for TFN0.1-0.5L and TFN0.1-0.5H, respectively), is observed, along with a decrease in PWP (83.7 and 53.0 LMH bar^{-1}, respectively). This demonstrates the formation of denser cross-linked thin film layers upon treatment with PEI. Compared to TFN0.1-0.5H, TFN0.1-0.5L has a 58% of increase in PWP, while with the similar dye rejection in MB filtration. This suggests that PEI with the lower molecular weight is optimum for the cross-linking between the modified CNCs, whereas the use of the high-molecular-weight PEI may cause narrowed water channels due to over cross-linking among the modified CNCs, thus compromising the PWP of TFN membranes. Figure 3.5c illustrates schematically the different cross-linking structures generated in the thin film coating layer upon the use of PEIs with low and high molecule weights. As such, the low-molecular-weight PEI has been chosen exclusively for all subsequent TFN membranes. Meanwhile, TFN membranes were prepared at varying concentrations of the PEI deposition solution within the range of $0.001 - 0.5$ g L^{-1} to evaluate its effect on the membrane performance.

As shown in Figure 3.5b, PWP of the TFN membrane decreases dramatically from 448.3 to 83.7 LMH bar^{-1} with the increasing PEI concentration from 0.001 to 0.5 g L^{-1}, while the MB rejection significantly increases from 78.77% to 99.49%. Clearly, the increasing PEI concentration leads to enhanced cross-linking in the thin film coating layer, which causes the reduced water permeation and enhanced dye rejection. In consideration of the trade-off between PWP and dye rejection, the concentration of 0.02 g L^{-1} for the low-molecular-weight PEI has been adopted as the optimized deposition condition for the fabrication of the following TFN membranes to investigate their separation abilities toward various dye/salt mixtures.
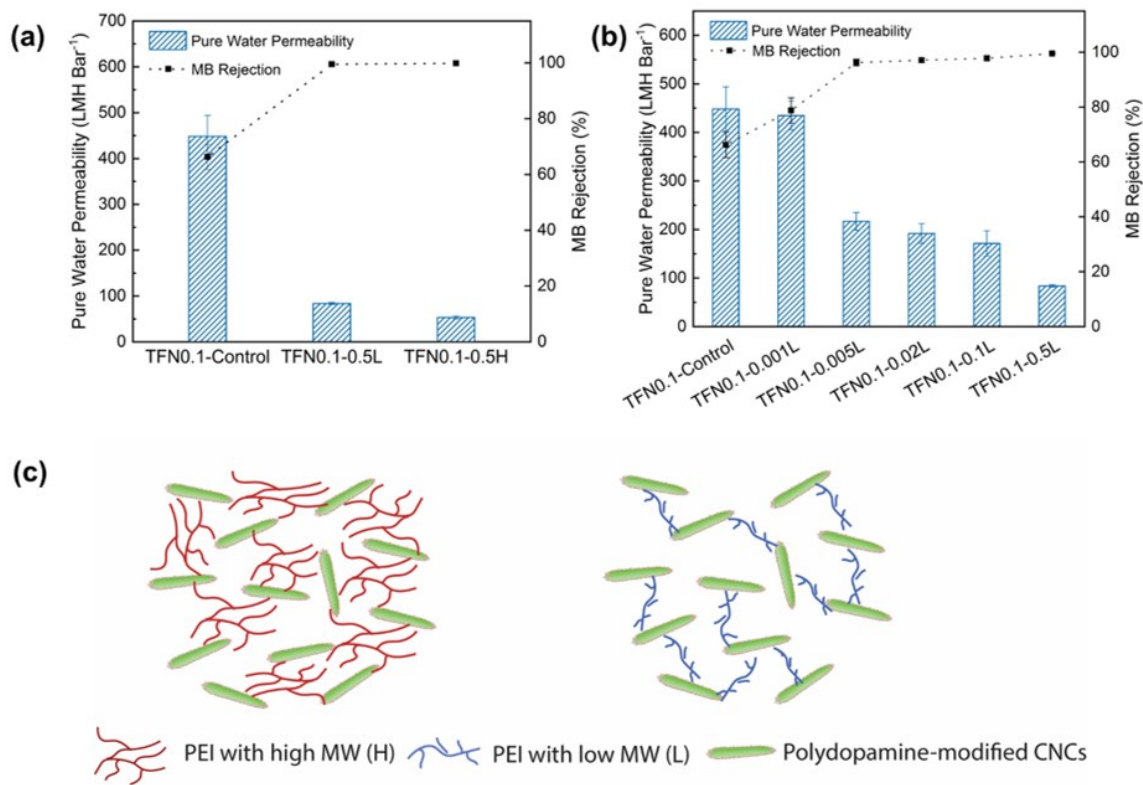
Figure 3.5 Pure water permeability and MB rejection: (a) effect of PEI molecular weight (L: 2000 g mol^{-1}; H: 25000 g mol^{-1}), (b) effect of PEI concentration in the range of 0.001 – 0.5 g L^{-1}, and (c) schematic illustration of the structures of the thin film coating layer.

Figure 3.6 shows the effect of the coating density (0.1 – 0.3 g m^{-2}) of the modified CNCs on the membrane separation performance. Generally, high PWPs (191.5 to 87.1 LMH/bar^{-1}) have been achieved with these TFN membranes owing to the use of the porous ENM substrate, which possesses numerous channels allowing water molecules to pass through. In particular, with the increase in the coating density, PWP decreases from 191.5 to 87.1 LMH bar^{-1} (Figure 3.6a). Clearly, increasing the coating density of the modified CNC active layer leads to the increased transmembrane resistance caused by the thicker and denser crosslinking networks in the active

layer. Meanwhile, as also shown in Figure 3.6a, the three membranes of different coating densities have relatively low water contact angles ($< 30°$). Confirming favorable surface hydrophilicities for membrane filtration, the low water contact angles are ascribed to the synergic effect of various hydrophilic groups, such as hydroxyl and amine groups, on the thin film layer, as well as the porous structure of ENMs. With the increase of coating density, the water contact angle increases from $21.1°$ to $28.8°$ due to the increased thickness and enhanced transmembrane resistance of the active layer, which is consistent with the decrease in PWP.
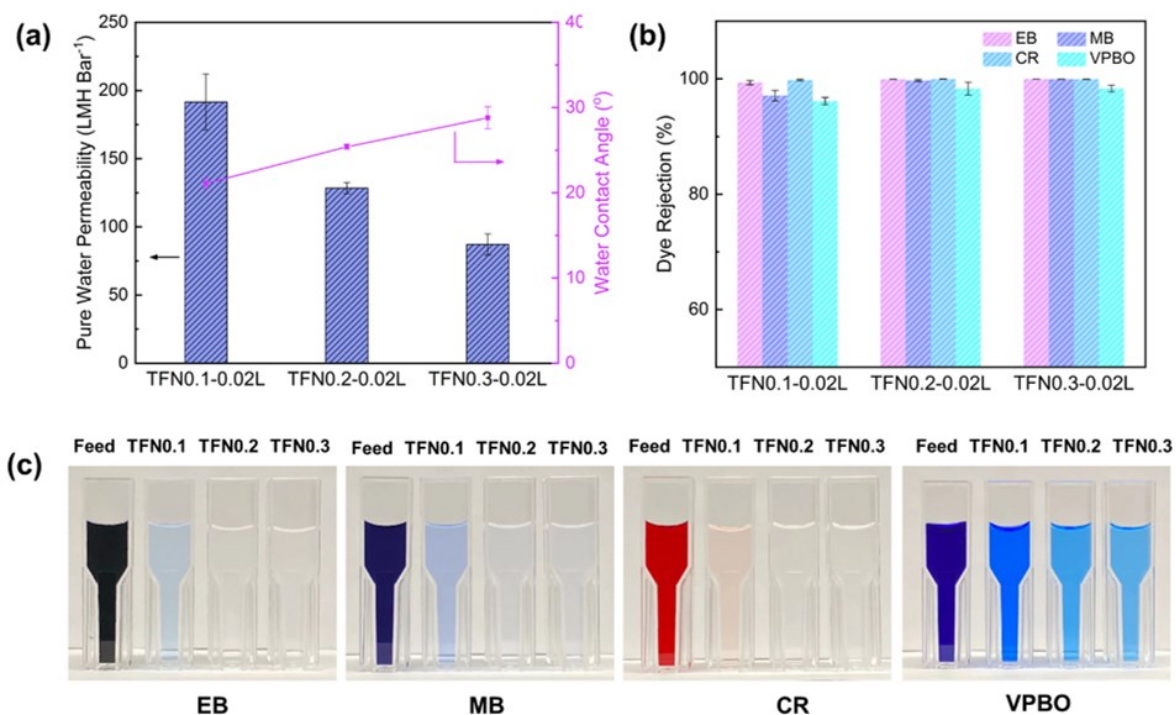
Figure 3.6 Membrane performance tests: (a) pure water permeability and water contact angle of TFN membranes with various coating densities of modified CNCs, (b) rejection of TFN membrane for four dyes (EB, MB, CR, and VPBO), and (c) digital photos of feed and permeate solutions (feed, TFN0.1-0.02L, TFN0.2-0.02L, and TFN0.3-0.02L from left to right for each dye).

The NF performance has been systematically investigated using four model dyes with different molecular sizes, E), MB, CR, and VPBO. The properties of these dyes are listed in Table 3.1. Four inorganic salts (NaCl, Na_2SO_4, $MgCl_2$, and $MgSO_4$) were used to investigate dye/salt separation ability of the TFN membranes. As shown in Figure S3.5, the dye solution permeability is slightly reduced compared to PWP due to the adsorption or deposition of dye molecules on the TFN membrane. As reported from previous researches, cross-linked coating layers constructed from PEI and polydopamine are prone to adsorb dyes via electrostatic interactions.[145,146] Meanwhile, it also decreases with the increasing coating density of the modified CNCs from 0.1 to 0.3 g m^{-2}. Figure 3.6b shows rejection characteristics of TFN0.1-0.02L, TFN0.2-0.02L, and TFN0.3-0.02L. The four model dyes can be effectively removed with all three membranes with high dye rejections (>96%). In particular, the rejection ratios with TFN0.1-0.02L for EB, MB, CR, and VPBO are 99.35%, 97.09%, 99.79%, and 96.16%, respectively, which show a general trend of increase with the increase of dye molecule size due to the size exclusion mechanism. However, the rejection characteristic of CR is the exception. The rejection ratio with TFN0.1-0.02L for CR with a moderate molecular size is the highest among four dyes. This is because CR molecules are prone to form larger aggregates in aqueous solution, therefore leading to the highest rejection ratio compared to other three dyes. The same trend is observed with TFN0.2-0.02L and TFN0.3-0.02L. With the increase of the coating density of modified CNCs from 0.1 to 0.3 g m^{-2}, the dye rejection ratio increases from 99.35% to 99.97% for EB, 97.09% to 99.93% for MB, and 99.79% to 99.96% for CR. Figure 3.6d compares the digital photos of aqueous dye solutions before and after filtration. It shows visually the increasing dye rejection ability with the increase of the modified CNCs coating density.

Inorganic salts as byproducts of the textile industry are common components in dye wastewaters. Therefore, high salt permeation is generally required in order to separate and recover dye/salt from dye wastewater. In this study, the separation of single salt component solutions and dye/salt mixture solutions has been performed to characterize the separation ability of the fabricated TFN membranes. As shown in Figure 3.7a, the permeation of four inorganic salts including monovalent (NaCl, Na_2SO_4) and bivalent salts ($MgCl_2$, $MgSO_4$) has been investigated by filtration with TFN0.2-0.02L. The permeations of both monovalent salts are higher than 99%, while the permeations of the two bivalent salts are also higher than 98%. The slightly lower permeations of

bivalent salts should result from their larger hydrated ionic radii than monovalent salts. Figure 3.7b presents the rejection performance of TFN0.2-0.02L for CR/salt mixture solutions. As we can see, the rejection ratio of CR is 99.91% for both CR/NaCl and CR/Na$_2$SO$_4$ mixture solutions, which is slightly lower compared to that for CR single-component solution (99.96%). This decrease is mainly caused by the dissolution of the dye (CR) aggregates, facilitated by the inorganic salt in aqueous solution.[147,148] Elimination of CR aggregates in aqueous solutions is conducive to the permeation of dye molecules. These performance results indicate the potential application of the fabricated TFN membranes for the separation of dye/salt wastewaters. It is worth noting that, to date, only few studies have demonstrate more than 99.9% of CR rejection in salt solutions while with maintained ultrahigh water permeability, e.g., 99.9% for ZDNMA membrane with PWP of 10.7 LMH Bar^{-1}, and 99.9% for PSF/GO membrane with PWP of 36.9 LMH Bar^{-1}.[147,149]
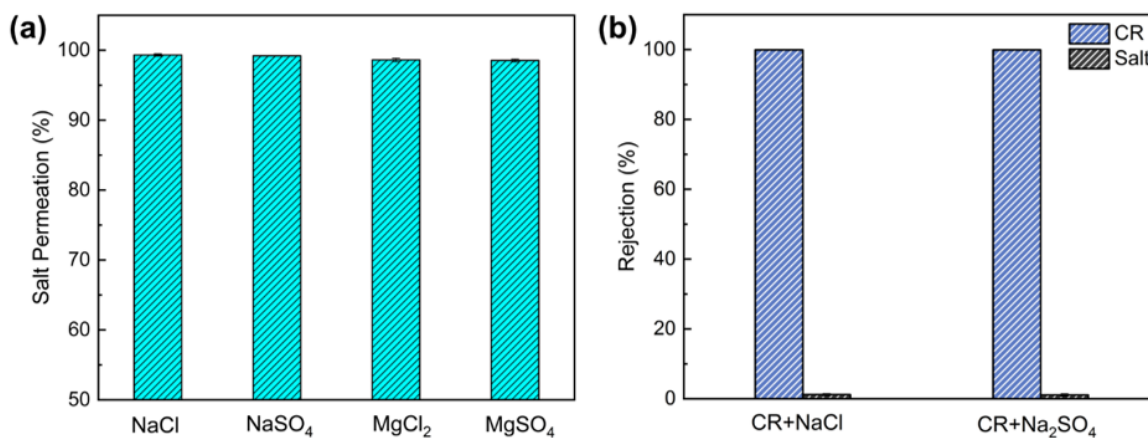
Figure 3.7 (a) Salt permeation performance of TFN0.2-0.02L membrane, (b) dye and salt rejection of CR/salt mixture solutions by TFN0.2-0.02L membrane.

3.3.4 Long-term separation stability

To investigate the long-term separation stability, the optimized membrane TFN0.2-0.02L has been employed for a long-term filtration of a CR (200 ppm) and NaCl (1000 ppm) mixture solution.

The permeability and rejection of solutes were recorded during the 40 h operation. As shown in Figure 3.8, the filtration permeability slightly declines from around 97 to 80 LMH bar^{-1} within first 2 h of operation and then maintains stable until the end of the filtration. The initial decline of the permeability is mainly ascribed to the accumulation of CR molecules on the membrane surface and the concentration polarization effect enhanced by the subsequent formation of the dye cake-layer.[53] However, a high level CR rejection (around 99%) is maintained throughout without distinct decline, while allowing more than 98% salt molecules passing through even after 40 h of filtration. This test confirms the long-term stability of the membrane for the separation of dye molecules and salts.
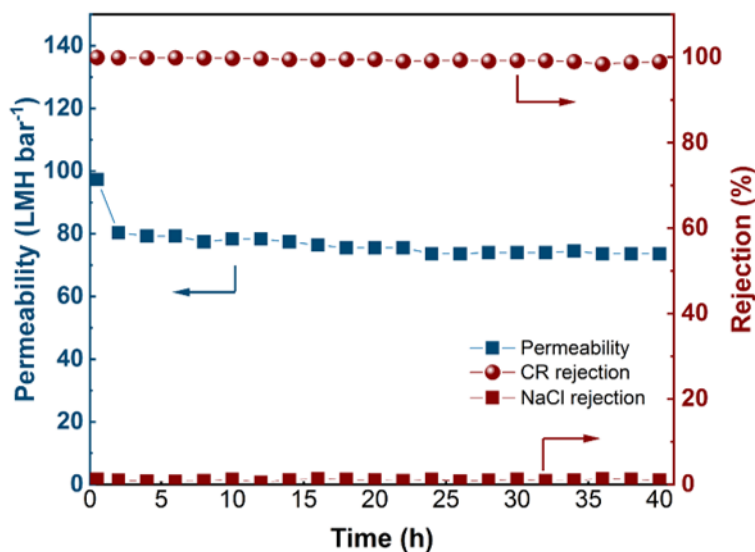
Figure 3.8 Long-term stability for dye and salt separation performance of the optimized membrane TFN0.2-0.02L. The feed solution was the mixture of CR and NaCl aqueous solution (CR concentration: 200 ppm, NaCl concentration: 1000 ppm, operation time: 40 h).

To highlight the outstanding performance of the TFN membrane in this study, a comparison of the fabricated TFN membrane is made with various NF membranes reported in the literature in terms of PWP, CR rejection, as well as selectivity of dye/salt mixture. As shown in Figure 3.9a and Table

S3.2, most of the membranes reported in the literature show relatively low PWPs, while TFN0.2-0.02L as our optimum membrane renders an ultrahigh PWP of 128.4 LMH bar^{-1} in combination of a CR rejection of 99.91%. The reported studies in Figure 3.9 show that achieving high PWP, high dye rejection, and high selectivity of dye/salt mixture simultaneously is still challenging because of the trade-off relationship between permeability and selectivity. For instance, one reported membrane (E-MSTF (+) AAO) showed a PWP of >300 LMH bar^{-1} with a compromised CR rejection, which is only 97.7%.[52] Furthermore, Figure 3.9b shows a comparison of selectivity factor among the membranes. The outstanding selectivity factor (1098 for CR/NaCl) achieved in this study is distinctly higher than those of reported membranes, demonstrating its superior potential for the separation of dye/salt mixtures. Therefore, with its ultrahigh PWP, superior dye rejection (more that 99.9% for CR in NaCl solution), outstanding selectivity for dye/salt mixture, as well as operational stability, we expect that the TFN membranes designed herein has a broad application scope, not only for the separation of dye/salt mixtures, but also for the removal of small molecules from wastewaters and purification in pharmaceutical industries.
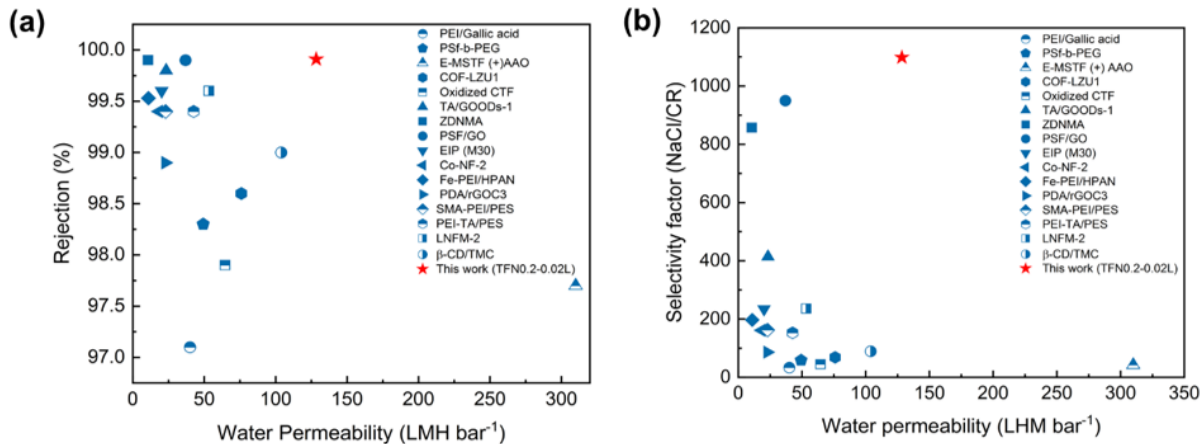
Figure 3.9 Performance comparison of TFN membranes in this work and other membranes (a) CR rejection versus permeability, (b) selectivity factor of NaCl/CR versus permeability.

3.4 Conclusions

We demonstrate in this work a new strategy for the fabrication of novel high-performance loose TFN membranes for the separation of dye/salt from textile wastewaters. In the strategy, polydopamine-modified CNCs with substantial quinonoid active sites have been prepared through oxidative auto-polymerization of dopamine, which enable the subsequent construction of controllable crosslinking networks. TFN membranes are fabricated with the modified CNCs as the active layer via facile vacuum filtration on ENMs followed by further cross-linking with PEI. The ideal linearity between the thickness and coating density demonstrates the feasibility for the tailored fabrication of the active layer. A systematic study on the effects of coating density of the modified CNCs, and the molecular weight and concentration of PEI cross-linker on the membrane performance has been undertaken. The optimum membrane, TFN0.2-0.02L, shows an ultrahigh PWP of 128.4 LMH bar^{-1}, a superior CR rejection of 99.91%, and a remarkable salt permeation of 99.33%. Moreover, an unprecedented salt/dye selectivity of 1098 is achieved on a CR/NaCl mixture, demonstrating its great potential for the effective separation of dye/salt mixtures and recovery of these valuable components. With their outstanding performance, these membranes have strong potential for other separation/purifications applications.

Chapter 4 Rapid covalent co-deposition of dopamine and diamine-zwitterion for nanofiltration membranes

The chapter is adapted from a paper submitted to *Journal of Water Process Engineering*, entitled as "High performance nanofiltration membranes with enhanced fouling-resistance by rapid covalent co-deposition of dopamine and diamine-zwitterion" by **Yang, L.**; Zhang, X.; Rahmatinejad, J.; Raisi, B.; Ye, Z., which is being revised following peer review.

Abstract

NF membranes have been extensively employed for the treatment of textile wastewater to produce clean water, due to their capability of retaining small organic molecules. In this study, zwitterionic nanofiltration (Z-NF) membranes have been successfully fabricated by the rapid co-deposition of dopamine and Z-DNMA via covalent bonds. The fabricated Z-NF membranes show improved hydrophilicity and enhanced fouling-resistant ability due to the incorporation of the zwitterionic functionality. Following the systematic investigation on the ratio between dopamine and Z-DNMA as well as the co-deposition time, the identified optimum membrane (Z-NF3) exhibits a high PWP of 32.0 LMH bar^{-1} and high organic dye rejections of 99.7% and 98.6% for CR and MB, respectively. In addition, the fouling experiments of Z-NF3 show that the flux recovery ratios (FRRs) for the filtration of bovine serum albumin (BSA), sodium alginate (NaAlg), and CR are 99.1%, 92.0%, and 82.2%, respectively, along with lower irreversible fouling ratios (R_{ir}) and higher reversible fouling ratios (R_r) values compared to those of the control membrane. The high PWP and high rejections to organic dyes, coupled with its superior fouling-resistant performance, indicate its great potential for practical applications in the treatment of textile wastewater.

4.1 Introduction

Water scarcity, exacerbated by climate change and anthropogenic pollution, is threating the ecological system, human health, and sustainable development of human society.[150,151] Especially, the pollution caused by the organic dyes from textile industries is becoming increasingly severe.[152] Therefore, the highly efficient and effective technologies for the production of clean water are intensively required. The conventional methods, including adsorption, flocculation, and

coagulation, have been widely used for wastewater treatment.[153-156] However, these methods generally require additional reagents and exhibit low sensitivity with extensive energy consumption. Apart from them, membrane separation technologies, as emerging alternative approaches, have attracted tremendous attention for the pretreatment of wastewater, desalination of seawater, and production of potable water due to their versatile properties, including low energy consumption, high separation efficiency and selectivity, easy scale-up, and no phase transfer.[157]

NF membranes, as one of the pressure-driven separation technologies, are capable of retaining small organic molecules, showing great merits in the treatment of wastewater from textile industry.[158] The state-of-the-art nanofiltration membranes are TFC membranes fabricated through the classical interfacial polymerization. However, the current TFC membranes often suffer from relatively low permeability and fouling propensity, which mainly result from the dense thin film selective layer and its inherently hydrophobic property, respectively. Over the development of the past decades, significant progress has been achieved towards enhancing the membrane permeability, selectivity and fouling-resistant ability. Among them, incorporating nanomaterials within the thin film selective layer is one of the most attractive strategies for NF membrane fabrication. To date, numerous nanomaterials have been developed to enhance NF membrane performance, including carbon-based nanomaterials (GO/reduced graphene oxide and CNTs), plant-based nanomaterials (CNCs and CNFs), and other types of nanomaterials (MXene nanosheets, covalent organic frameworks, and metal organic frameworks). These nanomaterials can be incorporated into thin film layer during the interfacial polymerization,[8] or pre-loading on the supporting layer before the interfacial polymerization as an interlayer to form a sandwich structure,[159,160] or coating on the porous supporting membrane directly to fabricate NF membranes.[100,161] Despite the progress, the limited permeability and compromised selectivity are still the restricting factors for the membranes by these strategies for practical applications due to the incompatibility between the nanomaterials and polymer matrices. To tackle this, an improved alternative strategy is to construct the thin film selective layer by employing the unique mussel-inspired chemistry. In this regard, tremendous achievements have been made since its first report on membrane surface modification with this unique strategy in 2007.[92]

Dopamine, as the most representative building block in the mussel-inspired chemistry, has been extensively employed for the fabrication of NF membranes by surface modification.[162] Based on

the previous researches, the functionality of mussel-inspired chemistry is ascribed to the abundant 3,4-dihydroxy-*L*-phenylalanine in mussel foot proteins, which involves covalent polymerization and non-covalent self-assembly under mild oxidative conditions.[92,124,163] In addition to the essential catechol structure for mussel-inspired chemistry, amine groups are also vital to facilitate the formation of covalent polymerization via Michael addition reaction and Schiff base reaction.[164] The increased proportion of covalent bonds in the coating layer can enhance the stability and hydrophilicity simultaneously, which are conducive to the membrane performance. On the basis of this understanding, numerous derivatives with a similar catechol structure from dopamine and their co-deposition with other amine-abundant polymers have been proposed for the fabrication of NF membranes, including catechol, tannic acid, gallic acid, and epigallocatechin gallate.[88,134,165-167] However, the time-consuming polymerization process and the limited hydrophilicity of coating layer still impede their applications in the fabrication of membranes. Tackling these challenges, different strategies have been developed to accelerate the oxidation and polymerization speed, including the use of copper sulfate/hydrogen peroxide, potassium persulfate, and UV irradiation.[136,168-171] In addition to improving the polymerization efficiency, co-depositions of dopamine with other zwitterions via non-covalent assembly have been reported to improve the hydrophilicity of coating layer.[172] However, the non-covalent assembly process of dopamine and zwitterions can not only decrease the polymerization efficiency but also the coating layer stability. Recently, a few studies on the covalent grafting of zwitterions with polydopamine for the surface modification of ultrafiltration membranes have been reported to improve fouling-resistant ability.[173,174] However, this has not yet been attempted thus far for NF membranes.

On the basis of the earlier studies, we hypothesize that the co-deposition of dopamine with zwitterions via covalent polymerization is also a promising strategy for the fabrication of NF membranes of improved performance. Herein, we propose a rapid bio-inspired strategy to construct a thin film selective layer by the co-deposition of a diamine-zwitterionic monomer (Z-DNMA) with dopamine via covalent bonds. Z-DNMA is conveniently synthesized by the protection of amine group from DNMA and the ring open reaction of tertiary amine group in DNMA with 1,3-PS, followed by the de-protection of amine group.[3] The two primary amine groups from Z-DNMA are able to form covalent bonds with polydopamine via Michael addition reaction and Schiff base reaction during the rapid co-deposition of $CuSO_4/H_2O_2$-triggered polymerization. The fabricated NF membranes with the incorporated zwitterionic structure from

Z-DNMA show enhanced surface hydrophilicity. An optimization of the co-deposition parameters has been undertaken to obtain the optimum NF membrane with superior fouling-resistant performance towards both typical hydrophobic contaminants (e.g., proteins) and organic molecules (e.g., organic dyes). The promising results obtained in this study, including PWP, dye rejection, and fouling-resistant performance, indicate its potential application in the treatment of wastewater from textile industries.

4.2 Experimental
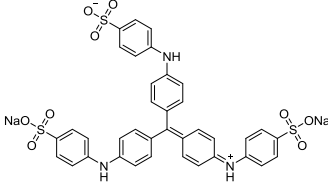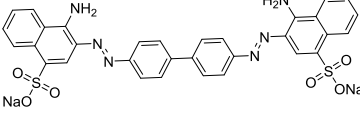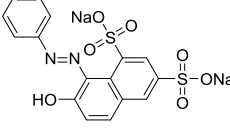
4.2.1 Materials

Commercial PES ultrafiltration membranes (molecular weight cut-off: 20 kDa) was supplied by Synder Filtration (Vacaville, USA). DNMA (96.0%), di-ter-butyl dicarbonate ((Boc)$_2$O, ≥98.0%), dopamine hydrochloride, Tris, copper sulfate (CuSO$_4$, ≥98.0%), BSA (68 kDa), NaAlg, acetonitrile, MB, CR, and orange G (OG) were obtained from Aldrich (Oakville, ON, Canada). Properties of all organic dyes are listed on Table 4.1.Hydrogen peroxide (H$_2$O$_2$, 30%), 1,3-PS, HCl (36.5%), dichloromethane (DCM), chloroform, and sodium hydroxide (99.0%) were provided by Thermo Fisher Scientific (St. Laurent, QC, Canada). DI water was prepared using a Milli-Q purification system (Millipore, Billerica, MA, USA). All the chemicals were used as received.

4.2.2 Synthesis of Z-DNMA

As shown in Figure 4.1a, Z-DNMA was synthesized according to a previously reported study with some modifications [3]. In brief, DNMA (20 mmol, 2.9 g) was firstly dissolved in DCM (40 mL), followed by the addition of (Boc)$_2$O (44 mmol, 9.6 g) in DCM (40 mL). The mixture was extracted with DI water after 12 h of stirring at room temperature. DNMA-Boc was obtained as a white solid after evaporating DCM. Subsequently, 1,3-propane sultone (7.0 mmol, 0.85 g) in chloroform (10 mL) was added dropwise into the solution of DNMA-Boc (5.8 mmol, 2.0 g) in chloroform (10 mL). The mixture was stirred at 40 ºC for 8 h. After that, the mixture was washed with DI water, followed by evaporation of chloroform to obtain Z-DNMA-Boc. The final compound Z-DNMA was obtained by the de-protection of Z-DNMA-Boc in HCl aqueous solution (4.0 M) at room temperature. The mixture was washed with acetonitrile to remove impurities, followed by the freeze drying to obtain the final solid Z-DNMA.

Table 4.1 Organic dyes used in this study.

Dyes	Chemical structure	Molecular weight (g mol^{-1})	λ_{max}^{a} (nm)
Methyl Blue (MB)		799.8	592
Congo Red (CR)		696.7	500
Orange G (OG)		452.4	475

^{a} Maximum absorption wavelength.
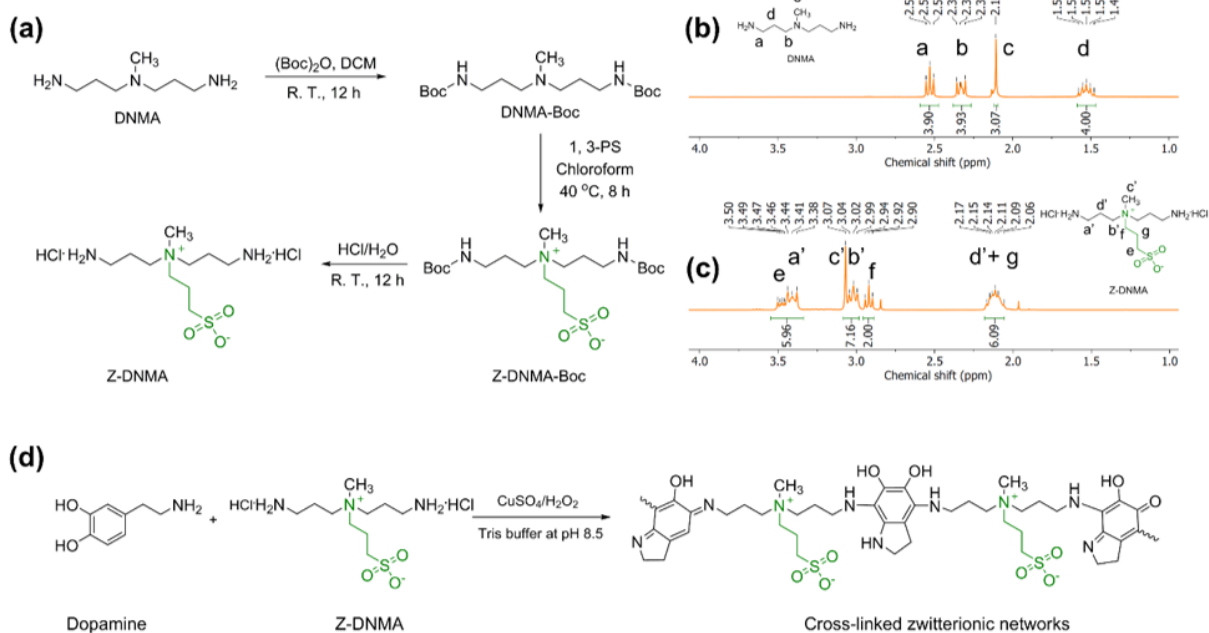
Figure 4.1 (a) Synthesis process of Z-DNMA; (b) [^1]H NMR spectrum of DNMA; (c) [^1]H NMR spectrum of Z-DNMA; (d) proposed co-deposition mechanism of dopamine and Z-DNMA for the construction of cross-linked zwitterionic networks.

4.2.3 Membrane fabrication

Z-NF membranes were fabricated by a rapid co-deposition of dopamine and Z-DNMA or DNMA via $CuSO_4/H_2O_2$-trigged oxidation. Firstly, a PES ultrafiltration membrane was immersed in DI water for at least 24 h in order to get the membrane surface completely wetted. Then, the wetted membrane was fixed into the lab-designed framework, which only allows the top surface of PES ultrafiltration membrane to contact with the following co-deposition solution of dopamine and diamine monomers (DNMA or Z-DNMA). The co-deposition solution was prepared by adding dopamine (2.0 mg mL^{-1}) into a Tris-HCl buffer solution (50 mM, pH = 8.5), followed by the addition of a different amount of Z-DNMA or DNMA. Considering that the prepared diamine

zwitterion (Z-DNMA) is a hydrochloride (shown in Figure 4.1a), the dissociated HCl may cause a pH deviation of Tris-HCl buffer solution. Therefore, a proper tuning of pH to 8.5 was performed by adding a diluted HCl (0.5 M) or NaOH (0.5 M) aqueous solution. Afterwards, $CuSO_4$ (5 mM) and H_2O_2 (19.6 mM) were added into the co-deposition solution sequentially [136]. The final solution was poured into the framework with a PES ultrafiltration membrane and shaken on a shaker under a constant shaking rate of 40 rpm for 1 h if there is no addition illustration. All solutions were freshly prepared for the co-deposition. The Z-NF membranes fabricated with Z-DNMA at the Z-DNMA/dopamine molar ratios of 0.2/1, 0.5/1, and 1/1 were denoted as Z-NF1, Z-NF2, and Z-NF3, respectively, while membranes fabricated from the pristine DNMA were donated as NF#. In addition, the membrane fabricated with dopamine (2.0 mg mL^{-1}) with no diamine monomers was denoted as NF0.

4.2.4 Characterization

The chemical structures of DNMA and Z-DNMA were characterized with ^{1}H nuclear magnetic resonance (^{1}H NMR, Bruker 300 MHz). Water contact angle (WCA) measurements were performed on a contact angle system (VCA, AST Products, Inc.). XPS was performed on a Thermo Scientific Theta Probe XPS spectrometer with a monochromatic Al Kα X-ray source at a spot area of 400 μm. Membrane surface morphologies were observed via a FE-ESEM after platinum coating (ca. 4 nm). The surface roughness of the NF membranes was investigated with an AFM (Tosca 400, Anton Paar) in the tapping mode.

4.2.5 Membrane separation performance

All membrane separation performance tests were conducted at 6.0 bar using a stirred dead-end filtration cell at a stirring speed 350 rpm. The effective area of membrane filtration was 12.56 cm^2. The NF membranes were compacted at 7.0 bar with DI water for around half an hour to reach a steady state before each testing. In this study, a series of dye solutions at a concentration of 100 ppm was employed as feed solutions if there was no additional illustration.

The NF membrane pure water permeability (P, LMH bar^{-1}) is calculated by using the following equation:

$$P = \frac{V}{A \times t \times \Delta P} \tag{4.1}$$

where V is the volume (L) of the permeate, A is the effective filtration area (m^2), t is the operation time (h) and ΔP is the trans-membrane pressure (bar). The solute rejection (R) is calculated according to:

$$R = \left(1 - \frac{C_p}{C_f}\right) \times 100\% \tag{4.2}$$

where C_p and C_f are solute concentrations of the permeate and feed dye solutions, respectively. Dye concentration was determined with a UV-vis spectrophotometer (Agilent Cary 8454).

4.2.6 Fouling-resistant performance

The fouling-resistance performance tests were carried out at 6.0 bar with three cycles of filtration with different model foulants, which were BSA (1.0 g L^{-1} in PBS buffer solution at pH 7.4), NaAlg (1.0 g L^{-1}), and CR (100 ppm), respectively. Firstly, PWP was recorded as the original permeability (J_0) for 0.5 h. Then, DI water was replaced with a corresponding model foulant. The filtration permeability (J_1) was recorded every 5.0 min for 1.0 h. The normalized flux (J_1/J_0) was employed to quantify the fouling-resistant ability during the filtration process. After 1.0 h of filtration, the fouled membrane was cleaned by hydraulic wash with DI water for 2.0 h, followed by the measurement of PWP again (J_2). This whole process was repeated three times. FRR, R_r, and R_{ir} are calculated according to the following equations:

$$FRR = \left(\frac{J_2}{J_0}\right) \times 100\% \tag{4.3}$$

$$R_r = \frac{J_2 - J_1}{J_0} \times 100\% \tag{4.4}$$

$$R_{ir} = \frac{J_0 - J_2}{J_0} \times 100\% \tag{4.5}$$

4.3 Results and discussion

4.3.1 Synthesis and characterization of Z-DNMA

The diamine zwitterion, Z-DNMA, is synthesized herein according to a previously reported study with some modifications.[175] As shown in Figure 4.1a, the two primary amine groups in DNMA are firstly protected with Boc (butyloxycarbonyl) to obtain DNMA-Boc to prevent from the reaction of these primary amine groups with 1,3-propane sultone in the next step. Then, the Boc-protected zwitterionic structure (Z-DNMA-Boc) is formed by the ring open reaction of DNMA-Boc and 1,3-PS. The subsequent de-protection of Z-DNMA-Boc under HCl aqueous solution renders Z-DNMA in the hydrochloride form. The chemical structures of DNMA and the synthesized Z-DNMA have been characterized with ^{1}H NMR spectroscopy. Figure 4.1b shows the ^{1}H NMR spectrum of DNMA, where the singlet peak c at 2.11 ppm (s, 3 H) is ascribed to the methyl group next to the tertiary amine group. The triplet peaks a and b at 2.53 ppm (t, 4 H) and 2.34 ppm (t, 4 H), and multiplet peak d at 1.53 ppm (m, 4H) are attributed to the methylene group next to the tertiary amine group, the methylene group next to the primary amine group, and the middle methylene group, respectively. Figure S4.1 shows the ^{1}H NMR spectrum of DNMA-Boc. Therein, the singlet peak at 1.37 ppm (s, 18 H) is ascribed to methyl groups on tert-butyloxycarbonyl (Boc), indicating the successful protection of the primary amine group. As shown in Figure 4.1c, after the introduction of zwitterionic moiety into DNMA, one can see that all the ^{1}H NMR peaks seen in DNMA shift to the relatively lower fields (higher chemical shifts) in the spectrum of Z-DNMA due to the formation of the quaternary ammonium group in Z-DNMA. In addition, the new peaks at 3.47 ppm, 2.92 ppm, and 2.11 ppm (integrated with peak d') are ascribed to the three methylene groups in the 1,3-propane sultone moiety. Therefore, these ^{1}H NMR results demonstrate the successful synthesis of Z-DNMA.

4.3.2 Fabrication and characterization of NF membranes

NF membranes have been fabricated by a rapid co-deposition of dopamine with Z-DNMA or DNMA via $CuSO_4/H_2O_2$-trigged oxidation, which can accelerate the polymerization rate and reduce the coating time.[136] Figure 4.2 shows the WCA of the fabricated membranes. One can see that the pristine PES membrane has a relatively high WCA value of around 80°, due to the inherent hydrophobicity of PES. After the deposition of polydopamine or co-deposition of polydopamine

with diamine monomers (DNMA and Z-DNMA), WCA decreases dramatically to less than 55°. Among the membranes other than PES, NF0 has a relatively high WCA (49.6°) value due to the limited hydrophilicity of polydopamine. With the co-deposition of dopamine and DNMA at a mole ratio of 1:1, NF3 shows a slightly higher WCA (53.1°) compared to NF0 (49.6°). However, Z-NF3 prepared at the same mass ratio but with Z-DNMA (Z-DNMA/dopamine = 1:1) shows a much lower WCA (30.0°). Meanwhile, prepared at the reduced Z-DNMA/dopamine mole ratio of 1:0.5, Z-NF2 shows an increased WCA of 42.8° compared to Z-NF3. These results indicate the successful formation of the coating layer and the enhanced hydrophilicity after the co-deposition with Z-DNMA.
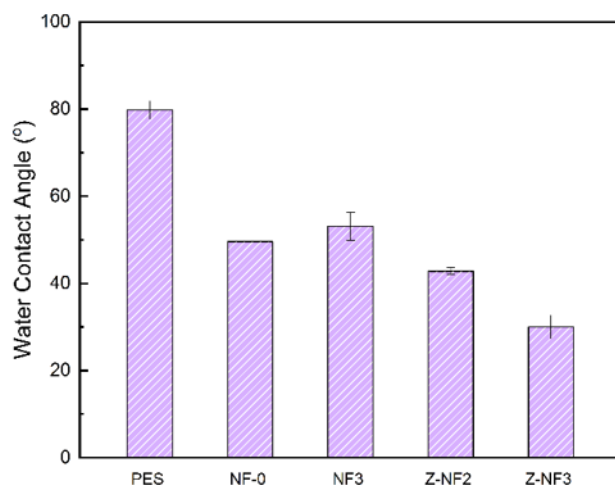
Figure 4.2 Water contact angles of different membranes.

Surface elemental compositions of NF membranes have been characterized with XPS. As shown in Figure 4.3, all three membranes (NF0, NF3, and Z-NF3) show the characteristic peak of N 1s, originating from dopamine and diamine monomers, and the peak of Cu 2p, due to the trace amount of Cu^{2+} residual on the membrane surface by the chelation with the amine group from dopamine.[169] In addition, one can observe that all three membranes show the peak of S 2p resulting from the PES substrate. The pristine PES membrane has a sulfur content of around 5%.[123] As shown in Table 4.2, NF0 shows a decreased sulfur content of 3.4% after the sole coating of dopamine,

indicating the formation of polydopamine layer on the PES surface. Compared to NF0, Z-NF3 shows an increased sulfur content of 4.2% due to the co-deposition of dopamine and sulfur-containing Z-DNMA. Furthermore, as shown in Table 4.2, the increased N/C ratios of NF3 and Z-NF3 also indicate the successful incorporation of both diamine monomers (DNMA and Z-DNMA).
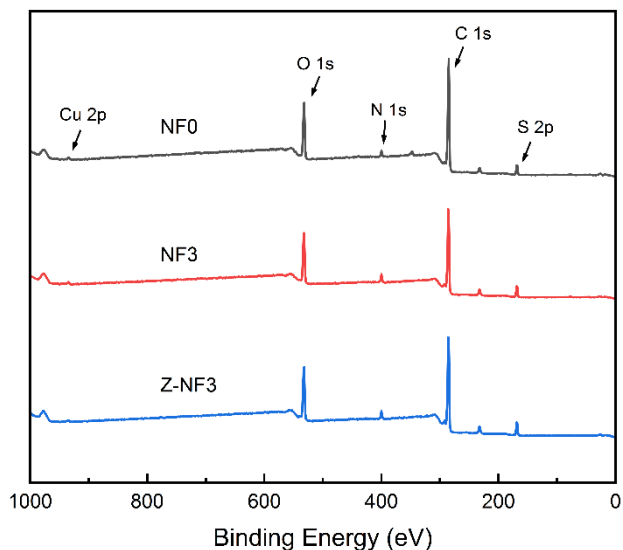
Figure 4.3 XPS spectra of NF0, NF3, and Z-NF3.

Table 4.2 Elemental compositions of membrane surfaces.

Membrane	Composition (%)					N/C (%)
	C	O	N	S	Cu	
NF0	75.2	17.9	3.1	3.4	0.3	4.1
NF3	71.4	19.9	4.3	4.2	0.3	6.0
Z-NF3	73.0	18.6	3.6	4.7	0.2	4.9

The surface morphologies of the pristine PES ultrafiltration membrane and the fabricated membranes have been characterized with SEM and AFM. As shown in Figure 4.4a, the SEM image of pristine PES membrane shows a relatively smooth surface. Compared to the PES membrane,

61

one can observe the obvious grainy surfaces after the deposition of dopamine and diamine monomers, due to the formation of polydopamine aggregates (Figure 4.4b-e). In addition, NF3 and Z-NF3 (Figure 4.4c,e) show increased quantities of polydopamine aggregates than NF0 (Figure 4.4b), which is mainly ascribed to the addition of diamine monomers since extra amine functional groups can facilitate the polymerization of dopamine by the formation of covalent bonds.[164] As shown in Figure 4.4e, Z-NF3 fabricated from the co-deposition solution with a highest diamine monomer content, exhibits the coarsest surface among all membranes, which further indicates the significance of diamine monomers for the formation of dopamine coating layer. The AFM images from Figure 4.4a'-e' show that the pristine PES has the lowest surface roughness (Ra = 6.6 nm). Among all membranes, NF0 possesses the highest surface roughness with Ra of 16.7 nm, while other modified membranes have relatively lower surface roughness. This is mainly ascribed to the addition of amine monomers and the formation of covalent bonds.[163]
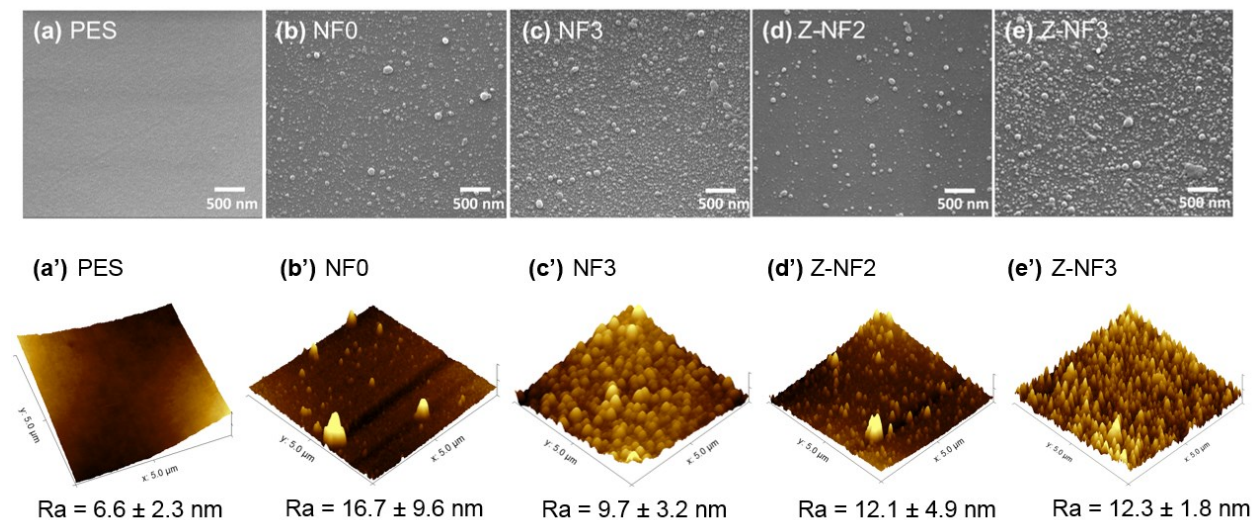
Figure 4.4 SEM images for surface morphology of membranes (a) PES; (b) NF0; (c) NF3; (d) Z-NF2; (e) Z-NF3; AFM images of the corresponding membranes (a') PES; (b') NF0; (c') NF3; (d') Z-NF2; (e') Z-NF3.

4.3.3 Separation performance of NF membranes

The separation performance of the fabricated NF membranes, including PWP and the filtration performance of BSA aqueous solution, has been systematically investigated. As shown in Figure 4.5a, the pristine PES ultrafiltration membrane shows the highest PWP (54.4 LMH bar^{-1}). After the deposition of dopamine, NF0 shows a decreased PWP of 47.8 LMH bar^{-1}, due to the formation of polydopamine coating layer on the PES membrane. Compared to NF0 with a single component polydopamine coating, NF membranes fabricated with the co-deposition of dopamine and Z-DNMA also show decreased PWPs, which are mainly caused by the formation of crosslinked zwitterionic networks via covalent bonding as shown in Figure 4.1d. Specifically, PWP decreases from 42.9 LMH bar^{-1} for Z-NF1 to 32.0 LMH bar^{-1} for Z-NF3 with the increase of Z-DNMA concentration, indicating the formation of the denser coating layer. In addition, compared to NF3, Z-NF3 prepared at the identical diamine monomer concentration, shows a relatively higher PWP (32.0 LMH bar^{-1}) due to the enhanced hydrophilicity, which is consistent with the WCA results shown in Figure 4.3.

Figure 4.5b shows the BSA filtration performance of NF membranes, including the normalized permeability for 0.5 h filtration and flux recovery ratio (FRR) after a hydraulic washing with DI water for around 2h. It shows that the PES membrane has the lowest normalized permeability and FRR (64.4%) among all NF membranes due to the inherent hydrophobicity of PES. After the polydopamine coating, NF0 exhibits a slightly enhanced FRR of 67.1%. Despite that the polydopamine coating helps improve the fouling-resistant ability to some extent, the limited hydrophilicity still restricts its further application in the modification of membrane surface. With the incorporation of Z-DNMA, on can observe that the normalized permeability increases dramatically from around 50% to more than 70%, while FRR increases significantly from around 70% to more than 95%. In addition, with the increase of Z-DNMA concentration, the normalized permeability and FRR increase gradually from 72.4% to 75.2%, and 87.5% to 97.7%, respectively. Furthermore, NF3 fabricated from DNMA shows the lower normalized permeability and FRR compared to Z-NF3 (69.7% vs 75.2%; 85.5% vs 97.7%, respectively), indicating the enhanced fouling-resistant ability with the incorporation of Z-DNMA.

In addition to the impact of diamine monomer concentration, the effect of the co-deposition time on the membrane performance has also been conducted under the Z-DNMA/dopamine molar ratio

of 1/1, which was used for the fabrication of Z-NF3. As shown in Figure 4.5c, with the coating time reduced from 60 min to 30 min, PWP increases from 32.0 LMH bar^{-1} to 42.5 LMH bar^{-1}. However, the normalized permeability and FRR decrease from 75.2% to 61.7% and 97.7% to 79.2%, respectively. Therefore, on the basis of the above filtration performance for all NF membranes, it can be concluded that the covalent incorporation of Z-DNMA into polydopamine coating endows the NF membranes with increased PWP and enhanced fouling-resistant ability. In consequence, Z-NF3 has been chosen as the optimum membrane for the following experiments given its high PWP and superior fouling-resistant ability.
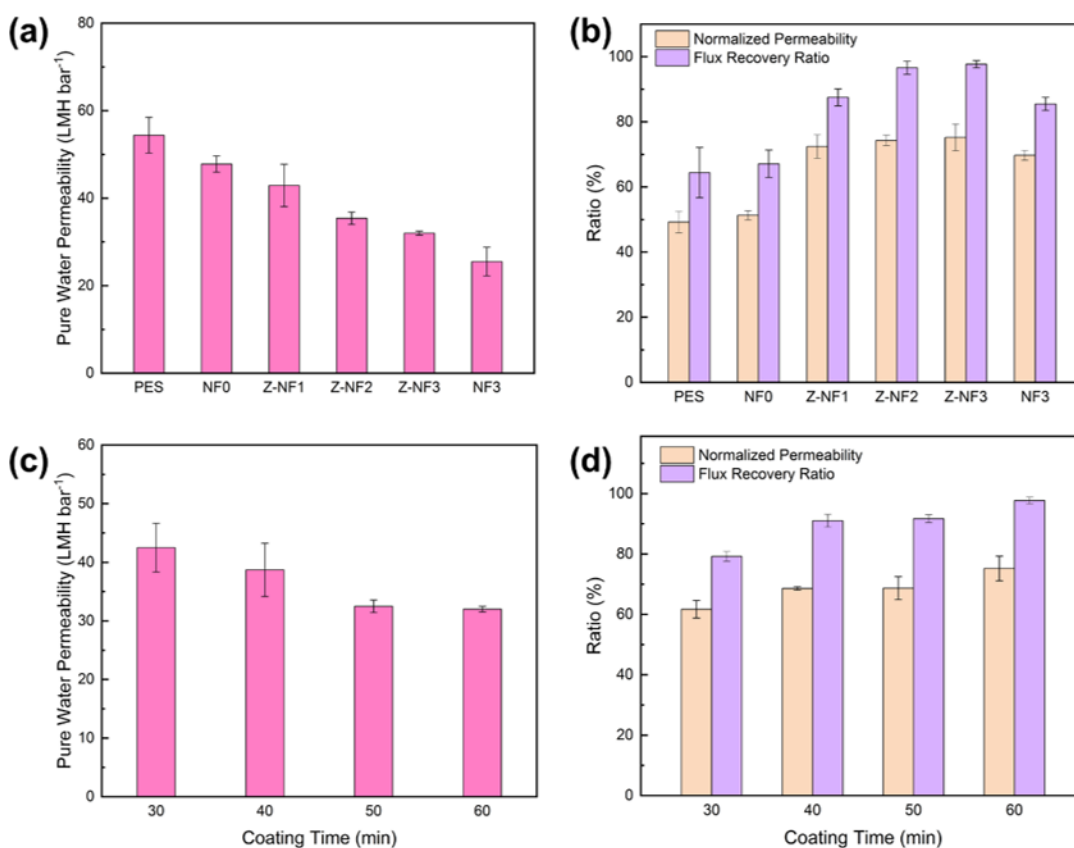
Figure 4.5 (a) Pure water permeability of NF membranes; (b) normalized permeability and flux recovery ratio of NF membranes for BSA filtration (1.0 g L^{-1}); (c) pure water permeability of NF membranes with different coating times (at the same Z-DNMA/dopamine mole ratio of 1/1); (d) normalized permeability and flux recovery ratio of NF membranes in (c) for BSA filtration (1.0 g L^{-1}).

To further investigate the filtration performance of the optimum membrane (Z-NF3), three organic dyes (CR, MB, and OG) with different molecular sizes have been chosen as the model contaminants. The detailed information of these three dyes is presented in Table 4.1. As shown in Figure 4.6a, NF3 and Z-NF3 exhibit similar rejections to all three dyes. With CR and MB, high dye rejections of more than 99% and 98%, respectively, have been achieved. However, with OG, the dye rejection decreases to around 65% for both NF membranes, due to the smaller molecular size of OG compared to CR and MB.[176] Figure 4.6b shows that the normalized permeabilities of Z-NF3 towards all three dyes are appreciably higher than the corresponding ones of NF3. Similarly, as shown in Figure 4.6c, Z-NF3 also exhibits enhanced FRRs compared to the corresponding ones of NF3. Especially, the FRR for CR is dramatically improved from 59.0% for NF3 to 80.8% for Z-NF3, due to the formation of the hydration layer with the enhanced membrane surface hydrophilicity.[80,177] All above results indicate the great potential of Z-DNMA in the construction of fouling-resistant membrane surface for the removal of organic dyes.
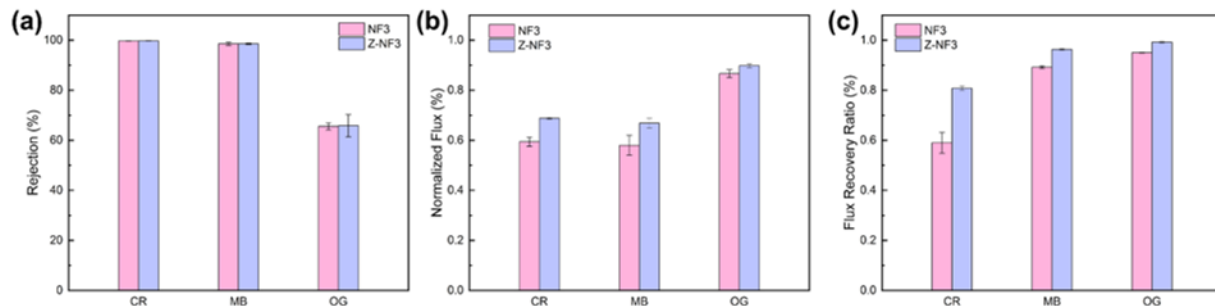
Figure 4.6 Dye filtration (CR, MB, and OG) performance of NF3 and Z-NF3 under 6.0 bar: (a) dye rejection; (b) normalized flux; (c) flux recovery ratio.

4.3.4 Fouling-resistant performance

A comparison of the fouling-resistant performance between Z-NF3 and NF3 has been undertaken by undertaking three cycles of filtration of CR (100 ppm), BSA (1.0 g L^{-1}), and NaAlg (1.0 g L^{-1}) to further verify the superior performance of Z-NF3. As shown in Figure 4.7a, both membranes

show an obvious permeability decrease in the first cycle due to the concentration polarization and deposition of CR molecules on the membrane surface. Then, it is followed by a relatively slower decrease in subsequent cycles, which is mainly ascribed to the deposition of CR molecules on the membrane surface.[175,178] After the hydraulic washing with DI water for 2 h, the FRRs are 52.5% and 82.2% for NF3 and Z-NF3, respectively, for the first cycle (Figure 4.7b). For the following two cycles, FRR of Z-NF3 decreases to 74.8% and 71.9%, while FRRs of NF3 decreases to 43.3% and 41.9%. After three cycles of CR filtration, the FRR value of Z-NF3 is 71.6% higher than that of NF3, demonstrating the superior fouling-resistance of Z-NF3 to organic dyes. Furthermore, as shown in Figure 4.7c and 4.7d, Z-NF3 has a much higher R_r and lower R_{ir} values compared to those of NF3 for all three cycles, which further confirms the enhanced fouling-resistance.
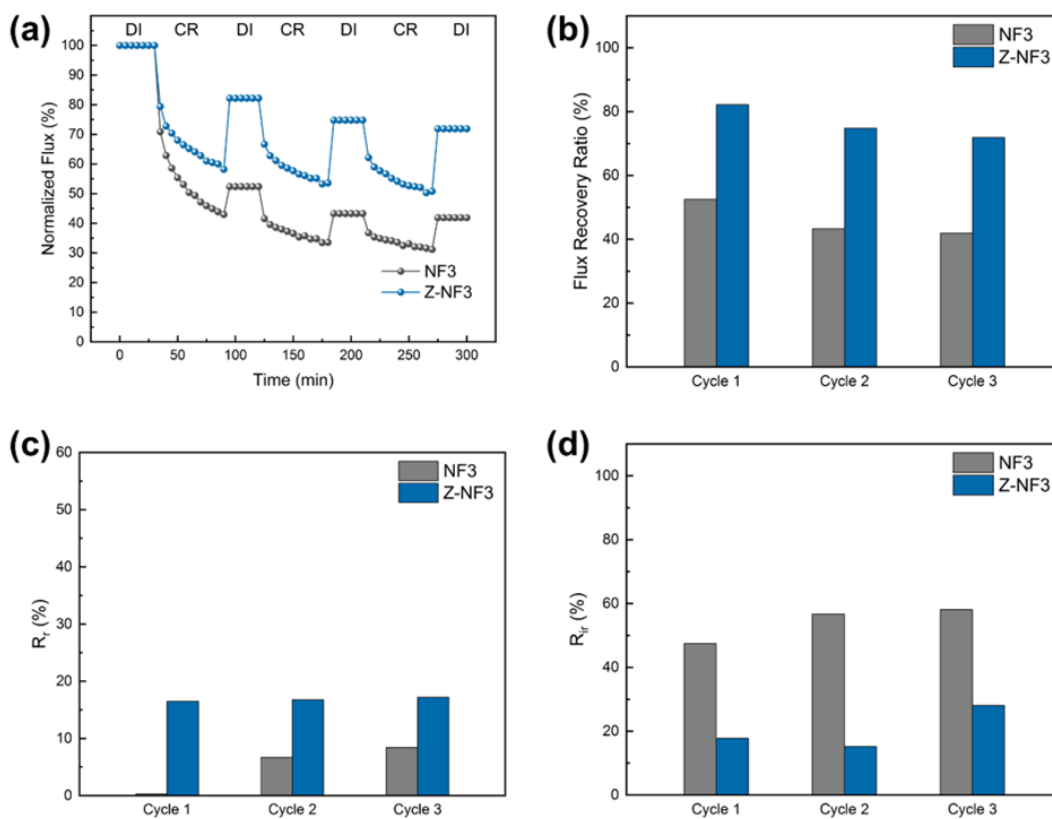
Figure 4.7 Reusability and fouling-resistant performance of Z-NF3 and NF3 using CR (100 ppm) as the model foulant under 6.0 bar: (a) normalized flux with three cycles filtration; (b) flux recovery ratio (FRR); (c) reversible fouling ratio (R_r); (d) irreversible fouling ratio (R_{ir}).

Figure 4.8 shows the fouling-resistant performance after three cycles of filtration of BSA solution. With the introduction of the zwitterionic moiety in Z-NF3, one can see a mild decrease in permeability compared to NF3 due to the increased hydrophilicity of membrane surface. After the cleaning of membrane surface, FRR of the first cycle reaches an ultrahigh level of 99.1%, while FRR of NF3 is only 84.0%. During the three cycles of filtration, FRR of Z-NF3 decreases slightly from 99.1% to 95.3%, demonstrating its superior stability and reusability (Figure 4.8b). As shown in Figure 4.8c and 4.8d, R_r and R_{ir} for BSA fouling follow the same pattern with the CR filtration, indicating its superior fouling-resistant ability for hydrophobicity contaminants.
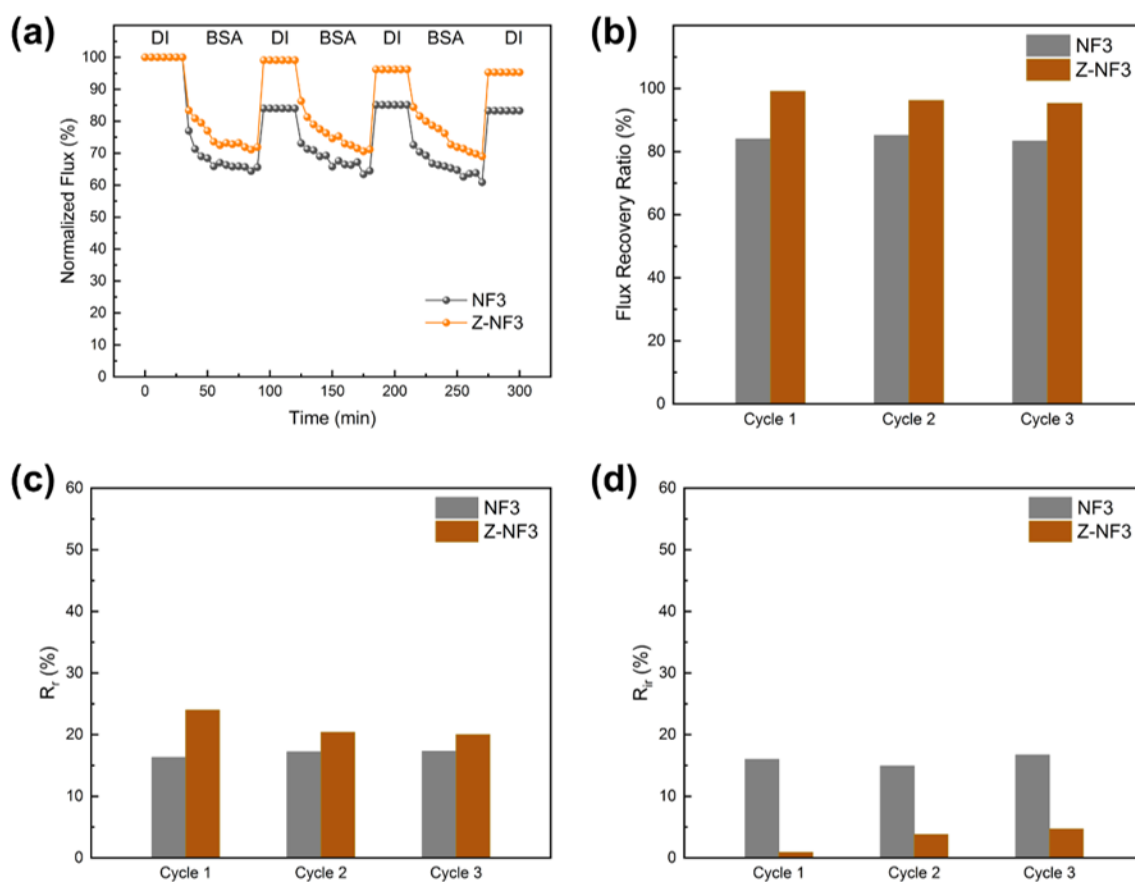
Figure 4.8 Reusability and fouling-resistant performance of Z-NF3 and NF3 using BSA (1.0 g L^{-1} in PBS buffer solution, pH 7.4) as the model foulant under 6.0 bar: (a) normalized flux with three cycles filtration; (b) flux recovery ratio (FRR); (c) reversible fouling ratio (Rr); (d) irreversible fouling ratio (Rir).

In addition to the filtration of CR and BSA, NaAlg as another typical contaminant has also been employed in order to fully investigate the fouling-resistant performance of Z-NF3. As shown in Figure 4.9a, it follows the similar trend observed above in the case with CR and BSA for the three cycles of filtration. Figure 4.9b shows the FRR values of Z-NF3 and NF3. One can see that the pristine NF3 has a lower FRR (87.7%) compared to Z-NF3 (92.0%) for the initial cycle and it dramatically decreases to 75.5% in the third cycle, while the FRR of Z-NF3 can still maintain at 84.5%. The higher R_r in Figure 4.9c and lower R_{ir} in Figure 4.9d further demonstrate the enhanced fouling-resistant ability of Z-NF3 to NaAlg relative to NF3. Based on the above results with the three model contaminants (CR, BSA, and NaAlg), it can be concluded that, after the introduction of the zwitterionic moiety in Z-NF3, the fouling-resistant ability has been significantly improved towards both hydrophobic contaminants and the deposition of textile organic molecules.
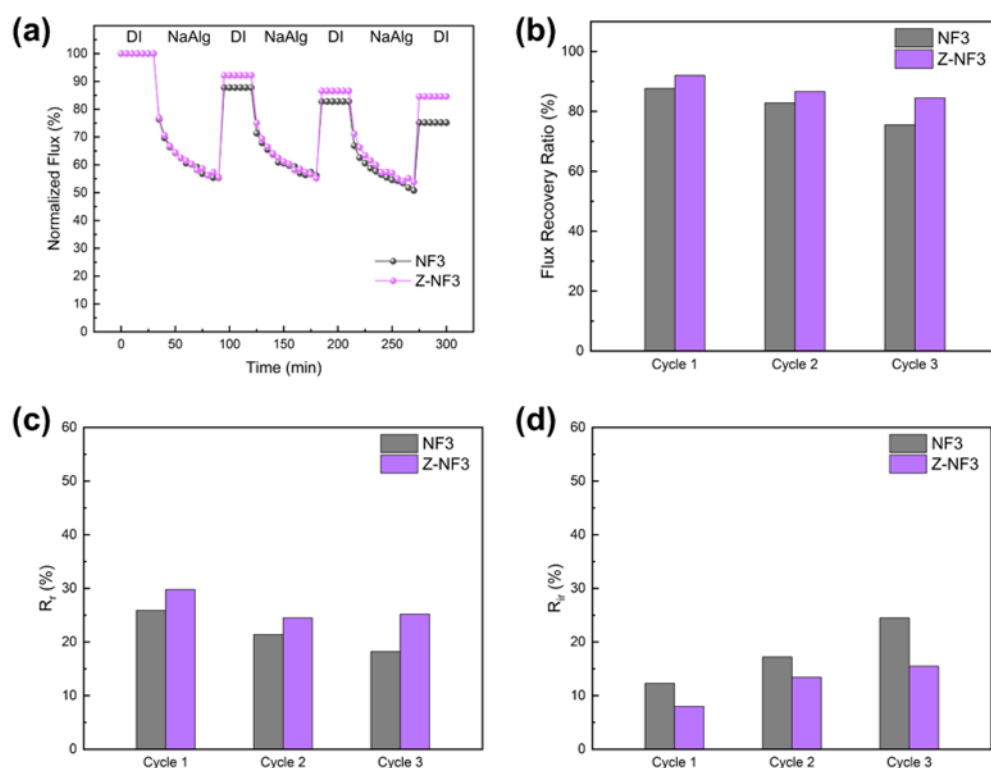
Figure 4.9 Reusability and fouling-resistant performances of Z-NF3 and NF3 using NaAlg (1.0 g L^{-1}) as the model foulant under 6.0 bar: (a) normalized flux with three cycles filtration; (b) flux recovery ratio (FRR); (c) reversible fouling ratio (R_r); (d) irreversible fouling ratio (R_{ir}).

To highlight the excellent performance of Z-NF3 fabricated in this study, a comparison of the performance in terms of PWP and dye rejection is made (see Table 4.3) in reference to reported NF membranes fabricated via various methodologies, including the conventional interfacial polymerization, polydopamine deposition, dopamine-involved layer-by-layer process, and dopamine rapid deposition. Though the NF membranes prepared via the conventional interfacial polymerization generally possess relatively higher dye rejections, their PWPs are much lower compared to Z-NF3membrane in this study. In addition, some of the reported NF membranes fabricated with dopamine deposition also show lower PWPs. For instance, the membrane GA-PEI fabricated with the co-deposition of gallic acid and branched polyethylenimine has a PWP of 8.3 LMH bar^{-1} with a low azithromycin (AH, molecular weight: 749.0 g mol^{-1}) rejection (96.2%). Other NF membranes (SPEI10k/PEI and (TA/JA)$_2$/PAN) have comparable PWPs and dye rejections as Z-NF3 in this study. However, the layer-by-layer methodology used their fabrication involves intricate processes. Furthermore, the reported membrane (RD-1S) prepared from a similar rapid deposition (non-covalent deposition) shows a lower PWP and also a lower dye rejection. This comparison indicates the superior performance of Z-NF3 for the potential applications in the treatment of dye-contaminated wastewater from textile industries

Table 4.3 Performance comparison of the NF membrane (Z-NF3) in this study with other reported NF membranes.

Membrane	Methodology	PWP (LMH bar^{-1})	Dye rejection (%)	Ref.
NF-SDA-0.1	Interfacial polymerization	10.4	CR: 99.9	[179]
M-3.0	Interfacial polymerization	16.6	MB: 95.4	[147]
ZM3	Interfacial polymerization	10.7	MB: 99.9	[175]
CNC-TFC-PDA	Deposition	23.1	CR: 99.9	[180]
Catechol-PEI	Deposition	2.6	BTB: 99.6	[89]
GA-PEI	Deposition	8.3	AH: 96.2	[181]
SPEI10k/PEI	Layer-by-layer	36.9	CR: 99.4	[182]
(TA/JA)$_2$/PAN	Layer-by-layer	37.0	CR: 99.5 MB: 98.0	[183]
RD-1S	Rapid deposition	27.4	CR: 98.2 DR23: 97.6	[184]
Z-NF3	Rapid deposition	32.0	CR: 99.7 MB: 98.6	This study

BTB: bromothymol blue; AH: azithromycin

4.4 Conclusions

In summary, zwitterionic NF membranes have been facilely fabricated through the rapid co-deposition of dopamine and diamine zwitterion (Z-DNMA) by $CuSO_4/H_2O_2$ triggered polymerization. The selective layer of Z-NF membranes is constructed by the covalent bonding of dopamine and Z-DNMA via Michael addition reaction and Schiff base reaction. Through the investigation on the effects of the co-deposition parameters, including the ratio between dopamine and Z-DNMA as well as the co-deposition time, the optimum membrane (Z-NF3) identified herein shows enhanced hydrophilicity (WCA of 30.0º), a high PWP of 32.0 LMH bar^{-1} with superior organic dye rejections to CR (99.7%) and MB (98.6%). The fouling experiments with three cycles of filtration of three model contaminants (CR, BSA, and NaAlg) confirm that Z-NF3 has an outstanding fouling-resistant ability and excellent stability. FRRs for the first cycle filtration of BSA, NaAlg, and CR are 99.1%, 92.0%, and 82.2%, respectively, with a lower irreversible fouling ratio (R_{ir}) and higher reversible fouling ratio (R_r) values compared to those of the control membrane (NF3). The high PWP and high rejection to organic dyes, coupled with its superior fouling-resistant performance, highlight its great potential for applications in the treatment of textile wastewater.

Chapter 5 Trimethylamine *N*-oxide-derived thin-film composite membranes

This chapter is adapted from a paper entitled "Trimethylamine N-oxide-derived zwitterionic polyamide thin-film composite nanofiltration membranes with enhanced anti-dye deposition ability for efficient dye separation and recovery" by **Yang, L.**; Zhang, X.; Ma, W.; Raisi, B.; Liu, X.; An, C.; Ye, Z., which has been accepted by *Journal of Membrane Science*.

Abstract

Organic dyes from textile industries are becoming the second largest pollutants in the world. In this study, inspired by the seawater fish, a new diamine monomer, DNMAO with a TMAO-derived "N⁺—O⁻" zwitterionic functionality, has been designed for the fabrication of polyamide TFC membranes to purify dye-contaminated water and recover organic dyes. The fabricated membranes show enhanced permeability and improved anti-dye-deposition performance. The optimum membrane fabricated at 0.5 wt% of DNMAO feed solution exhibits an ultrahigh PWP of 37.5 LMH bar^{-1}, a superior CR rejection of 99.93%, and a low NaCl rejection of 9.3%, indicating its outstanding performance for dye/salt separation. It can also achieve the complete CR removal from a feed with a low CR concentration of 1 ppm, demonstrating its superior separation performance for the production of clean potable water. In addition, the low dye loss rate (6.22%) and high salt removal rate (85.6%) are achieved during the purification and recovery test with CR/NaCl mixtures. Furthermore, the optimum membrane possesses an excellent anti-dye-deposition performance with a FRR of 92.1%. All these results demonstrate its potential for applications in not only textile wastewater treatment but also organic dye purification and recovery.

5.1 Introduction

Water scarcity and water pollution have become formidable challenges that severely restrict the sustainable development of human society. Highly efficient and effective water purification technologies are thus urgently required to ensure the adequate supply of clean and safe water.[185,186] Printing and dyeing industry, deemed as one of the most polluting industries, generates a significant amount of wastewater containing organic dyes annually, causing destructive impacts on the aquatic ecosystem.[187,188] Traditional methods, including adsorption, photo-degradation, and chemical degradation, have been widely adopted to remove organic dyes from the effluents of

printing and dyeing industry.[189,190] However, for adsorption, the limited removal efficiency, especially at low dye concentrations, and the intricate regeneration process of adsorbents make it unsuitable for the production of high quality water. Likewise, the toxic sludge produced from degradation also restricts its application in the treatment of dye-polluted wastewater.[191,192] Therefore, processes with high efficiency and sound sustainability are urgently required not only to produce high quality water by removal of toxic dyes, but also to recover and reuse the latter.[5]

NF has been considered as one of the most promising and attractive options for separation of organic molecules, including organic dye recovery and reuse, owing to its facile operation conditions, low energy consumption, and high separation efficiency.[193,194] To date, the state-of-the-art NF membranes are polyamide TFC membranes fabricated by interfacial polymerization.[80,195] Current NF membranes often offer high rejections to both organic dyes and inorganic salts and thus cannot facilitate the separation of dyes from the salts. The nondifferentiated simultaneous removal of both organic dyes and inorganic slats impacts the purity of recovered dyes.[53,113] In addition, the inadequate permeation of inorganic salts compromises the filtration flux due to the high osmotic pressure and concentration polarization.[175]

Various strategies have been explored to design high performance NF membranes, including the addition of nanomaterials as additives during the interfacial polymerization (SiO_2, TiO_2, GO, COFs, and MXenes),[67,196-199] the construction of thin-film layers with two-dimensional (2D) functional materials (GO, COFs, and MXenes),[111,200-202] and the application of bio-inspired chemistry (dopamine, catechol, and tannic acid) for the construction of thin-film selective layers.[88,89,131,167] Although the fabricated NF membranes have shown enhanced permeability and improved permeation of inorganic salts, the weak compatibility between the nanomaterial additives and polyamide matrix may lead to the release of the nanomaterials and thus compromise membrane performance. In addition, the high cost of 2D materials and the intricate bio-inspired chemistry limit their applications in NF membranes. Furthermore, membrane fouling associated with their relatively hydrophobic surface is another issue that strongly restricts their practical applications.[34] Therefore, it is of great importance to develop NF membranes with strong fouling-resistance for achieving the efficient separation of organic dyes and inorganic salts.

Zwitterions, possessing equimolar oppositely charged groups, have shown great potential in surface modification of membranes. Their strong water affinity facilitates the formation of a

hydration layer on the membrane surface for alleviating fouling.[183] To date, three well-established zwitterions have been extensively employed in the membrane fabrication, including PC, SB, and CB.[24,203] Previous studies have shown that the hydration capacity increases with the decrease in distance between oppositely charged groups.[204,205] TMAO inspired from saltwater fish, as a small organic osmolyte, possesses a positively charged quaternary amine group and a negatively charged oxygen atom. The equimolar oppositely charged groups in TMAO are connected directly without any spaces to provide a stronger hydration capacity compared to the well-established PC, SB, and CB-based zwitterions.[204,205] On the basis of this theory, TMAO inspired from saltwater fish has been designed as a new generation of zwitterion for constructing ultralow fouling surfaces.[204]
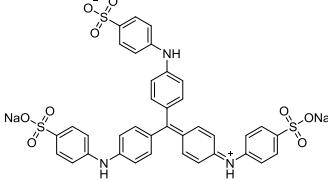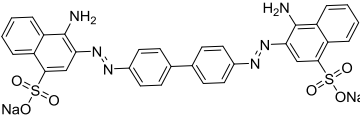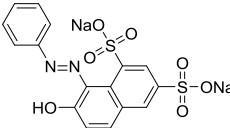
Herein, we report a new diamine monomer featured with TMAO structure, DNMAO, for the fabrication of polyamide TFC membranes via the interfacial polymerization. DNMAO is conveniently synthesized by the facile oxidation of tertiary amine group of DNMA with hydrogen peroxide. Its charged group (N^+-O^-) is directly connected without extra atoms and has the typical characteristics of zwitterions with enhanced polarity compared to DNMA. TFC membranes have been fabricated by incorporating DNMAO in the active layer. The optimum TFC membrane shows high water permeability, high dye/salt selectivity, and improved antifouling ability. In addition, the filtration of dye/salt mixture with four cycles shows superior dye recovery efficiency with low loss rate and high salt removal efficiency, demonstrating the potential of TMAO-inspired zwitterion for the fabrication of high-performance NF membranes in various separation applications.

5.2 Experimental

5.2.1 Materials

Polysulfone (PSf, M_w = 22,000 g/mol), PVP (M_w =40,000 g/mol), 1-methyl-2-pyrrolidinone (NMP, 99.5%), DNMA, TMC, MB, CR, OG, and PEG were obtained from Aldrich (Oakville, Canada). Properties of all organic dyes (MB, CR, and OG) are listed in Table 5.1. H_2O_2 (30%), DCM, NaCl (99.0%), Na_2SO_4 (98.0%), $MgCl_2$ (99.0%), and $MgSO_4$ (99.0%) were provided by Thermo Fisher Scientific (St. Laurent, Canada). DI water was prepared using a Milli-Q purification system (Millipore, Billerica, MA, USA). All the chemicals were used as received.

Table 5.1 Organic dyes used in this study.

Dyes	Chemical structure	Molecular weight (g mol^{-1})	λ_{max}[a] (nm)
MB		799.8	592
CR		696.7	500
OG		452.4	475

[a] Maximum absorption wavelength.

5.2.2 Synthesis of DNMAO monomer

DNMAO was synthesized via the oxidation of the tertiary amine group in DNMA according to a previously reported study.[206] In brief, DNMA (34.5 mmol, 5.0 g) was dissolved in DI water (20 mL). H_2O_2 (30%, 4 mL) was diluted with DI water (11 mL). Afterwards, the diluted H_2O_2 solution was added dropwise into the stirred DNMA solution in an ice-water bath. The mixed solution was exposed to air and stirred continuously at room temperature for 12 h. Then, the reaction mixture was extracted with dichloromethane to remove the un-oxidized precursor (DNMA) for at least three times. The final aqueous solution was freeze-dried and a viscous liquid with a light yellow color was obtained (yield: 71%).
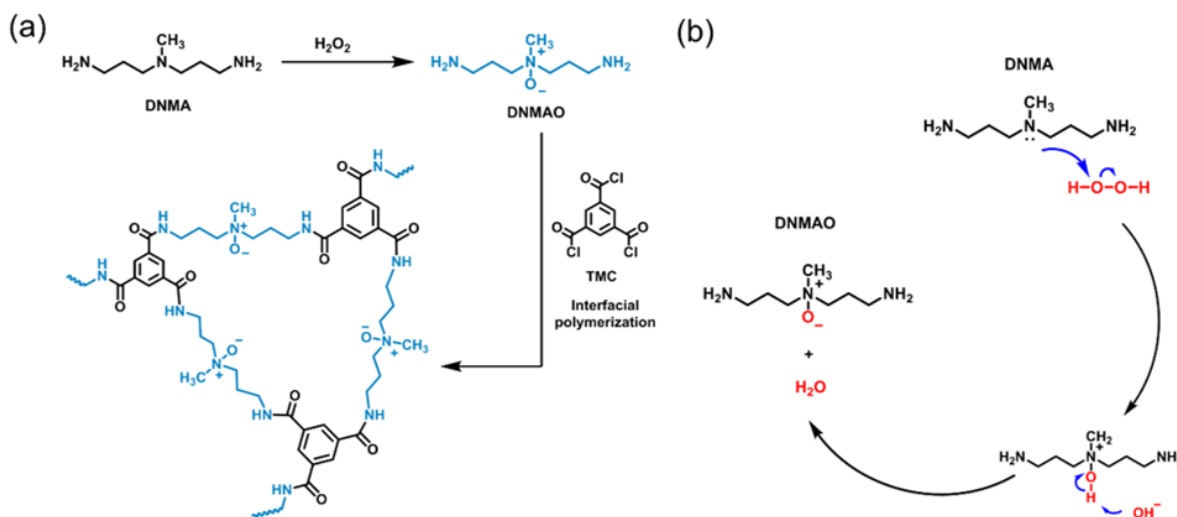
Figure 5.1 (a) Synthesis of DNMAO and fabrication of polyamide TFC membranes by interfacial polymerization, (b) mechanism of the oxidation process from DNMA to DNMAO with H_2O_2.[207,208]

5.2.3 Fabrication of polyamide TFC membranes

PSf ultrafiltration membranes were prepared by a phase-inversion method and were used as the support layer of polyamide TFC membranes.[209] Briefly, a solution of PSf (15 wt%) and PVP (2%) as the pore-forming agent in NMP (83 wt%) was cast on a glass plate by a casting knife with the thickness of 200 μm. Subsequently, the cast film was immersed into DI water to induce phase-inversion at room temperature. The obtained PSf ultrafiltration membrane was washed thoroughly with fresh DI water and dried at room temperature before usage.

Polyamide TFC membranes were fabricated by interfacial polymerization on PSf ultrafiltration membranes. Typically, the PSf ultrafiltration membrane fixed in a mould was exposed to an aqueous solution containing DNMA or DNMAO at different concentrations (0.1, 0.25, 0.5, and 1.0 wt%, respectively) for 1 min. The excess solution was removed by a rubber roller. Afterwards, the membrane was exposed to a hexane solution of TMC (0.2 wt%) for 2 min. The final membrane

was finally post-treated at 60 ºC for 10 min. Then, the prepared membrane was immersed in an ethanol solution (50 % in DI water) for 30 min, followed by wash with DI water to remove residual ethanol. The membranes fabricated with DNMA are termed as N-0.1, N-0.25, N-0.5, and N-1.0, respectively, and those fabricated with DNMAO are termed as NO-0.1, NO-0.25, NO-0.5, and NO-1.0, respectively, with the number in each name denoting DNMA/DNMAO monomer concentration in the synthesis.

5.2.4 Characterizations

The chemical structures of DNMA and DNMAO were characterized with ^{1}H NMR, Bruker 300 MHz). FTIR spectra were obtained on a Thermo Scientific Nicolet 6700 Analytical FTIR spectrometer. WCA measurements were performed on a contact angle system (VCA, AST Products, Inc.). Membrane surface and cross-sectional morphologies were observed via a FE-ESEM after platinum coating (ca. 4 nm). XPS was performed on a Thermo Scientific Theta Probe XPS spectrometer with a monochromatic Al Kα X-ray source at a spot area of 400 μm. The surface roughness of the TFN membranes was investigated with an AFM (Tosca 400, Anton Paar) in the tapping mode. The detection of CR in solutions of low CR concentrations was performed on a Tosca 400 series (Anton Paar) high performance liquid chromatography (HPLC) equipped with a UV-vis detector (the absorption wavelength set at 500 nm). The mobile phase used was 70% ammonium acetate buffer (0.1 M, pH 4.0) and 30% acetonitrile.

Pore size distribution of the fabricated polyamide TFC membranes was performed by measuring the rejections of PEG aqueous solutions (1.0 g L^{-1}) with different molecular weights (200, 400, 600, 1000, and 1500 Da). The mean effective pore radius (μ_p) is the solute geometric radius when the rejection R = 50%, while geometric standard deviation (σ_p) is the ratio of Stoke radius when rejection R = 84.13% to that of R = 50%. The Stoke radii of PEGs is calculated according to the following equation:

$$r = 16.73 \times 10^{-12} \times MW^{0.557} \quad (MW \leq 35{,}000) \qquad (MW \leq 35000) \tag{5.1}$$

where r is the Stoke radius, MW is the molecular weight of PEGs.

The pore size distribution is determined by the following equation:

$$\frac{dR(r_p)}{dr_p} = \frac{1}{r_p \ln\sigma_p \sqrt{2\pi}} exp\left[-\frac{(\ln r_p - \ln\mu_p)^2}{2(\ln\sigma_p)^2}\right] \qquad (5.2)$$

where r_p is the Stoke radius of PEG, μ_p is the mean effective pore radius, σ_p is the geometric standard deviation.

5.2.5 Membrane separation performance testing

The membrane performance testing was conducted at 6.0 bar with the use of a stirred dead-end filtration cell at a stirring speed of 350 rpm. The effective area of the membrane filtration was 12.56 cm^2. The TFC membranes were compacted at 7.0 bar with DI water for 30 min to reach a steady state before each testing. In this study, a series of solutions of dyes and inorganic salts at a concentration of 100 ppm and 1 g L^{-1}, respectively, was employed as feed solutions for single component filtration if there was no additional illustration.

The TFC membrane permeability (P, LMH bar^{-1}) is calculated by using the following equation:

$$P = \frac{V}{A \times t \times \Delta P} \qquad (5.3)$$

where V is the volume (L) of the permeate, A is the effective filtration area (m^2), t is the operation time (h) and ΔP is the trans-membrane pressure (bar). The solute rejection (R) is calculated according to:

$$R = \left(1 - \frac{C_p}{C_f}\right) \times 100\% \qquad (5.4)$$

where C_p and C_f are solute (dye or salt) concentrations of the permeate and feed solutions, respectively. Dye concentration was determined with a UV-vis spectrophotometer (Agilent Cary 8454), while salt concentration was measured by using a conductivity meter (OAKTON conductivity meter, CON 11 series, Vernon Hills, IL USA).

5.2.6 Dye purification and recovery process

The dye purification and recovery process was carried out with the optimum TFC membrane (NO-0.5). In detail, the feed solution (300 mL) with 100 ppm of CR and 1 g L^{-1} of NaCl was filtrated at 6 bar until the volume was reduced to half of the initial volume (150 mL). Then, 150 mL of DI

water was replenished to the feed solution in order to reach the initial volume. The whole operation was repeated for 4 cycles. The instantaneous concentrations of CR and NaCl in the feed and permeate were measured. The rejection of solutes is calculated by following Equation 2. The CR loss rate (R_c) and salt removal rate (R_s) are determined with Equations 3 and 4, respectively, to evaluate the desalination efficiency:

$$R_c = \left(1 - \frac{C_n}{C_0}\right) \times 100\% \qquad (5.5)$$

$$R_s = \left(1 - \frac{S_n}{S_0}\right) \times 100\% \qquad (5.6)$$

in which, C_o and S_o presents the initial CR and NaCl concentrations in the feed solution, which are 100 ppm and 1 g L^{-1}, respectively. C_n and S_n are solute concentrations in the feed solution for each cycle.

The theoretical solute concentrations are calculated according to Equation 5 during the dye desalination and recovery process, while the deviation ($\bar{\sigma}$) between the theoretical concentration (C_T) and experimental solute concentration (C_E) for each cycle is obtained by the Equation 6 [16,40]:

$$C_T = C_0(ac)^{-R}(1 + b)^{-n(1-R)} \qquad (5.7)$$

$$\bar{\sigma} = \left(\frac{C_E - C_T}{C_T}\right) \times 100\% \qquad (5.8)$$

in which, a is the volume concentration ratio (0.5) in pre-concentration step, b is the volume dilution ratio (1.0), and c is the volume concentration ratio (2.0) in post-concentration step. R and n are the solute rejection and the cycle number of DI water addition to the system, respectively. C_0 is the initial solute concentration in the feed solution.

The concentration ratio of CR/NaCl during the cycles is calculated according to the following equation:

$$R = \frac{C_{CR}}{C_{NaCl}} \qquad (5.9)$$

where C_{CR} and C_{NaCl} are CR and NaCl concentrations, respectively, in the retentate. For instance, the initial CR/NaCl ratio is 0.10 calculated by 0.1 g L^{-1} (CR)/1.0 g L^{-1} (NaCl), while the terminal CR/NaCl ratio is 0.66 calculated by 0.09482 g L^{-1} (CR)/0.144 g L^{-1} (NaCl).

5.2.7 Anti-dye-deposition performance testing

The anti-dye-deposition performance testing was conducted at 6.0 bar with CR as the foulant. Firstly, PWP was recorded as the original permeability (J_0) for 1 h. Then, DI water was replaced with 100 ppm CR solution. The filtration permeability (J_1) was recorded every 5.0 min for 5 h. The normalized permeability (J_0/J_1) was employed to quantify the anti-dye-deposition ability during the filtration process. After 5 h of filtration, the fouled membrane was cleaned by hydraulic wash with DI water for 2 h, followed by the measurement of PWP again (J_2). This whole process was repeated twice. Flux recovery ratio (FRR) and flux decline ratio (FDR) are calculated according to the following equations:

$$FRR = \left(\frac{J_2}{J_0}\right) \times 100\% \tag{5.10}$$

$$FDR = \left(1 - \frac{J_1}{J_0}\right) \times 100\% \tag{5.11}$$

5.3 Results and discussion

5.3.1 Synthesis and characterization of DNMAO

The TMAO-derived monomer, DNMAO, is synthesized herein by the facile oxidation of the tertiary amine group in DNMA with H$_2$O$_2$ (Figure 5.1a). The colorless DNMA turns into a light yellow viscous liquid after the oxidation. The typical nitrogen-oxide (N$^+$-O$^-$) functionality is the intermediate of the well-known "Cope Elimination" reaction.[207,208] The oxidation mechanism, illustrated in Figure 5.1b, involves the formation of a hydroxylamine group balanced with a negatively charged hydroxyl group through the nucleophilic attack of tertiary amine group of DNMA by H$_2$O$_2$, followed by the deprotonation of the hydroxylamine group.[138,209] The chemical structures of DNMA and DNMAO have been confirmed with ^{1}H NMR spectroscopy. Figure 5.2a

shows the ^{1}H NMR spectrum of DNMA, where the singlet peak a at 2.11 ppm (s, 3 H) is ascribed to the methyl group next to the tertiary amine group. The triplet peaks, including d at 2.53 ppm (t, 4 H) and b at 2.33 ppm (t, 4 H), and multiplet peak c at 1.53 ppm (m, 4H) are attributed to the methylene group next to the tertiary amine group, the methylene group next to the primary amine group, and the middle methylene group, respectively. After the oxidation of the tertiary amine groups, one can see that all peaks shift to the relatively lower fields (i.e., higher chemical shifts) due to the stronger electron-withdrawing ability of the N^+-O^- group (Figure 5.2b). These results demonstrate the successful synthesis of DNMAO.
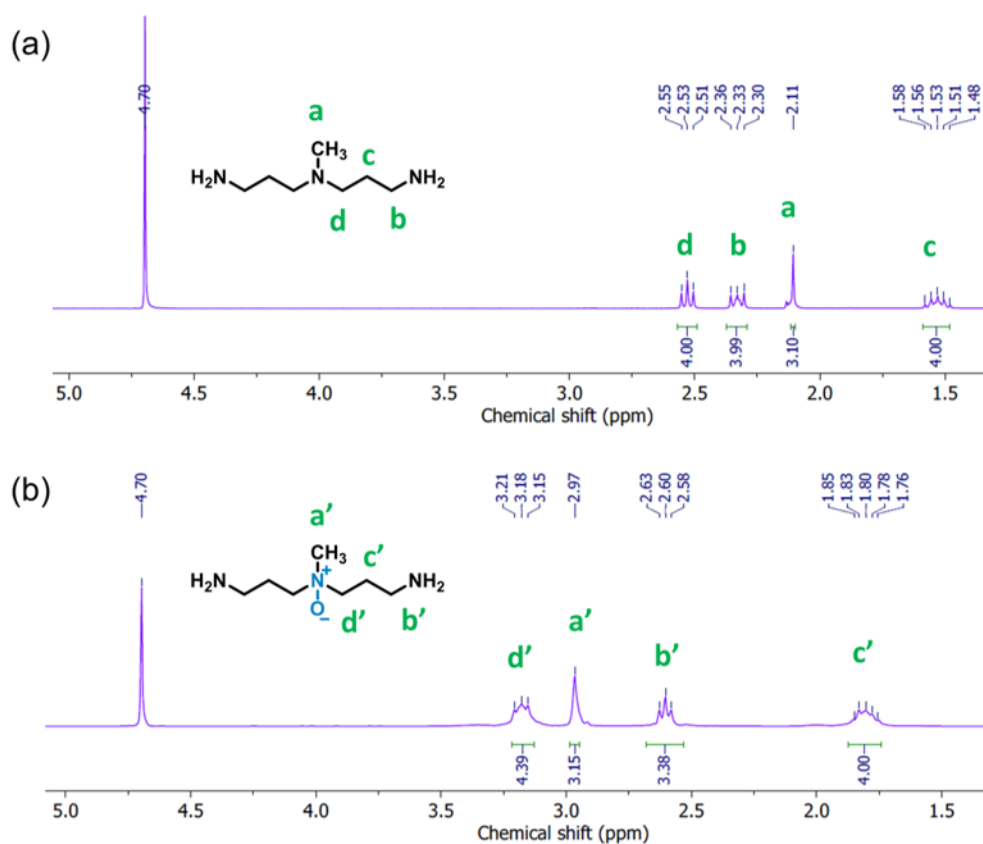
Figure 5.2 ^{1}H NMR spectra of DNMA (a) and DNMAO (b).

81

5.3.2 Fabrication and characterization of polyamide TFC membranes

Polyamide TFC membranes have been fabricated by the conventional interfacial polymerization on PSf ultrafiltration membranes with the use of DNMAO/DNMA and TMC as the monomer precursors. In particular, DNMAO/DNMA feed solutions at different concentrations were applied in the membrane fabrication to render the two sets of membranes (NO-# and N-#, respectively, with the number indicating DNMAO/DNMA concentration applied in the fabrication). The chemical compositions of resulting polyamide TFC membranes have been characterized with ATR-FTIR spectroscopy. As shown in Figure 5.3a, the bands at 1640 cm^{-1} and 1050 cm^{-1} are ascribed to the characteristic C=O stretching in the amide functionality and C-N stretching in the amine functionality, respectively, which indicate the formation of polyamide thin-film layers. XPS characterization (see Figure S5.1 and Table S5.1) shows that the nitrogen content in the membrane increases from 9.2% for NO-0.25 to 10.3% for NO-0.5 with the increase of DNMAO concentration from 0.25 to 0.5 wt% during fabrication. This indicates qualitatively the increasing cross-linking degree with the increase of DNMAO concentration during fabrication. In addition, N-0.5 has a higher nitrogen content (15.0%) than NO-0.5 (10.3%), suggesting a higher cross-linking degree in the former.

Figure 5.3b shows the WCA of the fabricated membranes. Compared to those fabricated from DNMAO except NO-0.1, the membrane N-0.5 has a relatively higher WCA (72.5º), which is caused by the inherent hydrophobicity of DNMA. It is obvious that the membrane NO-0.5 has a lower WCA than that of N-0.5 due to the enhanced hydrophilicity following incorporation of DNMAO with the highly polar zwitterionic functionality. In addition, with the increase of monomer concentration from 0.1 to 1.0 wt%, the WCA decreases from 75.3º to 60.6º.
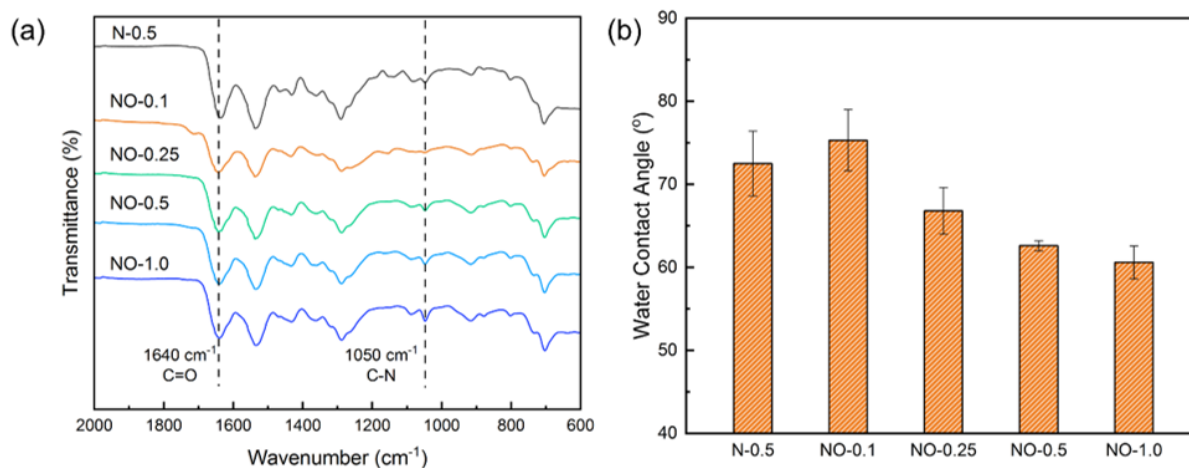
Figure 5.3 Membrane surface characterization: (a) ATR-FTIR spectra; (b) water contact angles.

Figure 5.4 shows the surface morphologies of the pristine PSf ultrafiltration membrane and the fabricated polyamide TFC membranes, including surface and cross-sectional SEM images, and surface AFM images. From surface and cross-sectional morphologies (Figure 5.4a-d and Figure 5.4a'-d'), one can observe the formation of a thin-film polyamide layer after the interfacial polymerization. In particular, the grainy surface structure is more visible (Figure 5.4d) with the increased monomer concentration used in the membrane fabrication. Cross-sectional images of the membranes show that the thickness of polyamide thin film layer increases from 149 to 244 nm with the increase of monomer concentration from 0.5 wt% (NO-0.5) to 1.0 wt% (NO-1.0). However, NO-0.5 exhibits a lower thickness (149 nm) compared to that of N-0.5 (185 nm), which should result from the restricted diffusivity of hydrophilic DNMAO towards hexane [16]. AFM has been used to characterize the membrane surface roughness (Figure 5.4a''- d''). The results show that the pristine PSf ultrafiltration membrane has a relatively rough surface (Ra = 37.7 nm) in comparison with the resulting polyamide TFC membranes, which is attributed to the formation of smooth thin-film layer covering the porous structure of the PSf ultrafiltration membrane [16,41]. As shown in Figure 5.4b'' and 5.4c'', N-0.5 and NO-0.5 membranes fabricated from the different monomers but at the same concentration have similar surface roughness. With the increase of

DNMAO concentration to 1.0 wt%, the membrane surface roughness is further reduced to 27.1 nm (Figure 5.4d"). On the basis of these results, it can be concluded that the thin-film layers have been constructed successfully.
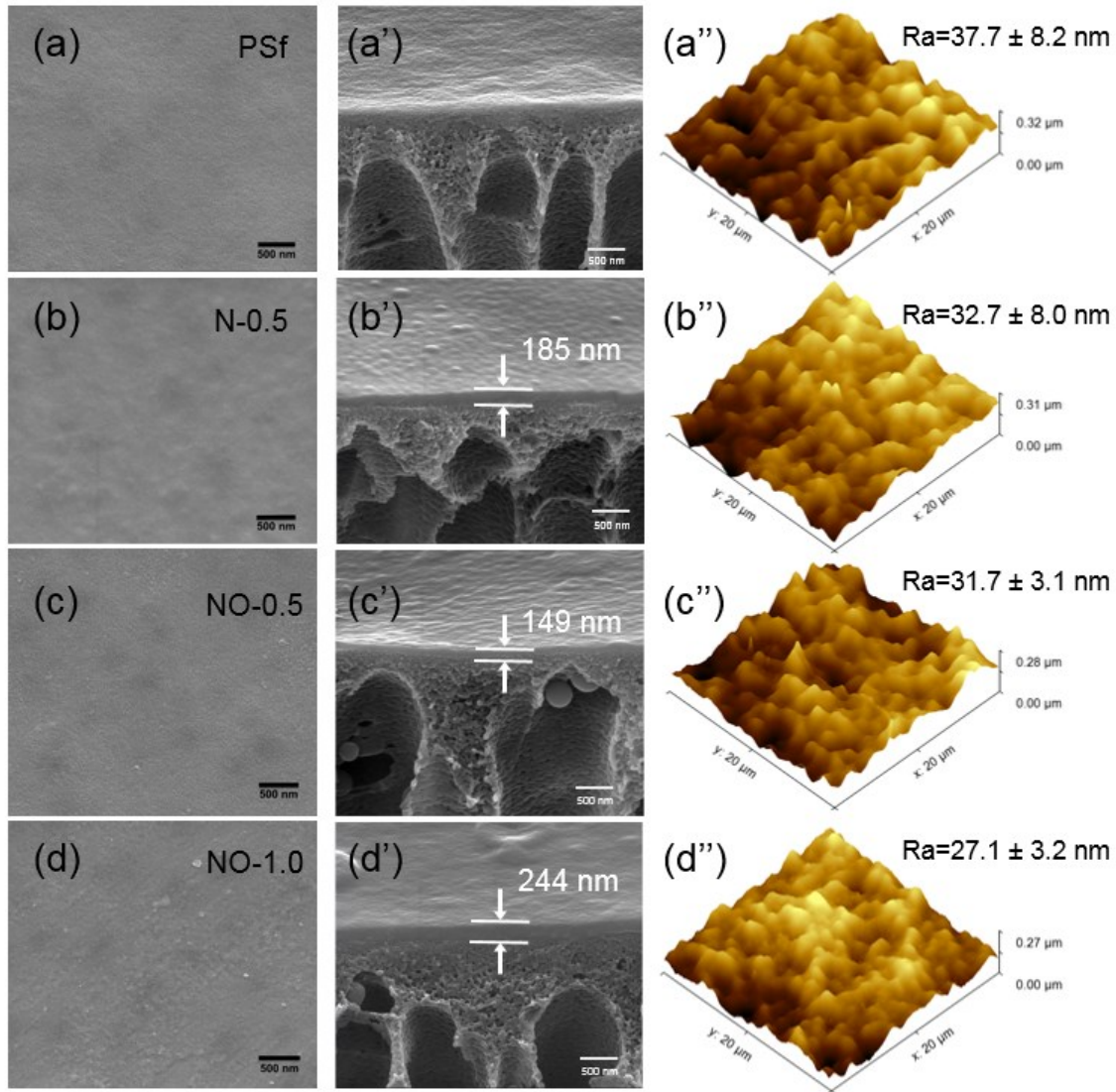
Figure 5.4 The surface morphologies of polyamide TFC membranes (PSf, N-0.5, NO-0.5, and NO-1.0): (a-d) surface SEM images, (a'-d') cross-sectional SEM images, and (a"-d") AFM images.

Figure S5.2 compares the pore size distributions of three membranes, N-0.5, NO-0.5 and NO-1.0, which were determined by measuring the rejections of PEG of different molecular weights (200, 400, 600, 1000, and 1500 Da; see Supporting Information for the procedure). With the increase of the DNMAO concentration during fabrication from 0.5 to 1.0 wt%, the pore size distribution of the membranes gets narrower. Meanwhile, N-0.5 shows a narrower pore size distribution compared to NO-0.5 due to the limited diffusivity of DNMAO towards hexane as mentioned above. In our determination of the pore size distributions, we have found that the rejections of PEG of the molecular weight of 1500 Da with N-0.5, NO-0.5, and NO-1.0 are 85.8, 84.5, and 88.8%, respectively. On the basis of these rejection data, we speculate that the molecular weight cut-offs of the three membranes should be around 2000 Da and should increase in the order of NO-1.0 < N-0.5 < NO-0.5.

5.3.3 Separation performance

The performance of TFC membranes, including PWP and dye/salt rejection ability, has been systematically investigated. A strong dependence of the membrane performance on the monomer type and concentration during the interfacial polymerization has been found. As shown in Figure 5.5a, N-0.1 and NO-0.1 have the highest pure water permeabilities in the corresponding sets, which are 37.1 and 50.2 LMH bar^{-1}, respectively. With the increase of DNMA/DNMAO concentrations from 0.1 to 1.0 wt% in each set, PWP decreases from 37.1 to 14.3 LMH bar^{-1} for membranes fabricated with DNMA and from 50.2 to 33.2 LMH bar^{-1} for those with DNMAO, respectively. Moreover, membranes fabricated with DNMAO show higher pure water permeabilities compared to the corresponding one with DNMA at each monomer concentration, which is ascribed to the increased hydrophilicity of membranes, the broader pore size distribution, the lower thickness of thin film layer, and the lower cross-linking degree upon incorporation of DNMAO having the zwitterion group.

In order to investigate the membrane separation ability, CR has been employed as the model dye for the membrane filtration. Figure 5.5b shows the filtration permeability and CR rejection results for all membranes. Clearly, all membranes achieve high CR rejection ratios of more than 99%, which shows a trend of slight increases with the increase of monomer concentration during fabrication. In particular, an ultrahigh CR rejection ratio of 99.95% has been achieved with

membranes fabricated at the highest DNMAO monomer concentration. The molecular weight cut-off of NO-0.5 is around 2000 Da as mentioned above, which is much higher than the molecular weight of CR. The high dye rejection achieved herein should thus be mainly ascribed to the aggregate formation of CR molecules in aqueous solution.[167] Meanwhile, one can also observe that the filtration permeability decreases with the increase of monomer concentration during fabrication. The ratio of permeability (both PWP and filtration permeability) between the membranes fabricated from the lowest and highest monomer concentrations can illustrate the impact of monomer concentration on the dye filtration performance. For PWP, the ratio between N-1.0 (14.3 LMH bar^{-1}) and N-0.1 (37.1 LMH bar^{-1}) is 38.5%, while it is 66.1% between NO-1.0 (33.2 LMH bar^{-1}) and NO-0.1 (50.2 LMH bar^{-1}). The ratio of filtration permeability is 17.8% between N-1.0/N-0.1 (4.9/27.6 LMH bar^{-1}) and 73.5% between NO-1.0/NO-0.1 (25.5/34.7 LMH bar^{-1}), respectively. For membranes fabricated with DNMA, the ratio decreases from 38.5% to 17.8%, while it increases from 66.1% to 73.5% for those with DNMAO. Therefore, it can be concluded that the higher concentration of DNMA compromises the filtration permeability, whereas the higher concentration of DNMAO is conducive to the filtration permeability due to the enhanced hydrophilicity of membrane surface after the incorporation of "N$^+$-O$^-$" zwitterionic functionality.

In order to obtain the optimum TFC membrane for the following experiments, the FRR values for all membranes after the filtration of CR have been evaluated (Figure 5.5c). From Figure 5.5c, one can find that, for DNMA membranes, FRR decreases with the increase of DNMA concentration during fabrication, while it increases with the increase of DNMAO concentration due to the enhanced hydrophilicity of membrane surface, which has been confirmed by the WCA in Figure 5.3b. These results are consistent with the above conclusions from permeability ratios of N-0.1/N-1.0 and NO-0.1/NO-1.0. Therefore, based on these results, the optimum membrane NO-0.5 has been employed for the following experiments.

In addition to the CR filtration, other organic dyes (OG and MB) and inorganic salts (NaCl, Na$_2$SO$_4$, MgCl$_2$, and MgSO$_4$) have also been used to investigate membrane rejection ability. Figure 5.5d shows that NO-0.5 has relatively low rejections to various inorganic salts, which decreases in the order of Na$_2$SO$_4$ > MgSO$_4$ > MgCl$_2$ > NaCl as a synergistic result of Donnan effect and steric hindrance [42,43]. Among the salts, divalent anions possess larger molecular sizes and stronger

electrostatic repulsions with the membrane surface, in turn rendering higher rejections. In addition to CR, the performance of NO-0.5 towards the filtration of two other dyes (MB and OG) has also been investigated. Like CR, NO-0.5 also exhibits a high rejection towards MB (99.29%). However, a relatively lower rejection (82.93%) is found towards OG, which is ascribed to its smaller molecular weight (452 g mol^{-1}) and size. With the high permeability and distinct difference in their rejections, NO-0.5 thus has a great potential for the effective separation of dye/salt mixtures.
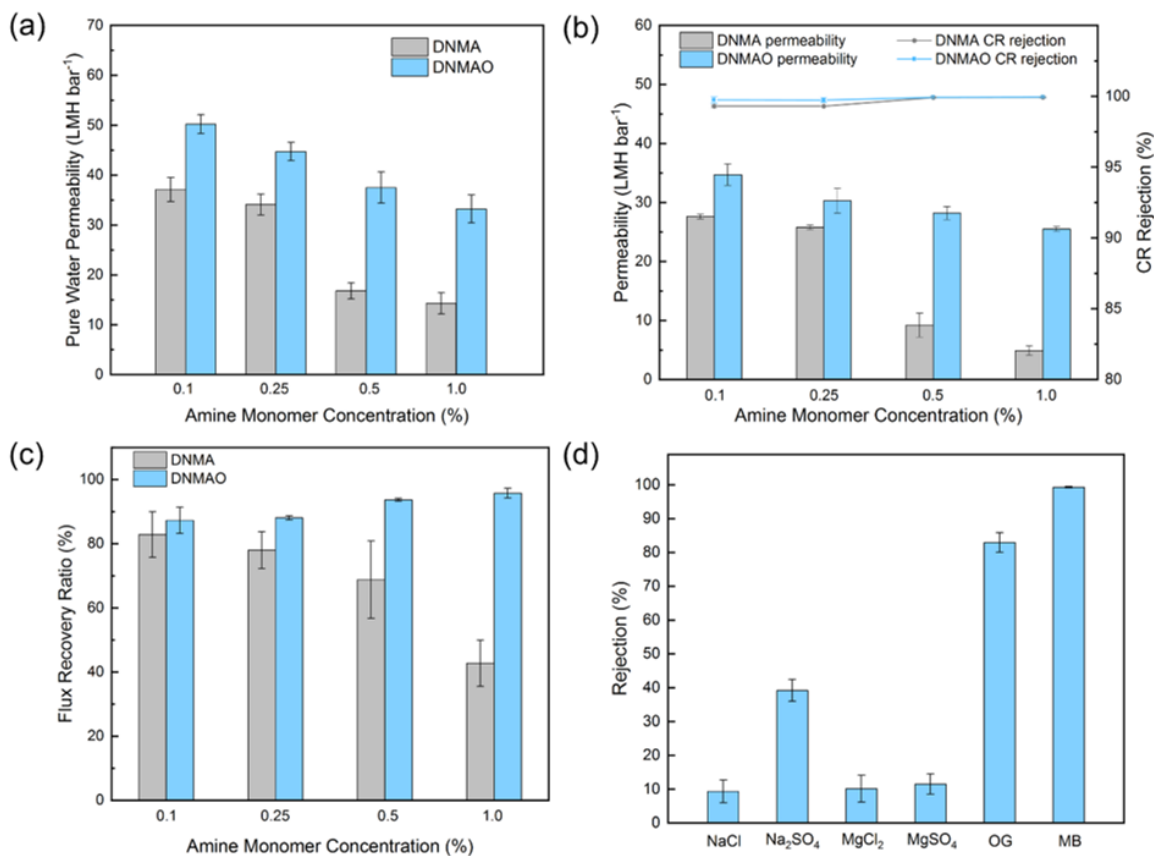
Figure 5.5 Separation performance of polyamide TFC membranes: (a) pure water permeability, (b) CR rejection (100 ppm) and filtration permeability, and (c) flux recovery ratio after CR filtration with various membranes; (d) rejections of inorganic salts (NaCl, Na$_2$SO$_4$, MgCl$_2$, and MgSO$_4$) and other dyes (OG and MB) with NO-0.5 membrane.

In addition to the single component filtration, the filtration of dye/salt mixtures (CR/NaCl) has also been performed with NO-0.5. Figure 5.6 shows the separation performance of NO-0.5 toward CR/NaCl mixtures at different combinations of concentrations (100 to 1000 ppm for CR and 1000 to 10000 ppm for NaCl). In Figure 5.6a, the NaCl rejection increases from 23.6% to 29.4% with the increase of CR concentration while at a fixed NaCl concentration of 1000 ppm, which is mainly ascribed to the enhanced electrostatic interaction between CR and NaCl.[210] Therefore, the higher CR concentration restricts the permeation of NaCl, leading to the higher NaCl rejection. This electrostatic interaction between CR and NaCl can also explain the phenomenon that NaCl rejection (23.6% at 100 ppm of CR, Figure 5.6a) in the dye/salt mixture is higher than that (9.3%, Figure 5.5d) in the filtration of single salt solution.[107] The decreased permeability shown in Figure 5.6a with the increase of CR concentration is caused by the CR adsorption as well as the formation of a cake layer on the membrane surface. Figure 5.6b shows the impact of the varying NaCl concentration on the separation performance of the CR/NaCl mixtures while at the fixed CR concentration of 100 ppm. With the increase of NaCl concentration, the permeability decreases only slightly. However, NaCl rejection decreases significantly from 23.6% to 7.6%, which is caused by the elevated osmotic pressure and the subsequent deterioration of membrane dielectric double layer.[175] In all cases, CR rejections are maintained more than 99%, which are slightly lower than that of the single CR filtration. This is mainly caused by the increased dye solubility and reduced dye aggregates due to the existence of NaCl.[167] On the basis of all above results, it is indisputable that high dye rejections have been achieved at high dye and salt concentrations, as well as the low salt rejection, especially at high salt concentrations.
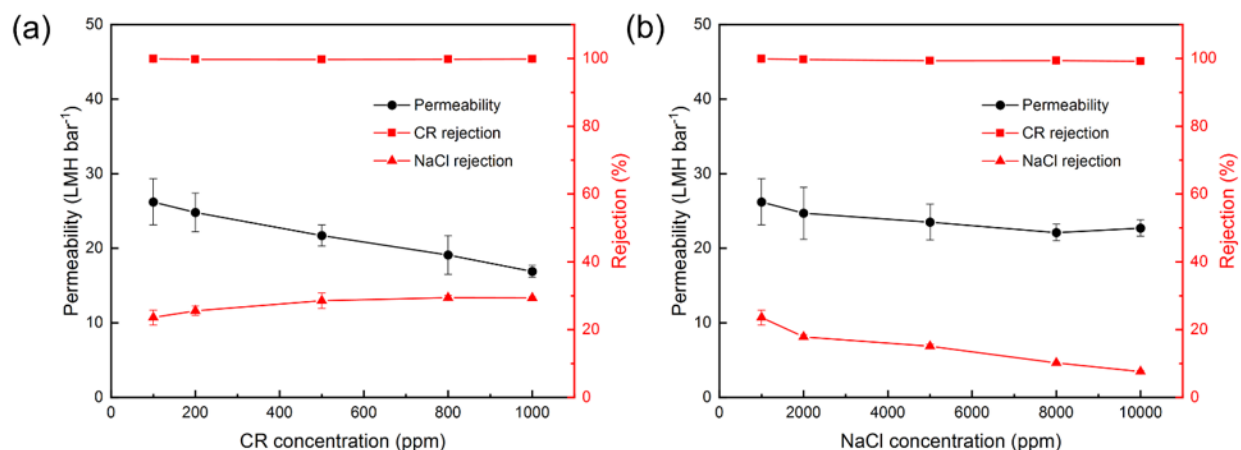
Figure 5.6 Dye/salt mixture separation of NO-0.5 membrane: (a) impact of CR concentration ranging from 100 to 1000 ppm at the fixed NaCl concentration of 1000 ppm; (b) impact of (NaCl concentration ranging from 1000 to 10000 ppm at the fixed CR concentration of 100 ppm.

Compared to other conventional methods, membrane-based filtration technologies often show high efficiency in the removal of organic dyes from wastewaters of high dye concentrations (a few hundred ppm). However, dye removal from wastewaters of very low dye concentrations (e.g., around 1 ppm) has often been neglected in the literature with the membrane-based technologies, while critically important in order to produce clean water for discharge or even for the production of potable water. To investigate the performance of NO-0.5 membrane in this extreme situation, we have undertaken the continuous filtration of a water solution of low CR concentration at 1 ppm for 10 h. As shown in Figure 5.7a, the filtration permeability decreases dramatically within the first 2 h of filtration and then maintains almost constant to the end of the filtration. The initial decrease of permeability is mainly ascribed to the CR adsorption on the membrane surface. Through the filtration, the CR has been completely removed as no CR is detected in the permeate via HPLC, which has the high sensitivity of detecting CR from a solution with a concentration of 0.05 ppm or even lower. As shown in Figure 5.7b, one can observe the obvious CR peak in the retentate, whereas there is no CR peak in the permeate at the retention time of around 5.5 min

(Figure 5.7c). This demonstrates the superior sensitivity and efficiency of NO-0.5 membrane for dye removal and the production of clean water.
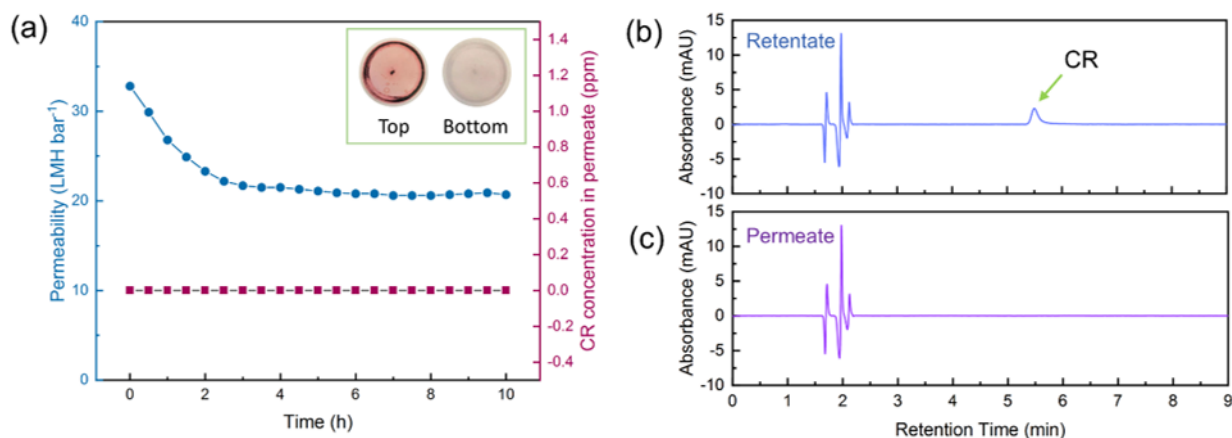
Figure 5.7 Separation performance of NO-0.5 membrane for water with a low CR concentration (1 ppm): (a) permeability and CR concentration in permeate (the inserted picture shows the top and bottom surface of NO-0.5 membrane after 10 h of CR filtration); the HPLC elution curves of the retentate (b) and permeate (c) for the CR analysis.

5.3.4 Dye purification and recovery performance

The purification and recovery test of a dye/salt mixture (100 ppm of CR and 1 g L of NaCl) at a constant-volume (300 mL) was performed with NO-0.5 membrane for four cycles at 2.0 bar. As shown in Figure 5.8a, the permeability decreases from 29.1 to 23.6 LMH bar[-1] in the first cycle, which is caused by the CR adsorption on the membrane as well as the elevated CR concentration with the gradual decrease of the mixture volume during the test. Nevertheless, the permeability recovers to 27.5 LMH bar[-1] at the start of the second cycle due to the addition of 150 mL of DI water into the retentate, then it follows the same trend of change as the first cycle. It is obvious that the permeability at the end of each cycle is almost constant. Figure 5.8b shows that the CR rejection ratio is well maintained above 99% during all four cycles of filtration, which is, however,

slightly lower than that of single component filtration of CR as found above in Figure 5.5. In each cycle, the CR concentration in the retentate increases significantly due to the high CR rejection and reaches less than 200 ppm (theoretical concentration if the rejection is 100%) when the retentate volume reduces to half. After the addition of DI water (150 mL) into the retentate at the start of each cycle, the CR concentration decreases to 99.26 ppm, 98.35 ppm, and 96.65 ppm in the second, third, and fourth cycle, respectively, compared to the initial value of 100 ppm. As shown in Figure 5.8c, the CR loss rates for each cycle are 0.94%, 1.73%, 3.35%, and 6.22%, respectively, showing the excellent dye purification and recovery performance without a significant dye loss even after four cycles.

Figure 5.8d shows NaCl concentration in the retentate and rejection during the filtration of the CR/NaCl mixture for fourth cycles. Notably, differing from the rapid increase of CR concentration (Fiure 5.9b), the NaCl concentration increases slightly in each cycle due to the low salt rejection. In addition, one can observe that the initial NaCl concentration in each cycle decreases dramatically from 1.0 in the first cycle to 0.144 g L^{-1} in the fourth cycle. Therefore, a total salt removal rate of 85.6% is achieved during the purification process. Correspondingly, NaCl rejection increases from 21.4% in the beginning to 45.0% at the end of four cycles, which is caused by the increasing concentration ratio between CR and NaCl, as well as the decreasing NaCl concentration during the filtration process. As we have discussed above with Figure 5.6a, the increasing CR concentration in the retentate can prevent the penetration of NaCl through the membrane, while the decreased osmotic pressure caused by the lower NaCl concentration can also improve the NaCl rejection. The concentration ratio between CR and NaCl increases from the initial value of 0.10 to 0.66 at the end of fourth cycle (Tables S5.2 and S5.3 and Equation S1). The enhanced ionic interaction between CR and NaCl caused by the increasing ratio of CR/NaCl leads to the increased NaCl rejection. The small deviations (Figure 5.8e) between theoretical and experimental concentrations of CR and NaCl indicate the low adsorption of both species and concentration polarization on the membrane surface, as well as the superior anti-dye-deposition performance of the membrane.
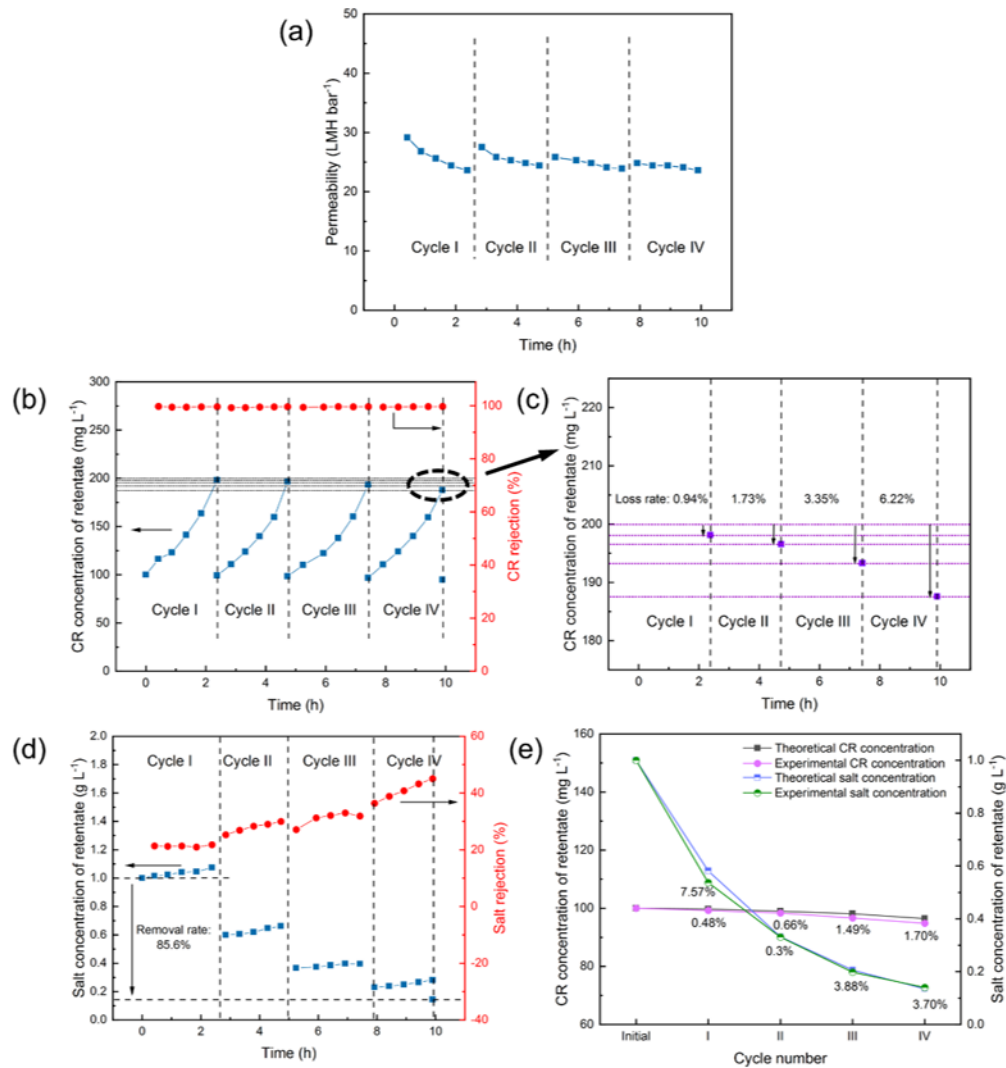
Figure 5.8 The purification and recovery test of a CR/NaCl mixture (100 ppm of CR and 1 g L of NaCl): (a) permeability in each cycle; (b) CR concentration in the retentate and its rejection in each cycle; (c) the magnified area in (b) showing CR concentration and loss rate at the end of each cycle; (d) NaCl concentration in the retentate and its rejection with in each cycle; (e) the comparison between theoretical and experimental concentrations of CR and NaCl. Test conditions: 2.0 bar and 25 °C.

5.3.5 Anti-dye-deposition performance

The test of anti-dye-deposition performance of N-0.5 and NO-0.5 was undertaken with the two-cycle filtration of the feed solution having 100 ppm of CR (see Figure 5.9). It is clearly seen that the permeability of both membranes decreases dramatically during the initial 2 h of filtration, which is caused by the concentration polarization and membrane fouling by dye deposition.[211,212] Subsequently, the permeability tends to be stable in the following 3 h. However, FDR of NO-0.5 is lower than that of N-0.5 (Figure 5.9b) in both cycles, which indicates the enhanced anti-dye-deposition performance of the former due to the formation of a hydration layer and thus the reduced adsorption of CR on the membrane surface.[34,45] In addition, NO-0.5 shows higher FRR values, which are 92.1% and 83.5% for the two respective cycles. On the contrary, the pristine N-0.5 membrane has much lower FRR values (52.7% and 48.2%). Therefore, all results demonstrate the superior anti-dye-deposition performance of TMAO-derived monomer (DNMAO) for the fabrication of polyamide TFC membranes.
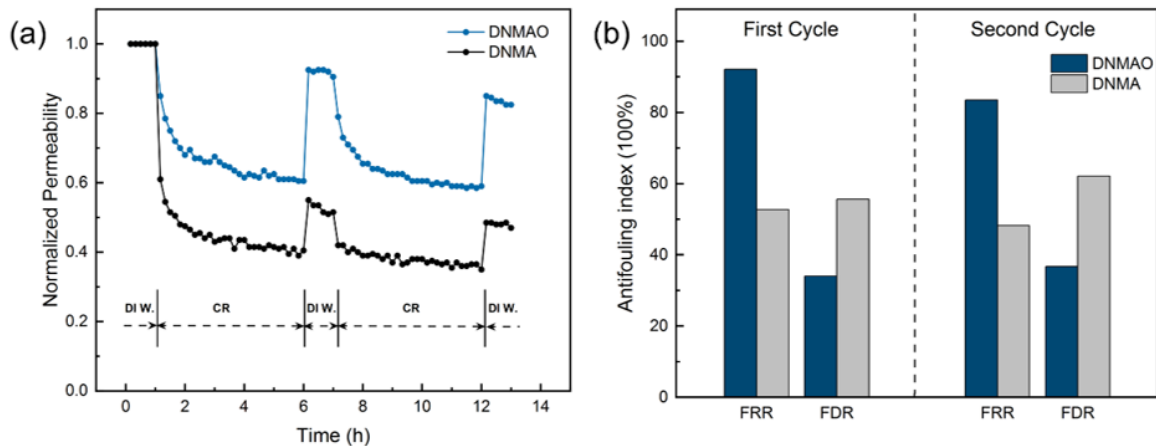
Figure 5.9 Anti-dye-deposition performances of N-0.5 and NO-0.5 by two-cycle filtration of CR (100 ppm) solution with 5 h for each cycle: (a) permeability and (b) FRR and FDR values.

5.3.6 Performance comparison with reported membranes for dye/salt separation

To highlight the superior performance of the polyamide TFC membrane fabricated in this study, a comparison is made with other reported nanofiltration membranes for dye/salt separation in terms of PWP, CR and MB rejection, and NaCl rejection. As shown in Table 5.2, most reported nanofiltration membranes show relatively low NaCl rejection, which make them good candidates for dye/salt separation. In addition to the low salt rejection, water permeability and dye rejection are other critical parameters that should be prioritized. As one can see in Table 5.2, PWPs of the most reported nanofiltration membranes are less than 30 LMH bar^{-1} in order to achieve high dye rejection. For instance, ZDNMA[175] and TA/GOQDs-1[213] membranes have low PWPs of 10.7 and 11.7 LMH bar^{-1}, respectively, with more than 99.9% of CR rejections. For other membranes like PEI/Gallic acid,[90] despite that a high PWP (~40 LMH bar^{-1}) is achieved, CR rejection (97.1%) is compromised. Notably, the optimum TFC membrane NO-0.5 in this study shows a combination of high permeability (37.5 LMH bar^{-1}) and high CR rejection (99.93%), demonstrating its superior potential for the treatment of textile wastewater and recovery of organic dyes.

Table 5.2 Performance comparison of the TFC membrane (NO-0.5) in this work with other reported membranes.

Membrane	PWP (LMH bar^{-1})	Rejection (%)		Ref.
		Dye	NaCl	
PIP/CNC-TMC	13.0	CR 99.8	~22.0	[80]
T-GO	33.4	CR 98.5 MB: 88.7	-	[205]
Catechin/chitosan NF	7.2	CR: 99.6	12.5	[138]
LNFM-2	53.3	CR: 99.6	5.6	[212]
SPEC	6.7	MB: 99.9	13.8	[214]
ZDNMA	10.7	MB: 99.9	14.3	[175]
TA/GOQDs-1	11.7	CR: 99.8 MB: 97.6	17.2	[213]
PEI/Gallic acid	~40	CR: 97.1	~3	[90]
Su0.6/TMC0.1	52.4	CR: 99.4	3.3	[215]
Fe-PEI/HPAN	11.0	CR: 99.5	7.5	[216]
PDA/rGOC3	22.8	CR: 98.9	~5	[217]
AM-PEI/HPAN	39.4	CR: 98.6 MB: 99.2	4.4	[218]
NO-0.5	37.5	CR: 99.93 MB: 99.29	9.32	This study

5.4 Conclusions

In summary, DNMAO, a new diamine monomer with a TMAO-derived "N^+-O^-" zwitterionic functionality has been designed and successfully synthesized via the facile oxidation with H_2O_2 for the fabrication of polyamide TFC membranes. The membranes fabricated with DNMAO show the higher permeability and FRR than those with un-oxidized DNMA under otherwise identical conditions. The optimum membrane NO-0.5 shows an ultrahigh PWP of 37.5 LMH bar^{-1}, a superior CR rejection of 99.93%, and a low NaCl rejection of 9.3%. The separation of CR/NaCl mixtures shows that NO-0.5 can well maintain its outstanding separation performance even under high CR/NaCl concentrations. In addition, the low dye loss rate (6.22%) and high salt removal rate (85.6%) have been achieved after four cycles filtration. Moreover, the enhanced anti-dye-deposition performance was conferred with the high FRR of 92.1% after 5 h of filtration. All these results, including permeability, rejection, and anti-dye-deposition performance, demonstrate its practical application for not only textile wastewater treatment but also purification and recovery of organic dyes.

Chapter 6 Triethanolamine-based polyester TFC membranes

Abstract

Water pollution and scarcity caused by small organic compounds (dyes and antibiotics) have attracted considerable attention due to their potential adverse effects to ecological environment and human body. Nanofiltration membranes with high performance, such as high rejection and fouling resistance, are expected to address these challenges. Herein, a new zwitterionic triethanolamine-based (Z-TEOA) monomer is proposed for the fabrication of zwitterionic polyester thin-film composite nanofiltration (ZNF) membranes. Z-TEOA is successfully prepared via the ring-open reaction between TEOA and 1,3-PS. ZNF membranes are fabricated via the interfacial polymerization under alkaline conditions. All fabricated membranes exhibit enhanced hydrophilicity and permeability due to the introduction of the zwitterionic functionality in the thin film layers. Specifically, the optimum membrane (ZNF1.5-5) shows an ultralow WCA of 20.2°, high rejections to CR (99.9%), MB (99.7%), OG (95.9%), and tetracycline (TC, 96.7%). The uncompromised MB rejection of the ZNF membrane after chlorine exposure (10000 ppm·h) indicates its excellent chlorine resistance. Furthermore, the achieved ultrahigh FRR (97.8%) for MB demonstrates its outstanding fouling-resistant performance. All results reveal its potential for applications in the treatment of wastewater from textile and pharmaceutical industries.

6.1 Introduction

Water pollution and scarcity caused by the rapid industrialization are threating the development of human society and human health.[219] Especially, the small organic compounds in the wastewater produced from textile and pharmaceutical industries are exacerbating the global water crisis and devastating our ecological environment due to their specific properties, such as aquatic toxicity, chronic toxicity to human body, and non-degradable property associated with their stable chemical structures.[220,221] Therefore, the presence of these organic compounds in water needs more attention. In order to eliminate these contaminants and alleviate their impacts on the environment, various methods have been developed, including flocculation, coagulation, adsorption, and degradation.[222,223] However, some limitations still restrict their practical applications in the

97

treatment of organic compounds-contaminated wastewaters, such as low efficiency, low selectivity, high cost, complicated operation process, as well as secondary pollution.[5]

Membrane-based separation processes, as emerging advanced separation technologies, are versatile platforms for the treatment of wastewater containing different types of contaminants via tuning the membrane pore size and other physicochemical properties.[224,225] Among them, NF membranes are attracting substantial attention for the separation of organic compounds due to their tunable molecular weight cut off range.[226] Over the decades of development, the state-of-the-art NF membranes are TFC membranes fabricated through the classical interfacial polymerization, mainly including polyamide and polyester TFC membranes.[227,228] To date, TFC polyamide membranes are generally constructed from tricarboxylic chloride and various aromatic or aliphatic amine monomers by interfacial polymerization. Despite the substantial progress that have been achieved, some limitations still restrict their extensive applications, such as low permeability and weak chlorine resistance.[229,230] Especially, TFC polyamide membranes usually exhibit severe fouling propensity due to their intrinsic surface hydrophobicity and other physicochemical characteristics.[231,232] Tremendous efforts have been dedicated to improve fouling-resistant performance of TFC polyamide membranes via various approaches, including adding hydrophilic additives (e.g., CNCs,[80] SiO$_2$,[233] or zwitterionic polymers[234]) into TFC layers and membrane surface modification with hydrophilic polymers.[235] Generally, the increased hydrophilicity can facilitate the formation of a hydration layer on the membrane surface and thus reduce the fouling propensity. However, these modifications always involve the complicated process and also may reduce the stability of TFC layers. In addition, the limited hydrophilicity achieved with these modifications is not sufficient enough to meet the requirements in practical applications.

TFC polyester NF membranes, as an alternative category, have attracted increasing attention and have been extensively explored recently. Compared to TFC polyamide NF membranes, polyester NF membranes have relatively higher hydrophilicity due to the abundant hydroxyl groups, thus produce better fouling-resistant performance.[236,237] To date, various polyhydroxyl-containing monomers have been employed, along with tricarboxylic chloride, to fabricate TFC polyester NF membranes via interfacial polymerization, including TEOA,[238,239] pentaerythritol,[240] *β*-cyclodextrin,[13,72,241] erythritol,[212,219] bis-tris propane,[242] resveratrol,[243] natural carbohydrates,[215] and porous organic polymer.[244] Though TFC polyester membranes show reduced fouling

propensities compared to TFC polyamide membranes, their fouling-resistant abilities still need further improvement in order to satisfy the requirements for practical applications.

Zwitterions, as a dominant class of hydrophilic modifiers, have been extensively used to enhance the hydrophilicity of membrane surface.[245] The equimolar oppositely charged groups in zwitterions exhibit stronger affinity to water molecules via hydrogen bonds, which facilitates the formation of a hydration layer on the membrane surface and prevents the deposition and attachment of hydrophobic contaminants.[47,183] Therefore, incorporation of zwitterionic functionalities into TFC layers is a well-established strategy and has been extensively investigated for enhancing fouling-resistant performance of TFC polyamide membranes. For instance, Li et al. has designed a zwitterionic diamine monomer (SB-based) for the fabrication of TFC polyamide membranes, which exhibited enhanced fouling resistance to bovine serum albumin.[43] In addition, another study reported a polyhydroxy-functionalized zwitterion-modified TFC polyamide membrane.[246] Though there have been some studies on the hydrophilic surface modifications of TFC polyester nanofiltration membranes, for example, with poly(acrylic acid),[41] zwitterionic TFC polyester nanofiltration membranes have not yet been reported and investigated so far, to the best of our knowledge.
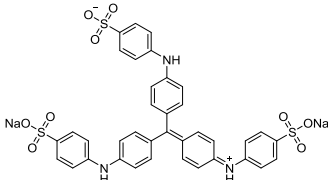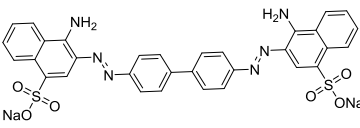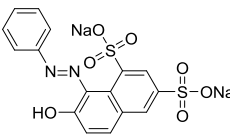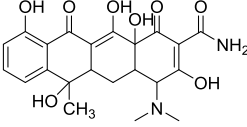
In the present work, we report the fabrication of a class of Z-TEOA TFC polyester NF membranes, along with their performance towards the purification of dye- or antibiotic-contaminated wastewaters. Z-TEOA is conveniently prepared by the ring-open reaction of tertiary amine group in TEOA with 1,3-PS. Z-TEOA endows a typical SB structure, which is one of the most widely used zwitterions in the fabrication of membranes. Zwitterionic TFC polyester NF (ZNF) membranes are subsequently fabricated through the conventional interfacial polymerization of Z-TEOA and tricarboxylic chloride under alkaline conditions. The resulting membranes have been systematically characterized for their structural and surface properties and evaluated for their performance towards the purification of dye- and antibiotic-contaminated wastewaters, with remarkable performance properties demonstrated. This work provides a new direction for the fabrication of fouling-resistant polyester membranes and demonstrates their potential applications in the treatment of wastewaters from the textile and pharmaceutical industries.

6.2 Experimental

6.2.1 Materials

Commercial PES ultrafiltration membranes (molecular weight cut-off: 100 kDa) was supplied by Synder Filtration (Vacaville, CA, USA). TEOA ($\geq$ 99.0%), 1,3-PS ($\geq$ 99.0%), TMC (98%), sodium hypochlorite (NaClO, available chlorine 4.00-4.99%), acetonitrile (anhydrous, 99.8%), MB, CR, OG, TC, and BSA (68 kDa) were obtained from Aldrich (Oakville, ON, Canada). Properties of all organic dyes and antibiotics (MB, CR, OG, and TC) are listed in Table 6.1. Sodium hydroxide (NaOH, 99.0%), NaCl (99.0%), and sodium sulfate (Na_2SO_4, 99.0%) were provided by Thermo Fisher Scientific (St. Laurent, QC, Canada). DI water was prepared using a Milli-Q purification system (Millipore, Billerica, MA, USA). All chemicals were used as received.

Table 6.1. Organic dyes and antibiotics used in this study.

Dyes	Chemical structure	Molecular weight (g mol^{-1})	λ_{max}[a] (nm)
MB		799.8	592
CR		696.7	500
OG		452.4	475
TC		444.4	276

[a] Maximum absorption wavelength.

6.2.2 Synthesis of the zwitterionic monomer Z-TEOA

Z-TEOA was synthesized via the ring-open reaction between TEOA and 1,3-PS as shown in Figure 6.1a. In brief, a round bottom flask was charged with TEOA (7.45 g, 50 mmol) in acetonitrile (10 mL). Then, 1,3-PS (7.32 g, 60 mmol) in acetonitrile (15 mL) was added dropwise into the above TEOA solution under stirring. The resulting mixture was stirred at 50 °C for 96 h,[42] with white precipitate formed gradually during the reaction. Afterwards, the mixture was cooled down and filtered via vacuum filtration. The obtained wet white solid was dissolved in DI water and filtered again to remove insoluble byproducts. The aqueous filtrate containing Z-TEOA was washed with acetonitrile for at least three times until fine white powder was produced, which was collected via vacuum filtration and dried overnight in a vacuum oven at 80 °C for use (yield: 91%).
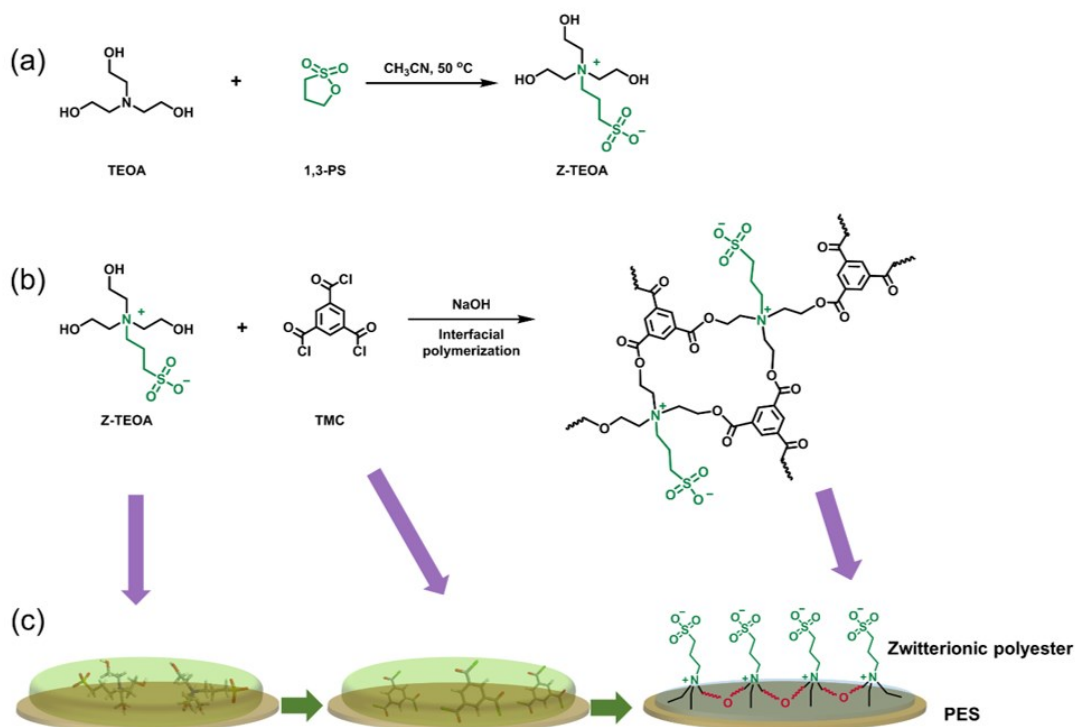
Figure 6.1 (a) Synthesis of Z-TEOA; (b) proposed cross-linked polyester structure of the TFC layer between Z-TEOA and TMC by interfacial polymerization; (c) schematic illustration of the fabrication process and structure of zwitterionic polyester membranes.

6.2.3 Fabrication of the TFC polyester nanofiltration membranes

The TFC polyester nanofiltration membranes were fabricated by the conventional interfacial polymerization on PES ultrafiltration membranes as shown in Figure 6.1b-c. Briefly, a PES membrane was fixed in a mould with only the top surface exposed to TEOA or Z-TEOA aqueous solution at different concentrations (wt%) for 5 min. Then, the excess solution was removed by a rubber roller. Afterwards, a hexane solution of TMC (0.2 wt%) was poured into the mould, allowing polymerization for a certain time (2 or 5 min). The final membrane was finally post-treated at 60 °C for 10 min. The membranes fabricated with TEOA are termed as NFx-y, and those fabricated with Z-TEOA are termed as ZNFx-y, where x presents TEOA or Z-TEOA concentration used for interfacial polymerization and y presents the polymerization time.

6.2.4 Characterizations

The chemical structures of TEOA and Z-TEOA were characterized with ^{1}H NMR Bruker 300 MHz. FTIR spectra were obtained on a Thermo Scientific Nicolet 6700 Analytical FTIR spectrometer. WCA measurements were performed on a contact angle system (VCA, AST Products, Inc.). XPS was performed on a Thermo Scientific Theta Probe XPS spectrometer with a monochromatic Al Kα X-ray source at a spot area of 400 μm. Membrane surface morphologies were observed via a FE-ESEM after platinum coating (ca. 4 nm). The surface roughness of the TFC polyester membranes was investigated with an AFM (Tosca 400, Anton Paar) in the tapping mode.

6.2.5 Membrane performance tests

All membrane separation performance tests were conducted at 6.0 bar using a stirred dead-end filtration cell at a stirring speed of 350 rpm. The effective area of membrane filtration was 12.56 cm^2. The NF membranes were compacted at 7.0 bar with DI water for around half an hour to reach a steady state before each test. In this study, dye solutions at 100 ppm and salt solutions at 1.0 g L^{-1} were generally employed as feed solutions unless otherwise specified.

Pure water permeability (P, LMH bar^{-1}) of the fabricated NF membranes is calculated by using the following equation:

$$P = \frac{V}{A \times t \times \Delta P} \qquad (6.1)$$

where V is the volume (L) of the permeate, A is the effective filtration area (m^2), t is the operation time (h) and ΔP is the trans-membrane pressure (bar). The solute rejection (R) is calculated according to:

$$R = \left(1 - \frac{C_p}{C_f}\right) \times 100\% \qquad (6.2)$$

where C_p and C_f are solute concentrations of the permeate and feed solutions, respectively. Dye concentration was determined with a UV-vis spectrophotometer (Agilent Cary 8454). Salt concentration was measured using a conductivity meter (OAKTON conductivity meter, CON 11 series, Vernon Hills, IL USA).

6.2.6 Chlorine resistance performance

To evaluate the chlorine resistance performance of the fabricated polyester NF membranes, the membranes were chlorinated by the static immersion of the fabricated membranes in NaClO solution (1000 ppm) for different time (1 h, 5 h, and 10 h). Afterwards, each chlorinated membrane was thoroughly rinsed by DI water and stored in DI water for at least 12 h prior to the subsequent performance tests. The degree of chlorination is expressed as ppm·h (1000, 5000, or 10000 ppm·h).

6.2.7 Fouling-resistant performance

The fouling-resistance performance tests were carried out at 6.0 bar with three cycles of filtration with different model foulants, which were MB (100 ppm) and BSA (1.0 g L^{-1}), respectively. Firstly, pure water permeability was recorded as the original permeability (J_0) for 0.5 h. Then, DI water was replaced with a corresponding model foulant. The filtration permeability (J_1) was recorded every 5.0 min for 2.0 h. The normalized flux (J_1/J_0) was employed to quantify the fouling-resistant ability during the filtration process. After 2.0 h of filtration, the fouled membrane was cleaned by hydraulic wash with DI water for 0.5 h, followed by the measurement of pure water permeability

again (J_2). This whole process was repeated three times. FRR is calculated according to the following equation:

$$FRR = \left(\frac{J_2}{J_0}\right) \times 100\% \qquad (6.3)$$

6.3 Results and Discussion

6.3.1 Synthesis and characterization of Z-TEOA

As shown in Figure 6.1a, Z-TEOA is prepared via the ring-open reaction between TEOA and 1,3-PS. With the ring-open reaction, the tertiary amine group in TEOA can form positively charged quaternary ammonium salt, while the sultone in 1,3-PS transfers to a negatively charged sulfonate, producing the equimolar oppositely charged zwitterionic structure (Z-TEOA). The chemical structures of TEOA and Z-TEOA have been characterized with ^{1}H NMR spectroscopy. Figure 6.2a shows the ^{1}H spectrum of TEOA, where the triplet peak a at 3.56 ppm (t, 6 H) is ascribed to the methylene group next to the hydroxyl group. Another triplet peak b at 2.62 ppm (t, 6H) is attributed to the methylene group close to the tertiary amine group. As shown in Figure 6.2b, after zwitterionic functionalization by 1,3-PS, one can see that all the ^{1}H NMR peaks seen in TEOA shift to the relatively lower fields (higher chemical shifts) in the spectrum of Z-TEOA due to the formation of the quaternary ammonium salt in Z-TEOA. In addition, three new peaks at 3.54 ppm, 2.68 ppm, and 2.14 ppm are assigned to the three corresponding methylene groups in 1,3-PS. Therefore, based on the above ^{1}H NMR results, Z-TEOA has been successfully synthesized via the ring-open reaction.
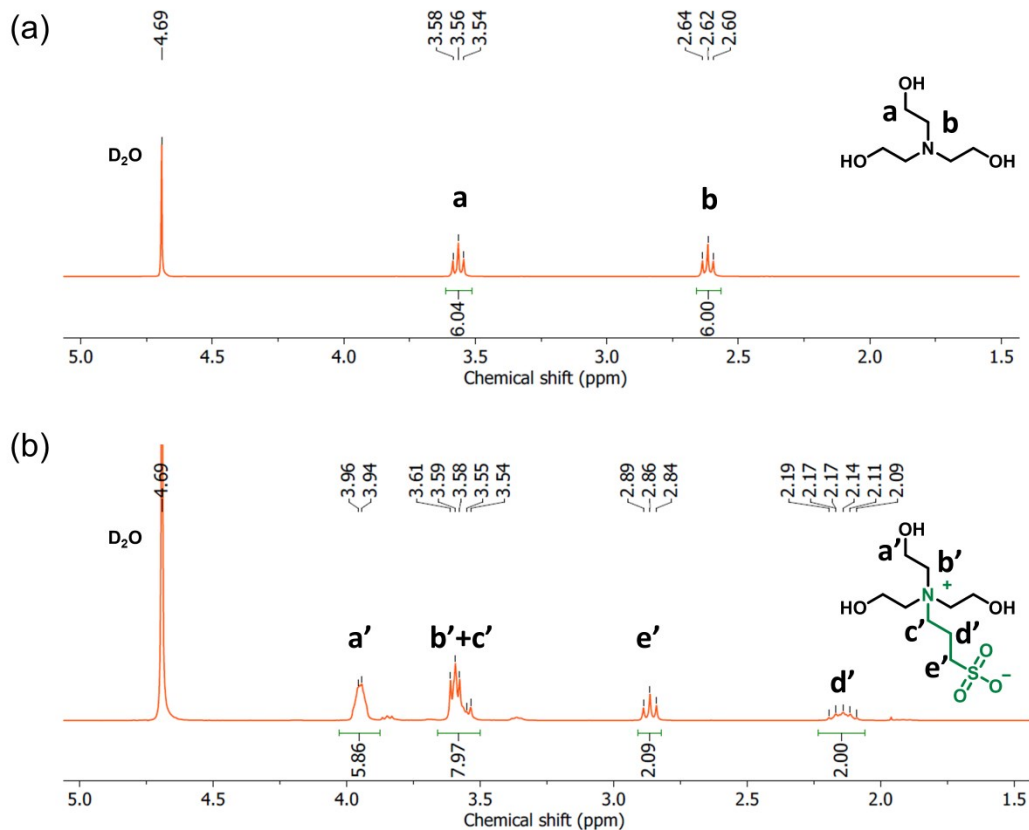
Figure 6.2 ^{1}H NMR spectra of TEOA (a) and Z-TEOA (b).

6.3.2 Fabrication and characterization of TFC polyester NF membranes

The surface characteristics of TFC polyester NF membranes have been investigated by ATR-FTIR and WCA measurements. Figure 6.3a shows the ATR-FTIR spectra of three types of membranes, the pristine PES ultrafiltration membrane, zwitterionic polyester NF membranes (ZNF), and non-zwitterionic polyester NF membranes. Compared to the pristine PES membrane, all TFC membranes exhibit the characteristic peaks at 3680-3130 cm^{-1} and 1730 cm^{-1}, which are ascribed to the O-H stretching and C=O stretching, respectively.[219,247] This indicates the successful formation of thin film polyester layers on the PES membranes. Figure 6.3b shows the WCAs of the pristine PES membranes and TFC polyester NF membranes. Among them, the pristine

membrane shows a relatively higher WCA (68.7º) due to the intrinsic hydrophobicity. With the formation of thin film polyester layers, WCA decreases to lower values. Especially, with the increase of Z-TEOA concentration from 0.5 to 2.0 wt% and polymerization time from 2 to 5 min, WCA decreases from 37.4º for ZNF0.5-2 to 18.9º for ZNF2.0-5. Compared to that (68.7º) of the pristine PES membrane, these reduced WCAs indicate tremendous improvements in the hydrophilicity of ZNF membranes. In addition, the non-zwitterionic membrane, NF1.5-2, shows a significantly higher water contact angle (55.1º) compared to ZNF1.5-2 (24.3º), which was fabricated under the same monomer concentration and polymerization time. All photos of water contact angles are provided in Figure S6.1. These results demonstrate that the zwitterionic-functionalized monomer (Z-TEOA) has an enormous potential for the enhancement of membrane surface hydrophilicity and, in turn, fouling-resistant ability.
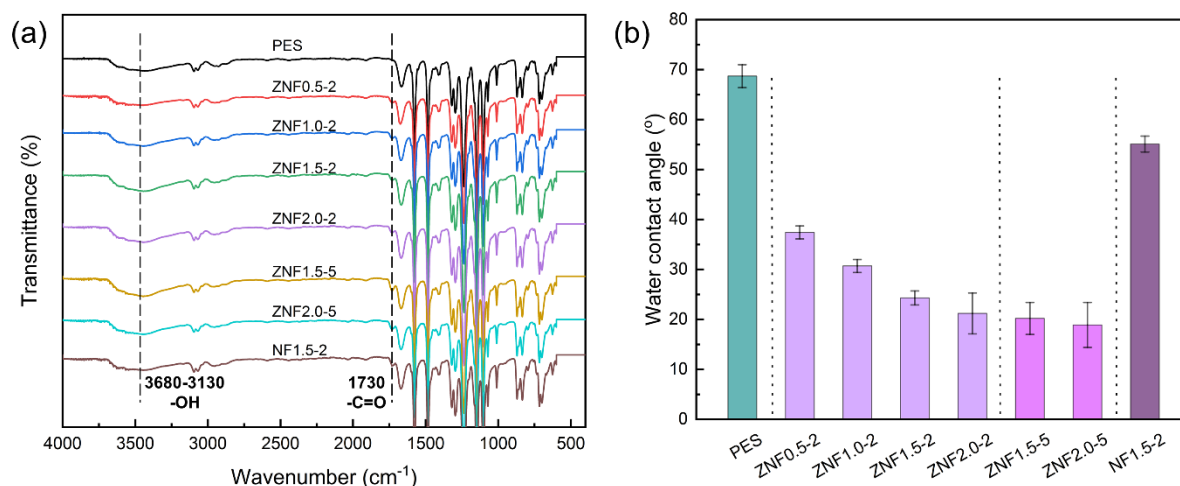
Figure 6.3 Membrane surface characterization: (a) ATR-FTIR spectra; (b) water contact angles.

The elemental compositions of the fabricated polyester NF membranes have been characterized with XPS. As shown in Figure 6.4, the pristine PES membrane presents the characteristic XPS peaks at 533, 287, and 168 eV, which are assigned to O 1s, C 1s, and S 2p, respectively. The unexpected N 1s peak at 400 eV is ascribed to the additives or extra surface coating layer

106

introduced during the fabrication of PES ultrafiltration membranes by the manufacturer.[149,248] Compared to the pristine PES membrane, TFC polyester NF membranes exhibit intensified N 1s peak due to the existence of tertiary amine group in TEOA or Z-TEOA and weakened S 2p peak due to the formation of thin film polyester layers. In addition, ZNF1.5-2 shows a relatively higher S content compared to NF1.5-2, which is mainly ascribed to the high S content of Z-TEOA after the ring-open reaction of TEOA with 1,3-PS. One can also see that the S 2p peak in NF1.5-2 is almost invisible because of the formation of the thin film layer. All detailed elemental compositions are listed on Table 6.2. Based on the above results, a thin film polyester layer has been successfully constructed on the PES ultrafiltration membranes.
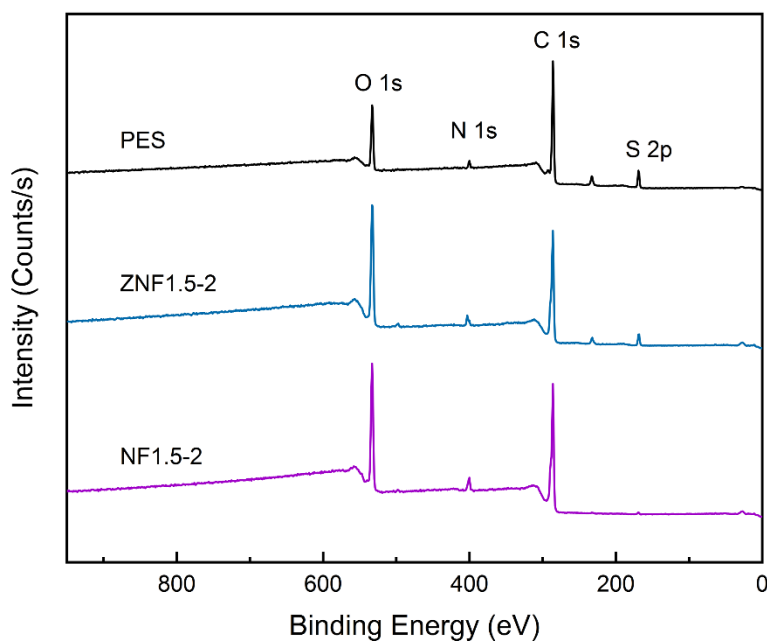
Figure 6.4 XPS spectra of the pristine PES ultrafiltration membrane, ZNF1.5-2 membrane, and NF1.5-2 membrane.

Table 6.2 Elemental compositions of membrane surfaces.

Membrane	Composition (%)			
	C	O	N	S
PES	72.7	19.2	3.0	5.1
ZNF1.5-2	63.8	29.6	4.0	2.6
NF1.5-2	66.7	28.0	4.8	0.5

The membrane surface morphology and roughness have been investigated with SEM and AFM, respectively. As shown in Figure 6.5a, the pristine PES membrane has a relatively smooth surface with Ra = 10.8 nm. Upon the formation of thin film polyester layer on the membrane surface, one can observe clearly that the membrane surfaces exhibit grainy and microspheric structures. In addition, it is found that the size and number of microspheres increase with the increase of monomer concentration from 0.5 to 1.5 wt% (ZNF0.5-2 vs ZNF 1.5-2) and interfacial polymerization time from 2 to 5 min (ZNF1.5-2 vs ZNF1.5-5). Moreover, NF1.5-2 fabricated under identical conditions as ZNF1.5-2 shows a relatively larger average microsphere size, which may be caused by the stronger hydrophobicity of TEOA compared to Z-TEOA. With its relatively stronger hydrophobicity, TEOA is expected to have a higher diffusion coefficient from aqueous solution into organic solution (hexane) during the interfacial polymerization, which renders a higher polymerization rate and in turn the formation of larger sized microspheres.[195,249] Figure 6.5b shows the surface roughness data of the membranes determined with AFM. The surface roughness also gradually increases from 10.8 nm for the pristine PES membrane to 14.1 nm for ZNF1.5-5 membrane with the increase of monomer concentration from 0.5 to 1.5 wt% and polymerization time from 2 min to 5 min. These characteristic surface morphology results can further demonstrate the formation of the TFC polyester layer on the surface of PES membrane.
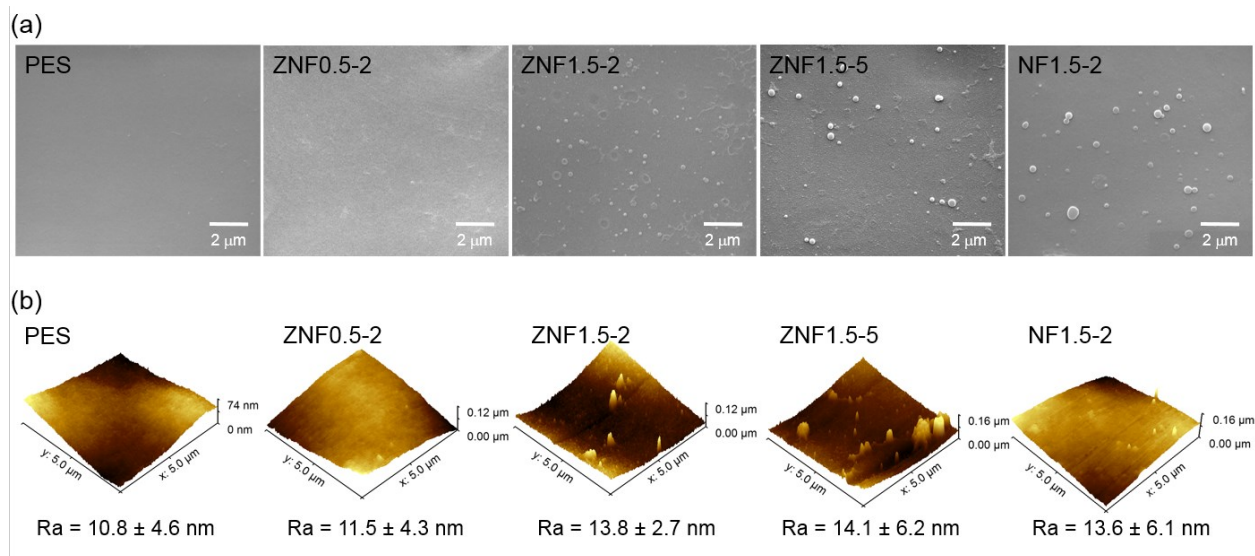
Figure 6.5 (a) SEM images and (b) AFM images of membranes (PES, ZNF0.5-2, ZNF1.5-2, ZNF1.5-5, and NF1.5-2).

6.3.3 Separation performance of TFC polyester membranes

The separation performance of TFC polyester NF membranes have been systematically evaluated for the filtration of three organic dyes of different molecular weights, CR, MB, and OG. As shown in Figure 6.6a, ZNF0.5-2 fabricated at the lowest monomer concentration (0.5 wt% of Z-TEOA) shows the highest pure water permeability (62.2 LMH bar^{-1}), which is more than twice of that (24.3 LMH bar^{-1}) of NF0.5-2 fabricated at otherwise identical conditions. In addition, the pure water permeability decreases from 62.2 to 22.1 LMH bar^{-1} for ZNF membranes while that of NF membranes decreases from 24.3 to 12.1 LMH bar^{-1} with the increase of both monomer concentrations from 0.5 wt% to 2.0 wt%. Compared to the pure water permeability data, all membranes show reduced filtration permeabilities toward the solutions of CR, MB, and OG (Figure 6.6b-d) due to the concentration polarization and the deposition of these organic dye molecules on the membrane surface. Figure 6.6b shows that the rejection of CR is well maintained at a high level (>99%) with all TFC membranes, even with those fabricated at the lowest monomer concentration. However, as shown in Figure 6.6c, ZNF membranes show lower MB rejections at

low monomer concentrations (1.0 wt% and 0.5 wt%) compared to NF membranes. Given the smaller molecular weight of CR than MB (696.7 and 799.8 g mol^{-1}, respectively), the relatively higher rejection towards CR is ascribed to the propensity of CR molecules to form larger aggregates in aqueous solutions.[167] Figure 6.6d shows that all membranes have lower OG rejections (<90%) compared to those of CR and MB due to its smallest molecule molecular weight (452.4 g mol^{-1}) among three dyes. Therefore, the separation performance towards OG requires further improvement by optimizing the fabrication parameters.
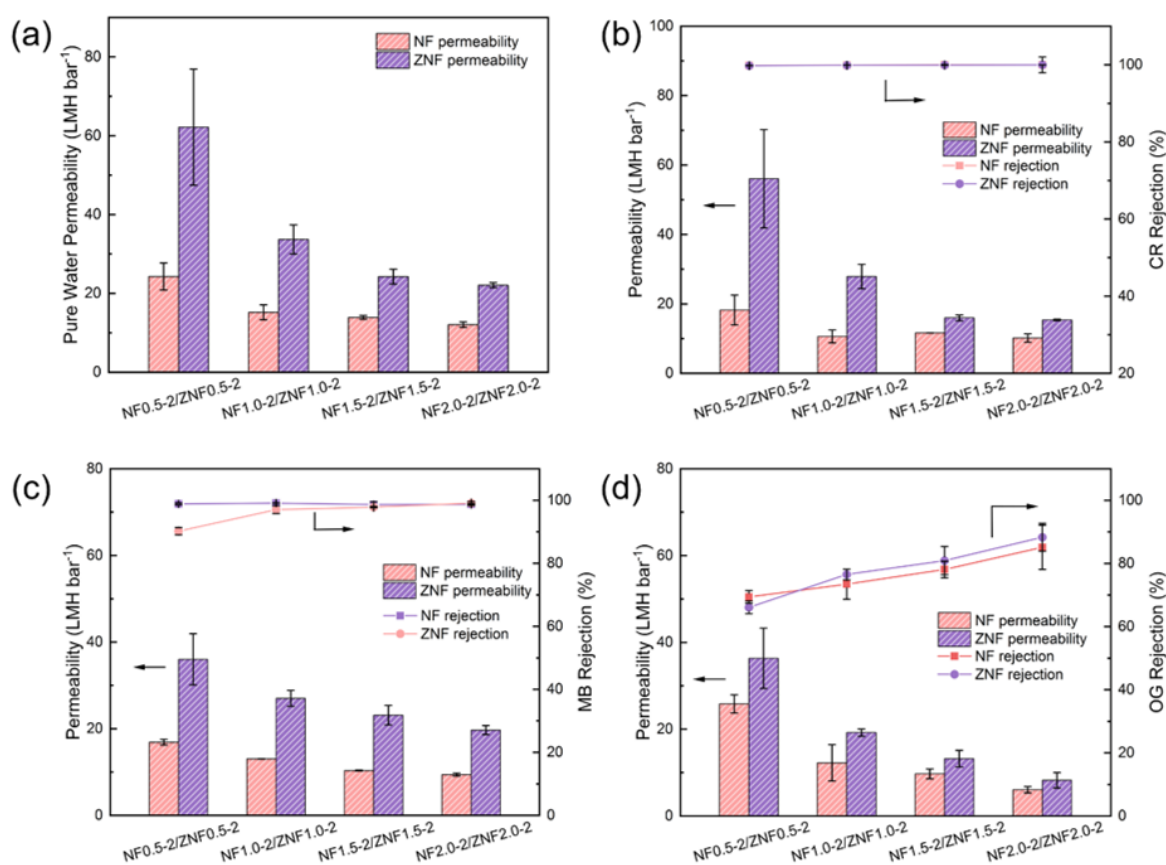
Figure 6.6 Separation performances of TFC polyester NF membranes (NF0.5-2/ZNF0.5-2, NF1.0-2/ZNF1.0-2, NF1.5-2/ZNF1.5-2, and NF2.0-2/ZNF2.0-2): (a) pure water permeability; (b) CR filtration permeability and rejection; (c) MB filtration permeability and rejection; (d) OG filtration permeability and rejection.

In order to further improve the filtration performance of ZNF membranes, the interfacial polymerization time has been increased from 2 min to 5 min with the resulting membranes termed as ZNFx-5, in which x presents the monomer concentration. As shown in Figure 6.7a, the pure water permeability decreases dramatically compared to that of the corresponding membrane fabricated with 2 min of interfacial polymerization (Figure 6.6a). These TFC polyester NF membranes have been investigated for the separation of aqueous solutions of two organic dyes (MB and OG) and one organic antibiotic (TC). Figure 6.7b shows the filtration of MB solutions. One can see that the filtration permeabilities are almost similar to the corresponding pure water permeabilities, indicating their excellent fouling-resistant ability. With all ZNFx-5 membranes, MB rejection is maintained over 98%, which is relatively higher than those of the ZNFx-2 membranes (Figure 6.6c) fabricated with 2 min of the interfacial polymerization. Especially, ZNF0.5-5 shows a significantly improved MB rejection from 90.2% (ZNF0.5-2 in Figure 6.6c) to 99.0% (Figure 6.7b).

Meanwhile, the OG rejection has also been significantly improved to up 96.0% (Figure 6.7c). Figure 6.7d shows the rejection of the organic antibiotic TC. The rejection increases from 22.1 to 96.1% with the increase of monomer concentration from 0.5 (ZNF0.5-5) to 2.0 wt% (ZNF2.0-5). In addition to these organic compounds, the filtration of aqueous solutions containing inorganic salts (NaCl and Na_2SO_4) has also been investigated with the ZNFx-5 membranes. As shown in Figure 6.7e-f, the rejection of NaCl increases from 23.1% to 45.2% with the increase of Z-TEOA concentration from 0.5 to 2.0 wt% during interfacial polymerization, while the rejection of Na_2SO_4 increases from 60.5% to 85.9%. Therefore, on the basis of the above separation results, ZNFx-5 membranes can not only effectively remove organic dyes and antibiotics, but also partially removal inorganic salts, which are commonly used additives in textile and pharmaceutical industries.[99,250,251]
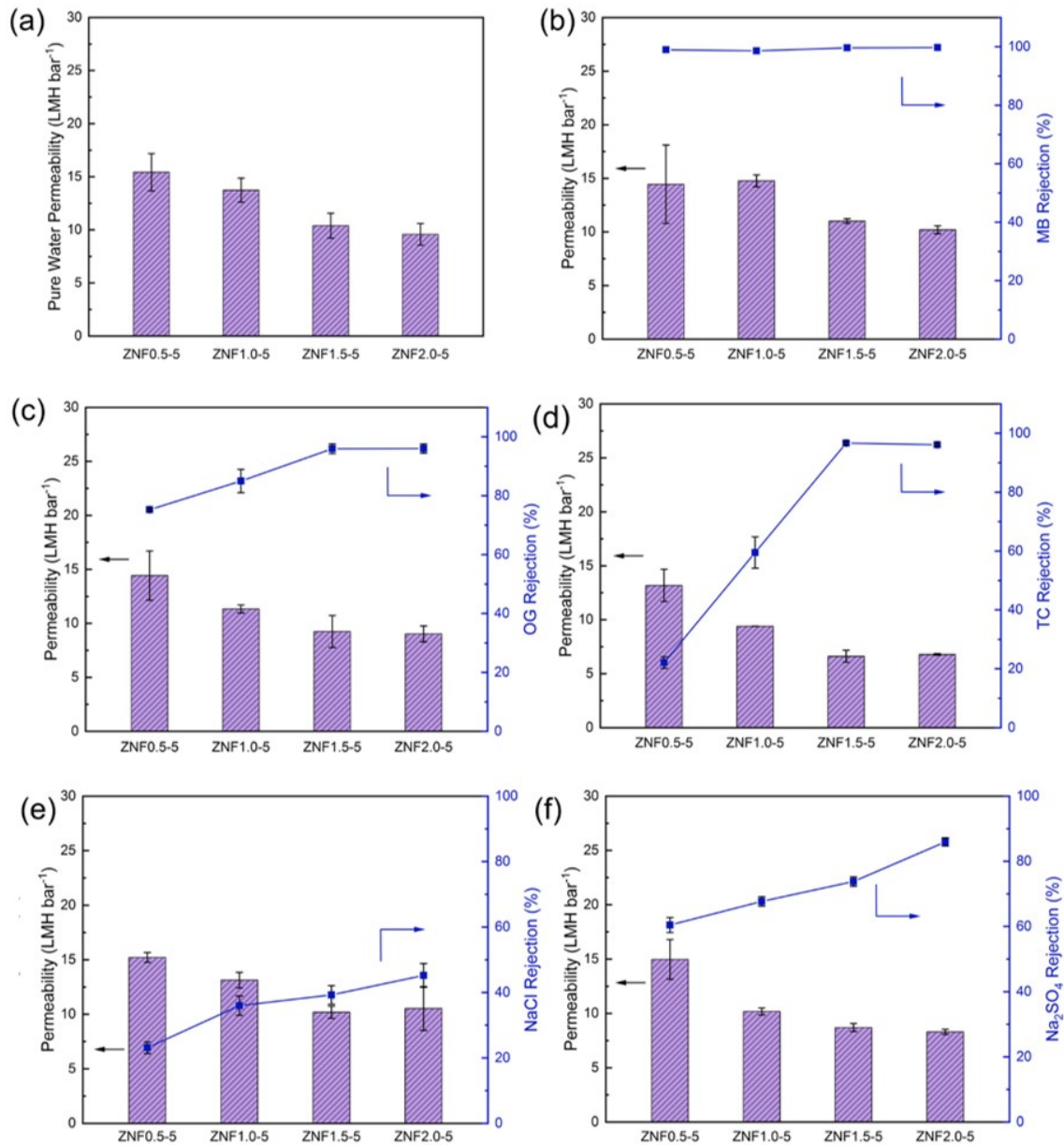
Figure 6.7 Separation performance of TFC polyester nanofiltration membranes (ZNF0.5-5, ZNF1.0-5, ZNF1.5-5, and ZNF2.0-5): (a) pure water permeability; (b) MB filtration permeability and rejection; (c) OG filtration permeability and rejection; (d) TC filtration permeability and rejection; (e) NaCl filtration permeability and rejection; (f) Na_2SO_4 filtration permeability and rejection.

6.3.4 Chlorine-resistant performance

To investigate the effects of chlorine exposure on the separation performance of ZNF membranes, the filtration of an MB solution (100 ppm) has been performed with chlorinated ZNF1.5-5 membrane, which have been chlorinated at various chlorine exposure doses from 0 ppm·h to 10000 ppm·h, at different pH values (10, 7, and 4). Figure 6.8a shows that the pure water permeability data. One can observe that the pure water permeability increases gradually from 10.4 to 12.3 LMH bar^{-1} with the increase of chlorine expose dose. As presented in Figure 6.8b, the chlorinated membranes show only a slight decrease of MB rejection from 99.7 to 99.2% after the 10000 ppm·h exposure of NaClO, indicating their excellent chlorine-resistant performance. In addition, Figure 6.8c-f show the separation performance of the chlorinated ZNF membranes at pH 7 and 4. Following the similar patterns seen with Figure 6.8a-b, the pure water permeability increases from 10.4 to 15.6 LMH bar^{-1} and 15.8 LMH bar^{-1} at pH of 7 and 4, respectively, with only slight decreases of MB rejection to 99.3% (pH 7) and 99.4% (pH 4). These slightly increased pure water permeabilities may be ascribed to the increased surface hydrophilic property upon chloration of the membrane.[252] Therefore, the above results demonstrate the excellent chlorine resistant performance of the TFC polyester membrane.
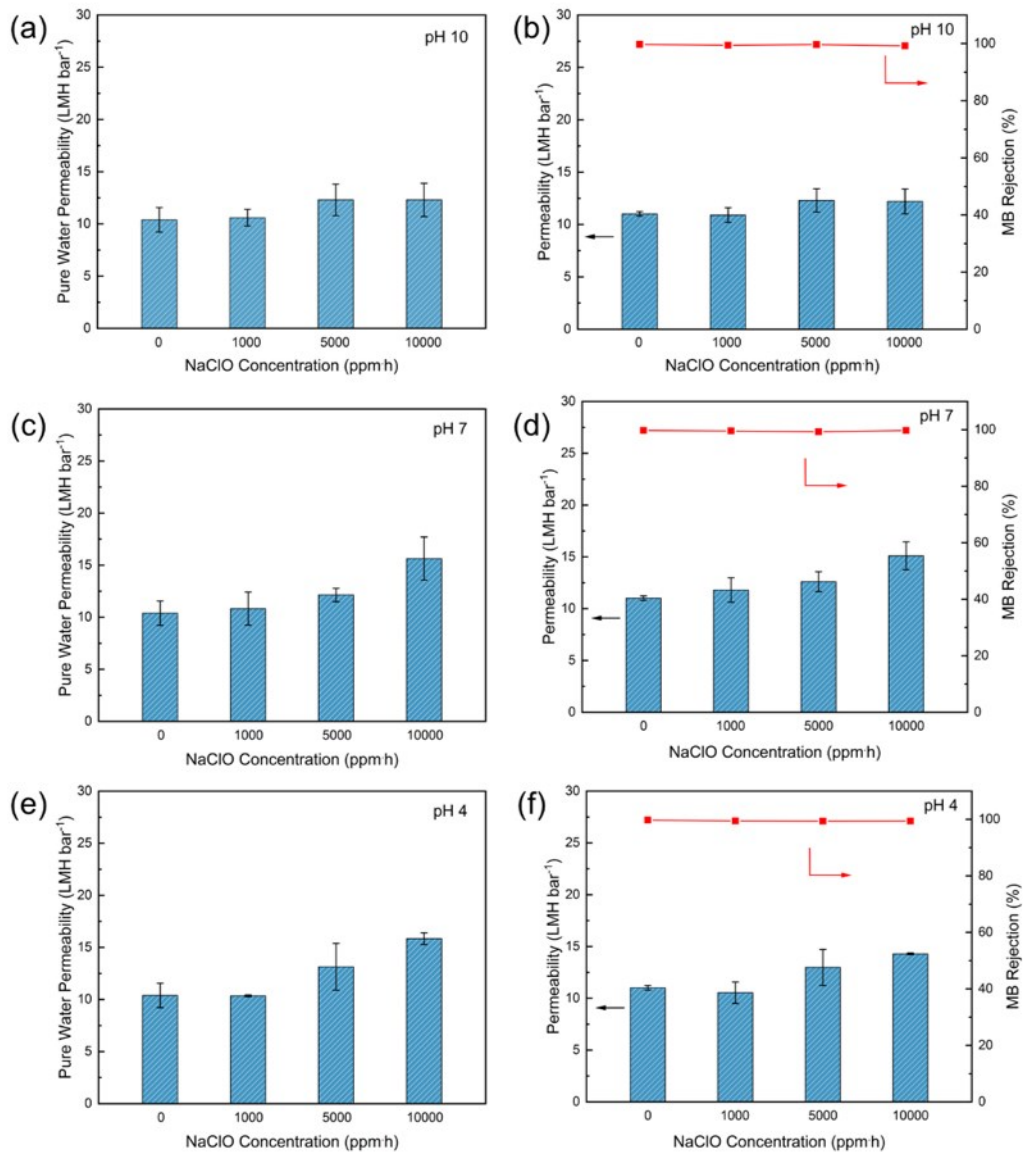
Figure 6.8 Separation performance of chlorinated ZNF1.5-5 following an exposure to different chlorine doses varying from 0 ppm·h to 10000 ppm·h toward filtration of MB solution (100 ppm) at different pH values: pure water permeability (a) and MB filtration permeability and rejection (b) at pH 10; pure water permeability (c) and MB filtration permeability and rejection (d) at pH 7; pure water permeability (e) and MB filtration permeability and rejection (f) at pH 4.

6.3.5 Fouling-resistant performance

The fouling-resistant performance of ZNF1.5-5 and NF1.5-5 membranes has been investigated by three-cycle filtration of MB (100 ppm) and BSA (1.0 g L^{-1}) solutions. As shown in Figure 6.9a, NF1.5-5 exhibits a dramatic decrease in permeability in the filtration of MB solution, which is caused by the simultaneous deposition of MB molecules and concentration polarization on the membrane surface.[253,254] However, ZNF1.5-5 shows an undifferentiated filtration permeability compared to the initial pure water permeability after the feeding of MB solution. After the hydraulic washing with DI water, the FRR of ZNF1.5-5 can achieve 114.7% (Figure 6.9c), while that of NF1.5-5 is 84.0%. After the following two cycles of MB filtration and washing of DI water, the FRR values for ZNF1.5-5 are 112.2% (second cycle) and 111.6% (third cycle), while those of NF1.5-5 are 76.5% (second cycle) and 74.7% (third cycle). However, considering that the maximum theoretical FRR is 100%, the above extraordinarily high FRR values (>100%) may be caused by the cleaning with DI water after the first cycle of filtration. In order to better evaluate FRR values of both membranes, Figure 6.9d shows alternative FRR results, which are calculated based on the pure water permeability after the DI water cleaning in the first cycle. It still shows that ZNF1.5-5 has ultrahigh FRR values, which are 97.8% (second cycle) and 97.3% (third cycle), while NF1.5-5 exhibits FRR values of 91.1% (second cycle) and 88.9% (third cycle). In addition, both membranes have MB rejections of around 99.8% (Figure 6.9b), which indicate that the above extraordinary FRR values (>100%) are not caused by the damage of thin film polyester layers during the washing with DI water. Therefore, on the basis of the above filtration results, the fouling-resistant performance of ZNF1.5-5 towards the filtration of MB has been significantly improved compared to NF1.5-5 due to the introduction of the zwitterionic functionality.
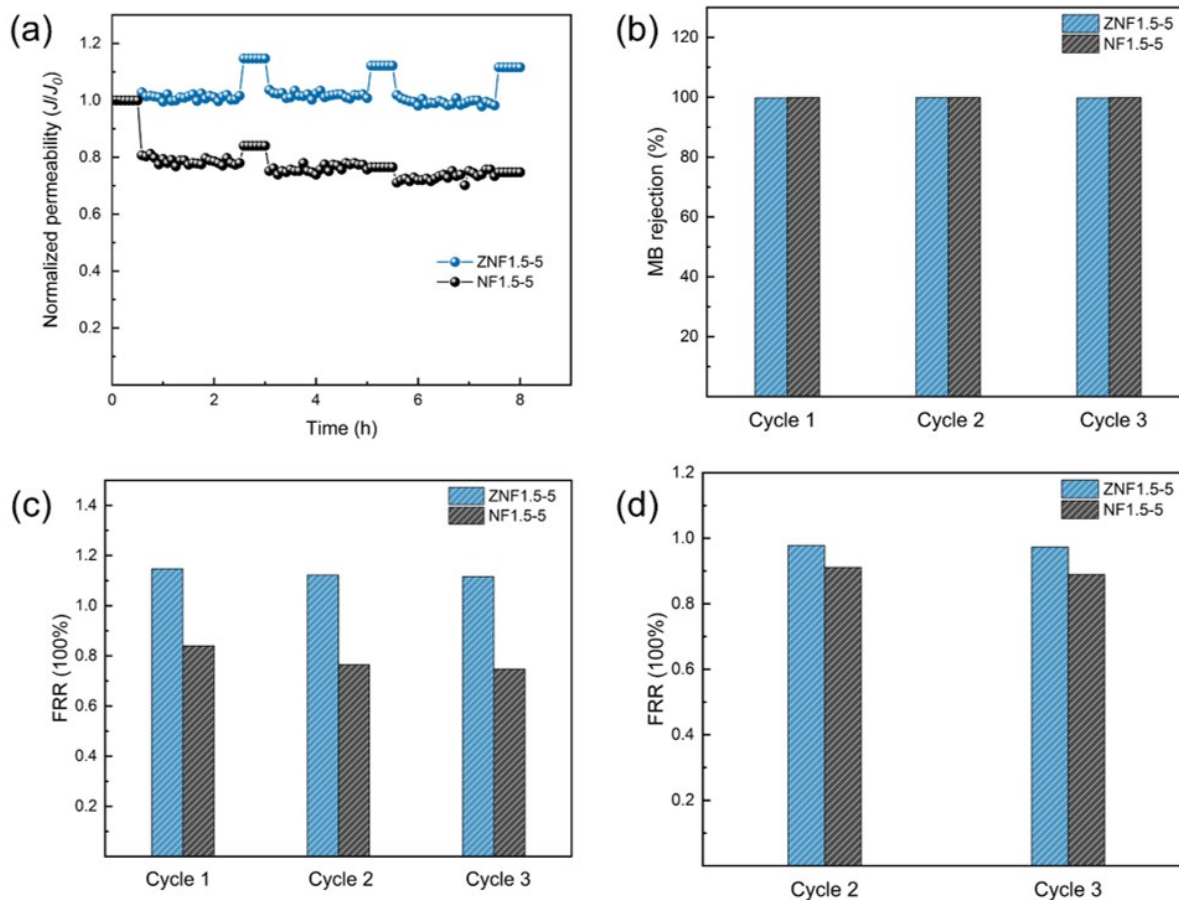
Figure 6.9 Fouling-resistant performance of ZNF1.5-5 and NF1.5-5 by three-cycle filtration of MB (100 ppm) solution: (a) permeability; (b) rejection; (c) FRR (calculated based on the initial pure water permeability); (d) FRR (calculated based on the pure water permeability after the cleaning in the first cycle).

In addition to the MB filtration, BSA (1.0 g L^{-1}) has also been chosen as another model contaminant to further evaluate the fouling-resistant performance of the two TFC membranes, ZNF1.5-5 and NF1.5-5. As shown in Figure 6.10a, both membranes show obvious permeability decreases during the filtration of BSA. After the hydraulic washing with DI water, FRRs are 88.4% and 70.6% for ZNF1.5-5 and NF1.5-5, respectively, after the first cycle (Figure 6.10b). Subsequently, FRR of ZNF1.5-5 decreases to 88.4% and 83.8% after the 2nd and 3rd cycle,

respectively, while that of NF1.5-5 decreases to 66.5% and 63.1%. The BSA filtration results further demonstrate the enhanced fouling-resistant performance of ZNF1.5-5 after the introduction of the zwitterionic functionality. Therefore, the fouling-resistance results with both model contaminants (MB and BSA) confirms the significantly improved performance of ZNF membranes and their potential applications.
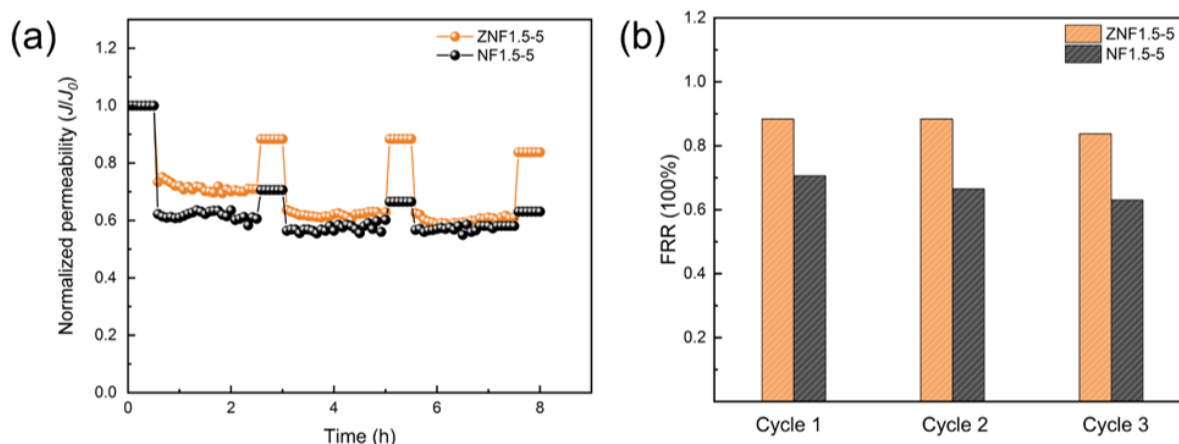
Figure 6.10 Fouling-resistant performance of ZNF1.5-5 and NF1.5-5 by three-cycle filtration of BSA (1.0 g L^{-1}) solution: (a) permeability; (b) FRR.

6.4 Conclusions

In this work, a zwitterionic TEOA-based monomer, Z-TEOA, has been successfully synthesized with its structured verified with ^{1}H NMR. This monomer has been used for the fabrication of zwitterionic polyester thin-film composite NF (ZNF) membranes via the interfacial polymerization with TMC as a comonomer under alkaline conditions. The effect of monomer concentrations and polymerization time on the membrane separation performance have been investigated in detail. With the introduction of zwitterionic functionality into the thin film layer, the fabricated membranes exhibit enhanced hydrophilicity and permeability due to the strong water affinity of

zwitterions. The optimum membrane (ZNF1.5-5) shows excellent rejections to three organic dyes (CR, MB, and OG) and an organic antibiotic (TC). Meanwhile, it also exhibits the uncompromised dye rejection after chloration, indicating its excellent chlorine-resistance. In addition, an ultrahigh FRR of 97.8% has been achieved with ZNF1.5-5 for the filtration of MB solution, demonstrating its outstanding fouling-resistant performance. All these results suggest the strong potential of this class of high-performance zwitterionic TFC polyester nanofiltration membranes for the treatment of textile and pharmaceutical wastewaters.

Chapter 7 Contributions and significance of thesis research, and suggestions for future work

7.1 Contributions and significance of thesis research

TFC membranes play a significant role in the treatment of wastewater for production of clean water and recycle of valuable contaminants, especially small organic compounds contaminated wastewaters from textile and pharmaceutical industries. However, the limited permeability and fouling propensity of TFC membranes still restrict their wide applications. To address the current challenges and limitations in TFC membranes, it is essential to develop new methodologies for the construction of thin film selective layers. In addition, development of new types of zwitterions with stronger hydrophilicity for the modification of TFC membranes is needed in order to enhance their fouling-resistant performance in the treatment of organic compounds contaminated wastewaters.

The contributions and significance of this thesis research can be summarized according to three aspects: (i) preparation of functional materials, including polydopamine-modified CNCs, TMAO-based zwitterion, SB-based diamine zwitterion, and SB-based polyhydroxy zwitterion; (ii) fabrication methodology of thin film selective layers and porous supporting layers, including bioinspired chemistry, interfacial polymerization, and electrospinning; (iii) systematic performance investigation of TFC membranes, including PWP, separation efficiency, and fouling-resistance.

(i) Synthesis of functional materials

Four functional materials have been successfully synthesized and characterized. All these materials have the potential to serve as active monomers for the construction of thin film selective layers, due to their functional and active groups. For instance, polydopamine-modified CNCs have substantial quinonoid active sites, which are able to form cross-linked networks with amine-functionalized monomers, such as PEI. Other synthesized functional materials (DNMAO, Z-DNMA, and Z-TEOA), as zwitterions possessing diamine or trihydroxy structures, are able to react with dopamine or TMC to form thin film selective layers. In particular, DNMAO, inspired from

TMAO, as a new generation zwitterion, has been designed, synthesized and employed for the fabrication of TFC membranes.

(ii) Fabrication methodology

A new strategy based on bio-inspired chemistry has been successfully developed for the fabrication of high-performance TFC membranes. The preloading polydopamine via polydopamine-modified CNCs on ENMs avoid the formation of polydopamine aggregates, which is beneficial to prevent the pore blocking of the porous supporting layer. In addition, the employment of ENMs from electrospinning as the porous supporting layer further enhance the membrane PWP. The ultrahigh PWP (128.4 LMH bar^{-1}), superior dye rejection, remarkable salt permeation, and excellent selectivity factor of CR/NaCl (1098), demonstrate its great potential for the effective separation of dye/salt mixtures and recovery of these valuable components. Furthermore, the conventional interfacial polymerization has also been used for the fabrication of TFC membranes with the new synthesized zwitterionic diamine and trihydroxy monomers. In particular, to the best of our knowledge, this thesis research shows the first direct fabrication of zwitterionic TFC polyester membranes via interfacial polymerization with zwitterionic monomer (Z-TEOA).

(iii) Systematic performance investigation of TFC membranes

The performance of all fabricated TFC membranes has been systematically investigated via varying the fabrication parameters. For instance, in chapter 3, the impact of polydopamine-modified CNCs loading density, PEI concentration, and PEI molecular weight on PWP and rejection has been conducted. The optimum TFC membrane with PWP of 128.4 LMH bar^{-1} and excellent dye/salt separation ability has been obtained. In other chapters, with the incorporation of zwitterionic monomers, all membranes has shown increased hydrophilicity and enhanced fouling resistance to model contaminants (CR, MB, BSA, and NaAlg), demonstrating that the prepared functional materials have the great potential in the fabrication of high-performance TFC membranes.

7.2 Suggestions for future work

On the basis of the findings from this thesis research, the following recommendations are proposed for the future study on the fabrication of high performance TFC membranes.

- Bioinspired chemistry is a promising alternative method to fabricate TFC membranes. However, the number of monomers with a catechol structure is still limited. Therefore, discovery of new monomers and design of more active monomers with a catechol structure for the application of bio-inspired chemistry in the fabrication of TFC membranes should be encouraged.

- The main drawbacks of bio-inspired chemistry are the formation of large sized aggregates and its time-consuming polymerization process. Therefore, the mLBL method can be employed to avoid the formation of aggregates, coupled with oxidants to improve the polymerization efficiency.

- TMAO-derived structure as a new generation of zwitterion shows a stronger hydration ability compared to other well-established zwitterions. This study has presented TMAO-derived diamine monomer (DNMAO) for the fabrication of polyamide TFC membranes. To further improve the hydrophilicity and fouling-resistant performance, ATRP is a promising process to graft TMAO-derived monomers on the surface of polyamide TFC membranes.

- The application of plant-derived nanomaterials (CNCs and CNFs) as additives has been investigated on the fabrication of TFN membranes via interfacial polymerization. However, the stability of these nanomaterial-incorporated TFC membranes and limited loading dose are the main obstacles. Hence, functionalization of these nanomaterials enables to improve the stability of TFC membranes and increase the loading dose to enhance membrane performance.

- Wastewaters from practical industries generally contain diverse contaminants. Therefore, the performance evaluation of the fabricated membranes in this research towards practical wastewaters from industries is needed to investigate their potential applications under harsh conditions.

References

1. Boretti, A.; Rosa, L., Reassessing the projections of the World Water Development Report. *npj Clean Water* **2019**, *2*, 15.

2. Ighalo, J.O.; Adeniyi, A.G., A comprehensive review of water quality monitoring and assessment in Nigeria. *Chemosphere* **2020**, *260*, 127569.

3. Samsami, S.; Mohamadizaniani, M.; Sarrafzadeh, M.-H.; Rene, E.R.; Firoozbahr, M., Recent advances in the treatment of dye-containing wastewater from textile industries: Overview and perspectives. *Process Saf. Environ. Prot.* **2020**, *143*, 138-163.

4. Al-Tohamy, R.; Ali, S.S.; Li, F.; Okasha, K.M.; Mahmoud, Y.A.G.; Elsamahy, T.; Jiao, H.; Fu, Y.; Sun, J., A critical review on the treatment of dye-containing wastewater: Ecotoxicological and health concerns of textile dyes and possible remediation approaches for environmental safety. *Ecotoxicol. Environ. Saf.* **2022**, *231*, 113160.

5. Holkar, C.R.; Jadhav, A.J.; Pinjari, D.V.; Mahamuni, N.M.; Pandit, A.B., A critical review on textile wastewater treatments: Possible approaches. *J. Environ. Manage.* **2016**, *182*, 351-366.

6. Khan, A.; Sherazi, T.A.; Khan, Y.; Li, S.; Naqvi, S.A.R.; Cui, Z., Fabrication and characterization of polysulfone/modified nanocarbon black composite antifouling ultrafiltration membranes. *J. Membr. Sci.* **2018**, *554*, 71-82.

7. Liao, Y.; Loh, C.-H.; Tian, M.; Wang, R.; Fane, A.G., Progress in electrospun polymeric nanofibrous membranes for water treatment: Fabrication, modification and applications. *Prog. Polym. Sci.* **2018**, *77*, 69-94.

8. Bai, L.; Liu, Y.; Bossa, N.; Ding, A.; Ren, N.; Li, G.; Liang, H.; Wiesner, M.R., Incorporation of cellulose nanocrystals (CNCs) into the polyamide layer of thin-film composite (TFC) nanofiltration membranes for enhanced separation performance and antifouling properties. *Environ. Sci. Technol.* **2018**, *52*, 11178-11187.

9. Kang, G.-d.; Cao, Y.-m., Development of antifouling reverse osmosis membranes for water treatment: a review. *Water Res.* **2012**, *46*, 584-600.

10. Kochkodan, V.; Hilal, N., A comprehensive review on surface modified polymer membranes for biofouling mitigation. *Desalination* **2015**, *356*, 187-207.

11. Zhong, Z.; Li, D.; Zhang, B.; Xing, W., Membrane surface roughness characterization and its influence on ultrafine particle adhesion. *Sep. Purif. Technol.* **2012**, *90*, 140-146.

12. Cai, H.; Fan, H.; Zhao, L.; Hong, H.; Shen, L.; He, Y.; Lin, H.; Chen, J., Effects of surface charge on interfacial interactions related to membrane fouling in a submerged membrane bioreactor based on thermodynamic analysis. *J. Colloid Interface Sci.* **2016**, *465*, 33-41.

13. Wang, X.; Cheng, W.; Wang, D.; Ni, X.; Han, G., Electrospun polyvinylidene fluoride-based fibrous nanocomposite membranes reinforced by cellulose nanocrystals for efficient separation of water-in-oil emulsions. *J. Membr. Sci.* **2019**, *575*, 71-79.

14. Khorshidi, B.; Thundat, T.; Fleck, B.A.; Sadrzadeh, M., A novel approach toward fabrication of high performance thin film composite polyamide membranes. *Sci. Rep.* **2016**, *6*, 1-10.

15. Karami, P.; Khorshidi, B.; McGregor, M.; Peichel, J.T.; Soares, J.B.P.; Sadrzadeh, M., Thermally stable thin film composite polymeric membranes for water treatment: A review. *J. Clean. Prod.* **2020**, *250*, 119447.

16. Maruf, S.H.; Ahn, D.U.; Pellegrino, J.; Killgore, J.P.; Greenberg, A.R.; Ding, Y., Correlation between barrier layer Tg and a thin-film composite polyamide membrane's performance: Effect of chlorine treatment. *J. Membr. Sci.* **2012**, *405*, 167-175.

17. Lau, W.; Ismail, A.; Misdan, N.; Kassim, M., A recent progress in thin film composite membrane: a review. *Desalination* **2012**, *287*, 190-199.

18. McGinnis, R.L.; Elimelech, M., Global challenges in energy and water supply: The promise of engineered osmosis. *Environ. Sci. Technol.* **2008**, *42*, 8625-8629.

19. Hermans, S.; Mariën, H.; Van Goethem, C.; Vankelecom, I.F., Recent developments in thin film (nano) composite membranes for solvent resistant nanofiltration. *Curr. Opin. Chem. Eng.* **2015**, *8*, 45-54.

20. Baker, R.W., *Membrane technology and applications*. 2012: John Wiley & Sons.

21. Yoon, K.; Hsiao, B.S.; Chu, B., High flux ultrafiltration nanofibrous membranes based on polyacrylonitrile electrospun scaffolds and crosslinked polyvinyl alcohol coating. *J. Membr. Sci.* **2009**, *338*, 145-152.

22. Zhang, Y.; Li, H.; Li, H.; Li, R.; Xiao, C., Preparation and characterization of modified polyvinyl alcohol ultrafiltration membranes. *Desalination* **2006**, *192*, 214-223.

23. Ong, C.S.; Goh, P.; Lau, W.; Misdan, N.; Ismail, A.F., Nanomaterials for biofouling and scaling mitigation of thin film composite membrane: A review. *Desalination* **2016**, *393*, 2-15.

24. He, M.; Gao, K.; Zhou, L.; Jiao, Z.; Wu, M.; Cao, J.; You, X.; Cai, Z.; Su, Y.; Jiang, Z., Zwitterionic materials for antifouling membrane surface construction. *Acta Biomater.* **2016**, *40*, 142-152.

25. Shahkaramipour, N.; Tran, T.N.; Ramanan, S.; Lin, H., Membranes with surface-enhanced antifouling properties for water purification. *Membranes* **2017**, *7*, 13.

26. Miller, D.J.; Dreyer, D.R.; Bielawski, C.W.; Paul, D.R.; Freeman, B.D., Surface modification of water purification membranes. *Angew. Chem. Int. Ed.* **2017**, *56*, 4662-4711.

27. Jiang, S.; Li, Y.; Ladewig, B.P., A review of reverse osmosis membrane fouling and control strategies. *Sci. Total Environ.* **2017**, *595*, 567-583.

28. Bokhary, A.; Tikka, A.; Leitch, M.; Liao, B., Membrane fouling prevention and control strategies in pulp and paper industry applications: A review. *J. Membr. Sci. Res* **2018**, *4*, 181-197.

29. Kim, S.; Hoek, E.M., Modeling concentration polarization in reverse osmosis processes. *Desalination* **2005**, *186*, 111-128.

30. Chong, T.; Wong, F.; Fane, A., Enhanced concentration polarization by unstirred fouling layers in reverse osmosis: detection by sodium chloride tracer response technique. *J. Membr. Sci.* **2007**, *287*, 198-210.

31. Kim, E.-S.; Liu, Y.; Gamal El-Din, M., The effects of pretreatment on nanofiltration and reverse osmosis membrane filtration for desalination of oil sands process-affected water. *Sep. Purif. Technol.* **2011**, *81*, 418-428.

32. Le, T.-N.; Au-Duong, A.-N.; Lee, C.-K., Facile coating on microporous polypropylene membrane for antifouling microfiltration using comb-shaped poly (N-vinylpyrrolidone) with multivalent catechol. *J. Membr. Sci.* **2019**, *574*, 164-173.

33. Zhang, M.; Liao, B.-q.; Zhou, X.; He, Y.; Hong, H.; Lin, H.; Chen, J., Effects of hydrophilicity/hydrophobicity of membrane on membrane fouling in a submerged membrane bioreactor. *Bioresour. Technol.* **2015**, *175*, 59-67.

34. Mi, Y.-F.; Zhao, F.-Y.; Guo, Y.-S.; Weng, X.-D.; Ye, C.-C.; An, Q.-F., Constructing zwitterionic surface of nanofiltration membrane for high flux and antifouling performance. *J. Membr. Sci.* **2017**, *541*, 29-38.

35. Ahmed, F.; Lalia, B.S.; Kochkodan, V.; Hilal, N.; Hashaikeh, R., Electrically conductive polymeric membranes for fouling prevention and detection: A review. *Desalination* **2016**, *391*, 1-15.

36. Rana, D.; Matsuura, T., Surface modifications for antifouling membranes. *Chem. Rev.* **2010**, *110*, 2448-2471.

37. Yin, J.; Zhu, G.; Deng, B., Graphene oxide (GO) enhanced polyamide (PA) thin-film nanocomposite (TFN) membrane for water purification. *Desalination* **2016**, *379*, 93-101.

38. Ismail, A.; Padaki, M.; Hilal, N.; Matsuura, T.; Lau, W., Thin film composite membrane—Recent development and future potential. *Desalination* **2015**, *356*, 140-148.

39. Lowe, A.B.; McCormick, C.L., Synthesis and solution properties of zwitterionic polymers. *Chem. Rev.* **2002**, *102*, 4177-4190.

40. Le, N.L.; Duong, P.H.H.; Pulido, B.A.; Nunes, S.P., Zwitterionic triamine monomer for the fabrication of thin-film composite membranes. *Ind. Eng. Chem. Res.* **2021**, *60*, 583-592.

41. Wu, Y.; Gao, M.; Chen, W.; Lü, Z.; Yu, S.; Liu, M.; Gao, C., Efficient removal of anionic dye by constructing thin-film composite membrane with high perm-selectivity and improved anti-dye-deposition property. *Desalination* **2020**, *476*, 114228.

42. An, Q.-F.; Sun, W.-D.; Zhao, Q.; Ji, Y.-L.; Gao, C.-J., Study on a novel nanofiltration membrane prepared by interfacial polymerization with zwitterionic amine monomers. *J. Membr. Sci.* **2013**, *431*, 171-179.

43. Li, S.-L.; Shan, X.; Zhao, Y.; Hu, Y., Fabrication of a novel nanofiltration membrane with enhanced performance via interfacial polymerization through the incorporation of a new zwitterionic diamine monomer. *ACS Appl. Mater. Interfaces* **2019**, *11*, 42846-42855.

44. Ma, R.; Ji, Y.-L.; Weng, X.-D.; An, Q.-F.; Gao, C.-J., High-flux and fouling-resistant reverse osmosis membrane prepared with incorporating zwitterionic amine monomers via interfacial polymerization. *Desalination* **2016**, *381*, 100-110.

45. Li, S.-L.; Shan, X.; Zhao, Y.; Hu, Y., Fabrication of a novel nanofiltration membrane with enhanced performance via interfacial polymerization through the incorporation of a new zwitterionic diamine monomer. *ACS Appl. Mater. Interfaces* **2019**, *11*, 42846-42855.

46. Wang, J.; Zhang, S.; Wu, P.; Shi, W.; Wang, Z.; Hu, Y., In situ surface modification of thin-film composite polyamide membrane with zwitterions for enhanced chlorine resistance and transport properties. *ACS Appl. Mater. Interfaces* **2019**, *11*, 12043-12052.

47. Guo, Y.-S.; Weng, X.-D.; Wu, B.; Mi, Y.-F.; Zhu, B.-K.; Ji, Y.-L.; An, Q.-F.; Gao, C.-J., Construction of nonfouling nanofiltration membrane via introducing uniformly tunable zwitterionic layer. *J. Membr. Sci.* **2019**, *583*, 152-162.

48. Ye, G.; Lee, J.; Perreault, F.; Elimelech, M., Controlled architecture of dual-functional block copolymer brushes on thin-film composite membranes for integrated "defending" and "attacking" strategies against biofouling. *ACS Appl. Mater. Interfaces* **2015**, *7*, 23069-23079.

49. Elimelech, M.; Phillip, W.A., The future of seawater desalination: energy, technology, and the environment. *science* **2011**, *333*, 712-717.

50. Chowdhury, M.R.; Steffes, J.; Huey, B.D.; McCutcheon, J.R., 3D printed polyamide membranes for desalination. *Science* **2018**, *361*, 682-686.

51. Freger, V., Nanoscale heterogeneity of polyamide membranes formed by interfacial polymerization. *Langmuir* **2003**, *19*, 4791-4797.

52. Yang, J.; Lin, G.; Mou, C.; Tung, K., Mesoporous silica thin membrane with tunable pore size for ultrahigh permeation and precise molecular separation. *ACS Appl. Mater. Interfaces* **2020**, *12*, 7459-7465.

53. Kang, Y.; Jang, J.; Kim, S.; Lim, J.; Lee, Y.; Kim, I.S., PIP/TMC interfacial polymerization with electrospray: novel loose nanofiltration membrane for dye wastewater treatment. *ACS Appl. Mater. Interfaces* **2020**, *12*, 36148-36158.

54. Ma, X.-H.; Yang, Z.; Yao, Z.-K.; Guo, H.; Xu, Z.-L.; Tang, C.Y., Interfacial polymerization with electrosprayed microdroplets: Toward controllable and ultrathin polyamide membranes. *Environ. Sci. Technol.* **2018**, *5*, 117-122.

55. Yang, S.; Wang, J.; Fang, L.; Lin, H.; Liu, F.; Tang, C.Y., Electrosprayed polyamide nanofiltration membrane with intercalated structure for controllable structure manipulation and enhanced separation performance. *J. Membr. Sci.* **2020**, *602*, 117971.

56. Liu, Z.; Qi, L.; An, X.; Liu, C.; Hu, Y., Surface engineering of thin film composite polyamide membranes with silver nanoparticles through layer-by-layer interfacial polymerization for antibacterial properties. *ACS Appl. Mater. Interfaces* **2017**, *9*, 40987-40997.

57. Agarwal, P.; Tomlinson, I.; Hefner, R.E.; Ge, S.; Rao, Y.; Dikic, T., Thin film composite membranes from polymers of intrinsic microporosity using layer-by-layer method. *J. Membr. Sci.* **2019**, *572*, 475-479.

58. Karan, S.; Jiang, Z.; Livingston, A.G., Sub–10 nm polyamide nanofilms with ultrafast solvent transport for molecular separation. *Science* **2015**, *348*, 1347-1351.

59. Gu, J.E.; Lee, S.; Stafford, C.M.; Lee, J.S.; Choi, W.; Kim, B.Y.; Baek, K.Y.; Chan, E.P.; Chung, J.Y.; Bang, J., Molecular layer‐by‐layer assembled thin‐film composite membranes for water desalination. *Adv. Mater.* **2013**, *25*, 4778-4782.

60. Johnson, P.M.; Yoon, J.; Kelly, J.Y.; Howarter, J.A.; Stafford, C.M., Molecular layer-by-layer deposition of highly crosslinked polyamide films. *J. Polym. Sci. B: Polym. Phys.* **2012**, *50*, 168-173.

61. Mulhearn, W.D.; Oleshko, V.P.; Stafford, C.M., Thickness-dependent permeance of molecular layer-by-layer polyamide membranes. *J. Membr. Sci.* **2021**, *618*, 118637.

62. Tousley, M.E.; Shaffer, D.L.; Lee, J.-H.; Osuji, C.O.; Elimelech, M., Effect of final monomer deposition steps on molecular layer-by-layer polyamide surface properties. *Langmuir* **2016**, *32*, 10815-10823.

63. Roduner, E., Size matters: why nanomaterials are different. *Chem. Soc. Rev.* **2006**, *35*, 583-592.

64. Ozin, G.A.; Arsenault, A., *Nanochemistry: a chemical approach to nanomaterials*. 2015: Royal Society of Chemistry.

65. Misdan, N.; Ismail, A.F.; Hilal, N., Recent advances in the development of (bio)fouling resistant thin film composite membranes for desalination. *Desalination* **2016**, *380*, 105-111.

66. Anand, A.; Unnikrishnan, B.; Mao, J.-Y.; Lin, H.-J.; Huang, C.-C., Graphene-based nanofiltration membranes for improving salt rejection, water flux and antifouling–A review. *Desalination* **2018**, *429*, 119-133.

67. Lai, G.S.; Lau, W.J.; Goh, P.S.; Ismail, A.F.; Yusof, N.; Tan, Y.H., Graphene oxide incorporated thin film nanocomposite nanofiltration membrane for enhanced salt removal performance. *Desalination* **2016**, *387*, 14-24.

68. Shen, Q.; Lin, Y.; Kawabata, Y.; Jia, Y.; Zhang, P.; Akther, N.; Guan, K.; Yoshioka, T.; Shon, H.; Matsuyama, H., Engineering heterostructured thin-film nanocomposite membrane with functionalized graphene oxide quantum dots (GOQD) for highly efficient reverse osmosis. *ACS Appl. Mater. Interfaces* **2020**, *12*, 38662-38673.

69. Zhang, C.; Wei, K.; Zhang, W.; Bai, Y.; Sun, Y.; Gu, J., Graphene oxide quantum dots incorporated into a thin film nanocomposite membrane with high flux and antifouling properties for low-pressure nanofiltration. *ACS Appl. Mater. Interfaces* **2017**, *9,* 11082-11094.

70. Zarrabi, H.; Yekavalangi, M.E.; Vatanpour, V.; Shockravi, A.; Safarpour, M., Improvement in desalination performance of thin film nanocomposite nanofiltration membrane using amine-functionalized multiwalled carbon nanotube. *Desalination* **2016**, *394*, 83-90.

71. Daraei, P.; Madaeni, S.S.; Ghaemi, N.; Khadivi, M.A.; Astinchap, B.; Moradian, R., Enhancing antifouling capability of PES membrane via mixing with various types of polymer modified multi-walled carbon nanotube. *J. Membr. Sci.* **2013**, *444*, 184-191.

72. Wu, H.; Tang, B.; Wu, P., Preparation and characterization of anti-fouling β-cyclodextrin/polyester thin film nanofiltration composite membrane. *J. Membr. Sci.* **2013**, *428*, 301-308.

73. Son, M.; Choi, H.-g.; Liu, L.; Celik, E.; Park, H.; Choi, H., Efficacy of carbon nanotube positioning in the polyethersulfone support layer on the performance of thin-film composite membrane for desalination. *Chem. Eng. J.* **2015**, *266*, 376-384.

74. Ma, W.; Chen, T.; Nanni, S.; Yang, L.; Ye, Z.; Rahaman, M.S., Zwitterion-functionalized graphene oxide incorporated polyamide membranes with improved antifouling properties. *Langmuir* **2019**, *35*, 1513-1525.

75. Chan, W.-F.; Chen, H.-y.; Surapathi, A.; Taylor, M.G.; Shao, X.; Marand, E.; Johnson, J.K., Zwitterion functionalized carbon nanotube/polyamide nanocomposite membranes for water desalination. *Acs Nano* **2013**, *7*, 5308-5319.

76. Pourjafar, S.; Rahimpour, A.; Jahanshahi, M., Synthesis and characterization of PVA/PES thin film composite nanofiltration membrane modified with TiO_2 nanoparticles for better performance and surface properties. *J. Ind. Eng. Chem.* **2012**, *18*, 1398-1405.

77. Wu, H.; Tang, B.; Wu, P., Optimizing polyamide thin film composite membrane covalently bonded with modified mesoporous silica nanoparticles. *J. Membr. Sci.* **2013**, *428*, 341-348.

78. Ma, N.; Wei, J.; Liao, R.; Tang, C.Y., Zeolite-polyamide thin film nanocomposite membranes: Towards enhanced performance for forward osmosis. *J. Membr. Sci.* **2012**, *405*, 149-157.

79. Asempour, F.; Emadzadeh, D.; Matsuura, T.; Kruczek, B., Synthesis and characterization of novel Cellulose Nanocrystals-based Thin Film Nanocomposite membranes for reverse osmosis applications. *Desalination* **2018**, *439*, 179-187.

80. Bai, L.; Liu, Y.; Ding, A.; Ren, N.; Li, G.; Liang, H., Fabrication and characterization of thin-film composite (TFC) nanofiltration membranes incorporated with cellulose nanocrystals (CNCs) for enhanced desalination performance and dye removal. *Chem. Eng. J.* **2019**, *358*, 1519-1528.

81. Huang, S.; Wu, M.-B.; Zhu, C.-Y.; Ma, M.-Q.; Yang, J.; Wu, J.; Xu, Z.-K., Polyamide nanofiltration membranes incorporated with cellulose nanocrystals for enhanced water flux and chlorine resistance. *ACS Sustain. Chem. Eng.* **2019**, *7*, 12315-12322.

82. Gong, G.; Wang, P.; Zhou, Z.; Hu, Y., New insights into the role of an interlayer for the fabrication of highly selective and permeable thin-film composite nanofiltration membrane. *ACS Appl. Mater. Interfaces* **2019**, *11*, 7349-7356.

83. Wu, M.-B.; Lv, Y.; Yang, H.-C.; Liu, L.-F.; Zhang, X.; Xu, Z.-K., Thin film composite membranes combining carbon nanotube intermediate layer and microfiltration support for high nanofiltration performances. *J. Membr. Sci.* **2016**, *515*, 238-244.

84. Wang, J.-J.; Yang, H.-C.; Wu, M.-B.; Zhang, X.; Xu, Z.-K., Nanofiltration membranes with cellulose nanocrystals as an interlayer for unprecedented performance. *J. Mater. Chem. A* **2017**, *5*, 16289-16295.

85. Zhou, Z.; Hu, Y.; Boo, C.; Liu, Z.; Li, J.; Deng, L.; An, X., High-performance thin-film composite membrane with an ultrathin spray-coated carbon nanotube interlayer. *Environ. Sci. Technol.* **2018**, *5*, 243-248.

86. Wang, J.; Zhu, J.; Tsehaye, M.T.; Li, J.; Dong, G.; Yuan, S.; Li, X.; Zhang, Y.; Liu, J.; Van der Bruggen, B., High flux electroneutral loose nanofiltration membranes based on rapid deposition of polydopamine/polyethyleneimine. *J. Mater. Chem. A* **2017**, *5*, 14847-14857.

87. Qiu, W.-Z.; Zhong, Q.-Z.; Du, Y.; Lv, Y.; Xu, Z.-K., Enzyme-triggered coatings of tea catechins/chitosan for nanofiltration membranes with high performance. *Green Chem.* **2016**, *18*, 6205-6208.

88. Zhang, N.; Jiang, B.; Zhang, L.; Huang, Z.; Sun, Y.; Zong, Y.; Zhang, H., Low-pressure electroneutral loose nanofiltration membranes with polyphenol-inspired coatings for effective dye/divalent salt separation. *Chem. Eng. J.* **2019**, *359*, 1442-1452.

89. Xu, Y.C.; Wang, Z.X.; Cheng, X.Q.; Xiao, Y.C.; Shao, L., Positively charged nanofiltration membranes via economically mussel-substance-simulated co-deposition for textile wastewater treatment. *Chem. Eng. J.* **2016**, *303*, 555-564.

90. Zhao, S.; Wang, Z., A loose nano-filtration membrane prepared by coating HPAN UF membrane with modified PEI for dye reuse and desalination. *J. Membr. Sci.* **2017**, *524*, 214-224.

91. Li, Q.; Liao, Z.; Fang, X.; Wang, D.; Xie, J.; Sun, X.; Wang, L.; Li, J., Tannic acid-polyethyleneimine crosslinked loose nanofiltration membrane for dye/salt mixture separation. *J. Membr. Sci.* **2019**, *584*, 324-332.

92. Lee, H.; Dellatore, S.M.; Miller, W.M.; Messersmith, P.B., Mussel-Inspired Surface Chemistry for Multifunctional Coatings. *Science* **2007**, *318*, 426-430.

93. Yin, C.; Zhang, Z.; Zhou, J.; Wang, Y., Single-layered nanosheets of covalent triazine frameworks (CTFs) by mild oxidation for molecular-sieving membranes. *ACS Appl. Mater. Interfaces* **2020**, *12*, 18944-18951.

94. He, Y.; Lin, X.; Chen, J.H.; Guo, Z.; Zhan, H., Homogeneous polymerization of self-standing covalent organic framework films with high performance in molecular separation. *ACS Appl. Mater. Interfaces* **2020**.

95. Kiani, S.; Mousavi, S.M.; Shahtahmassebi, N.; Saljoughi, E., Hydrophilicity improvement in polyphenylsulfone nanofibrous filtration membranes through addition of polyethylene glycol. *Appl. Surf. Sci.* **2015**, *359*, 252-258.

96. Wang, Z.; Yu, H.; Xia, J.; Zhang, F.; Li, F.; Xia, Y.; Li, Y., Novel GO-blended PVDF ultrafiltration membranes. *Desalination* **2012**, *299*, 50-54.

97. Farahani, M.H.D.A.; Vatanpour, V., A comprehensive study on the performance and antifouling enhancement of the PVDF mixed matrix membranes by embedding different nanoparticulates: clay, functionalized carbon nanotube, SiO_2 and TiO_2. *Sep. Purif. Technol.* **2018**, *197*, 372-381.

98. Islam, M.S.; McCutcheon, J.R.; Rahaman, M.S., A high flux polyvinyl acetate-coated electrospun nylon 6/SiO_2 composite microfiltration membrane for the separation of oil-in-water emulsion with improved antifouling performance. *J. Membr. Sci.* **2017**, *537*, 297-309.

99. Tavangar, T.; Karimi, M.; Rezakazemi, M.; Reddy, K.R.; Aminabhavi, T.M., Textile waste, dyes/inorganic salts separation of cerium oxide-loaded loose nanofiltration polyethersulfone membranes. *Chem. Eng. J.* **2020**, *385*, 123787.

100. Huang, L.; Huang, S.; Venna, S.R.; Lin, H., Rightsizing nanochannels in reduced graphene oxide membranes by solvating for dye desalination. *Environ. Sci. Technol.* **2018**, *52*, 12649-12655.

101. Jiang, M.; Ye, K.; Deng, J.; Lin, J.; Ye, W.; Zhao, S.; Van der Bruggen, B., Conventional ultrafiltration as effective strategy for dye/salt fractionation in textile wastewater treatment. *Environ. sci. technol.* **2018**, *52*, 10698-10708.

102. Liang, C.; Sun, S.; Li, F.; Ong, Y.; Chung, T., Treatment of highly concentrated wastewater containing multiple synthetic dyes by a combined process of coagulation/flocculation and nanofiltration. *J. Membr. Sci.* **2014**, *469*, 306-315.

103. Ye, W.; Ye, K.; Lin, F.; Liu, H.; Jiang, M.; Wang, J.; Liu, R.; Lin, J., Enhanced fractionation of dye/salt mixtures by tight ultrafiltration membranes via fast bio-inspired co-deposition for sustainable textile wastewater management. *Chem. Eng. J.* **2020**, *379*, 122321.

104. Paździor, K.; Bilińska, L.; Ledakowicz, S., A review of the existing and emerging technologies in the combination of AOPs and biological processes in industrial textile wastewater treatment. *Chem. Eng. J.* **2019**, *376*, 120597.

105. Oulad, F.; Zinadini, S.; Zinatizadeh, A.A.; Derakhshan, A.A., Fabrication and characterization of a novel tannic acid coated Boehmite/PES high performance antifouling NF membrane and application for licorice dye removal. *Chem. Eng. J.* **2020**, *397*, 125105.

106. Liu, C.; Wang, C.; Guo, Y.; Zhang, J.; Cao, Y.; Liu, H.; Hu, Z.; Zhang, C., High-performance polyamide membrane with tailored water channel prepared via bionic neural networks for textile wastewater tsreatment. *J. Mater. Chem. A* **2019**, *7*, 6695-6707.

107. Soyekwo, F.; Liu, C.; Wen, H.; Hu, Y., Construction of an electroneutral zinc incorporated polymer network nanocomposite membrane with enhanced selectivity for salt/dye separation. *Chem. Eng. J.* **2020**, *380*, 122560.

108. Zhao, S.; Zhu, H.; Wang, Z.; Song, P.; Ban, M.; Song, X., A loose hybrid nanofiltration membrane rabricated via chelating-assisted in-situ growth of Co/Ni LDHs for dye wastewater treatment. *Chem. Eng. J.* **2018**, *353*, 460-471.

109. Ye, C.; Zhao, F.; Wu, J.-K.; Weng, X.; Zheng, P.; Mi, Y.; An, Q.; Gao, C., Sulfated polyelectrolyte complex nanoparticles structured nanoflitration membrane for dye desalination. *Chem. Eng. J.* **2017**, *307*, 526-536.

110. Hu, J.; Li, M.; Wang, L.; Zhang, X., Polymer brush-modified graphene oxide membrane with excellent structural stability for effective fractionation of textile wastewater. *J. Membr. Sci.* **2021**, *618*, 118698.

111. Su, Y.; Yan, X.; Chen, Y.; Guo, X.; Chen, X.; Lang, W., Facile fabrication of COF-LZU1/PES composite membrane via interfacial polymerization on microfiltration substrate for dye/salt separation. *J. Membr. Sci.* **2021**, *618*, 118706.

112. Chowdhury, M.R.; Steffes, J.; Huey, B.D.; McCutcheon, J.R., 3D printed polyamide membranes for desalination. *Science* **2018**, *361*, 682-686.

113. Mehrabi, N.; Lin, H.; Aich, N., Deep eutectic solvent functionalized graphene oxide nanofiltration membranes with superior water permeance and dye desalination performance. *Chem. Eng. J.* **2021**, *412*, 128577.

114. Zhang, Q.; Fan, L.; Yang, Z.; Zhang, R.; Liu, Y.-n.; He, M.; Su, Y.; Jiang, Z., Loose nanofiltration membrane for dye/salt separation through interfacial polymerization with in-situ generated TiO_2 nanoparticles. *Appl. Surf. Sci.* **2017**, *410*, 494-504.

115. Wang, J.; Yang, H.; Wu, M.; Zhang, X.; Xu, Z., Nanofiltration membranes with cellulose nanocrystals as an interlayer for unprecedented performance. *J. Mater. Chem. A* **2017**, *5*, 16289-16295.

116. Karan, S.; Jiang, Z.; Livingston, A.G., Sub–10 nm polyamide nanofilms with ultrafast solvent transport for molecular separation. *Science* **2015**, *348*, 1347-1351.

117. Hoover, L.A.; Schiffman, J.D.; Elimelech, M., Nanofibers in thin-film composite membrane support layers: Enabling expanded application of forward and pressure retarded osmosis. *Desalination* **2013**, *308*, 73-81.

118. Dobosz, K.M.; Kuo-Leblanc, C.A.; Bowden, J.W.; Schiffman, J.D., Robust, small diameter hydrophilic nanofibers improve the flux of ultrafiltration membranes. *Ind. Eng. Chem. Res.* **2021**, *60*, 9179-9188.

119. Huang, L.; Arena, J.T.; Manickam, S.S.; Jiang, X.; Willis, B.G.; McCutcheon, J.R., Improved mechanical properties and hydrophilicity of electrospun nanofiber membranes for filtration applications by dopamine modification. *J. Membr. Sci.* **2014**, *460*, 241-249.

120. Bui, N.-N.; Lind, M.L.; Hoek, E.M.V.; McCutcheon, J.R., Electrospun nanofiber supported thin film composite membranes for engineered osmosis. *J. Membr. Sci.* **2011**, *385-386*, 10-19.

121. Amirilargani, M.; Yokota, G.N.; Vermeij, G.H.; Merlet, R.B.; Delen, G.; Mandemaker, L.D.B.; Weckhuysen, B.M.; Winnubst, L.; Nijmeijer, A.; de Smet, L.C.P.M.; Sudhölter, E.J.R., Melamine-based microporous organic framework thin films on an alumina membrane for high-flux organic solvent nanofiltration. *ChemSusChem* **2020**, *13*, 136-140.

122. Kandambeth, S.; Biswal, B.P.; Chaudhari, H.D.; Rout, K.C.; Kunjattu H., S.; Mitra, S.; Karak, S.; Das, A.; Mukherjee, R.; Kharul, U.K.; Banerjee, R., Selective molecular sieving in self-standing porous covalent-organic-framework membranes. *Adv. Mater.* **2017**, *29*, 1603945.

123. Zhang, X.; Li, H.; Wang, J.; Peng, D.; Liu, J.; Zhang, Y., In-situ grown covalent organic framework nanosheets on graphene for membrane-based dye/salt separation. *J. Membr. Sci.* **2019**, *581*, 321-330.

124. Lee, H.; Scherer, N.F.; Messersmith, P.B., Single-molecule mechanics of mussel adhesion. *PNAS* **2006**, *103*, 12999-13003.

125. Wang, J.; Wang, Y.; Zhu, J.; Zhang, Y.; Liu, J.; Van der Bruggen, B., Construction of TiO_2@graphene oxide incorporated antifouling nanofiltration membrane with elevated filtration performance. *J. Membr. Sci.* **2017**, *533*, 279-288.

126. Qiu, W.; Zhong, Q.; Du, Y.; Lv, Y.; Xu, Z., Enzyme-triggered coatings of tea catechins/chitosan for nanofiltration membranes with high performance. *Green Chem.* **2016**, *18*, 6205-6208.

127. Arena, J.T.; McCloskey, B.; Freeman, B.D.; McCutcheon, J.R., Surface modification of thin film composite membrane support layers with polydopamine: Enabling use of reverse osmosis membranes in pressure retarded osmosis. *J. Membr. Sci.* **2011**, *375*, 55-62.

128. Arena, J.T.; Manickam, S.S.; Reimund, K.K.; Freeman, B.D.; McCutcheon, J.R., Solute and water transport in forward osmosis using polydopamine modified thin film composite membranes. *Desalination* **2014**, *343*, 8-16.

129. Yang, Z.; Wang, F.; Guo, H.; Peng, L.E.; Ma, X.-h.; Song, X.-x.; Wang, Z.; Tang, C.Y., Mechanistic insights into the role of polydopamine interlayer toward improved separation performance of polyamide nanofiltration membranes. *Environ. sci. technol.* **2020**, *54*, 11611-11621.

130. Choi, H.-g.; Shah, A.A.; Nam, S.-E.; Park, Y.-I.; Park, H., Thin-film composite membranes comprising ultrathin hydrophilic polydopamine interlayer with graphene oxide for forward osmosis. *Desalination* **2019**, *449*, 41-49.

131. Zhao, J.; Su, Y.; He, X.; Zhao, X.; Li, Y.; Zhang, R.; Jiang, Z., Dopamine composite nanofiltration membranes prepared by self-polymerization and interfacial polymerization. *J. Membr. Sci.* **2014**, *465*, 41-48.

132. Xu, L.; Xu, J.; Shan, B.; Wang, X.; Gao, C., Novel thin-film composite membranes via manipulating the synergistic interaction of dopamine and m-phenylenediamine for highly efficient forward osmosis desalination. *J. Mater. Chem. A* **2017**, *5*, 7920-7932.

133. Xu, Y.; Li, Z.; Su, K.; Fan, T.; Cao, L., Mussel-inspired modification of PPS membrane to separate and remove the dyes from the wastewater. *Chem. Eng. J.* **2018**, *341*, 371-382.

134. Li, B.; Jain, P.; Ma, J.; Smith, J.K.; Yuan, Z.; Hung, H.-C.; He, Y.; Lin, X.; Wu, K.; Pfaendtner, J., Trimethylamine N-oxide–derived zwitterionic polymers: A new class of ultralow fouling bioinspired materials. *Sci. Adv.* **2019**, *5*, eaaw9562.

135. Hong, S.; Kim, J.; Na, Y.S.; Park, J.; Kim, S.; Singha, K.; Im, G.I.; Han, D.K.; Kim, W.J.; Lee, H., Poly (norepinephrine): ultrasmooth material‐independent surface chemistry and nanodepot for nitric oxide. *Angew. Chem. Int. Ed.* **2013**, *125*, 9357-9361.

136. Zhang, C.; Ou, Y.; Lei, W.X.; Wan, L.S.; Ji, J.; Xu, Z.K., $CuSO_4/H_2O_2$‐induced rapid deposition of polydopamine coatings with high uniformity and enhanced stability. *Angew. Chem. Int. Ed.* **2016**, *55*, 3054-3057.

137. Dobosz, K.M.; Kuo-LeBlanc, C.A.; Emrick, T.; Schiffman, J.D., Antifouling ultrafiltration membranes with retained pore size by controlled deposition of zwitterionic polymers and poly (ethylene glycol). *Langmuir* **2018**, *35*, 1872-1881.

138. Liu, S.; Wang, Z.; Song, P., Free radical graft copolymerization strategy to prepare catechin-modified chitosan loose nanofiltration (NF) membrane for dye desalination. *ACS Sustain. Chem. Eng.* **2018**, *6*, 4253-4263.

139. Bai, L.; Liu, Y.; Ding, A.; Ren, N.; Li, G.; Liang, H., Surface coating of UF membranes to improve antifouling properties: A comparison study between cellulose nanocrystals (CNCs) and cellulose nanofibrils (CNFs). *Chemosphere* **2019**, *217*, 76-84.

140. Chen, T.; Soroush, A.; Rahaman, M.S., Highly hydrophobic electrospun reduced graphene oxide/poly(vinylidene fluoride-co-hexafluoropropylene) membranes for use in membrane distillation. *Ind. Eng. Chem. Res.* **2018**, *57*, 14535-14543.

141. Chen, L.; Berry, R.M.; Tam, K.C., Synthesis of β-cyclodextrin-modified cellulose nanocrystals (CNCs)@ Fe_3O_4@ SiO_2 superparamagnetic aanorods. *ACS Sustain.Chem. Eng.* **2014**, *2*, 951-958.

142. Huang, L.; Ye, Z.; Berry, R., Modification of cellulose nanocrystals with quaternary ammonium-containing hyperbranched polyethylene ionomers by ionic assembly. *ACS Sustain.Chem. Eng.* **2016**, *4*, 4937-4950.

143. Luo, C.; Liu, Q., Oxidant-induced high-efficient mussel-inspired modification on PVDF membrane with superhydrophilicity and underwater superoleophobicity characteristics for oil/water separation. *ACS appl. mater. interfaces* **2017**, *9*, 8297-8307.

144. Ding, Y.; Weng, L.; Yang, M.; Yang, Z.; Lu, X.; Huang, N.; Leng, Y., Insights into the aggregation/deposition and structure of a polydopamine film. *Langmuir* **2014**, *30*, 12258-12269.

145. Ma, F.-f.; Zhang, N.; Wei, X.; Yang, J.-h.; Wang, Y.; Zhou, Z.-w., Blend-electrospun poly (vinylidene fluoride)/polydopamine membranes: self-polymerization of dopamine and the excellent adsorption/separation abilities. *J. Mater.Chem. A* **2017**, *5*, 14430-14443.

146. Zhu, Z.; Wu, P.; Liu, G.; He, X.; Qi, B.; Zeng, G.; Wang, W.; Sun, Y.; Cui, F., Ultrahigh adsorption capacity of anionic dyes with sharp selectivity through the cationic charged hybrid nanofibrous membranes. *Chem. Eng. J.* **2017**, *313*, 957-966.

147. Mi, Y.; Xu, G.; Guo, Y.; Wu, B.; An, Q., Development of antifouling nanofiltration membrane with zwitterionic functionalized monomer for efficient dye/salt selective separation. *J. Membr. Sci.* **2020**, *601*, 117795.

148. Ding, J.; Wu, H.; Wu, P., Preparation of highly permeable loose nanofiltration membranes using sulfonated polyethylenimine for effective dye/salt fractionation. *Chem. Eng. J.* **2020**, *396*, 125199.

149. Ji, D.; Xiao, C.; An, S.; Zhao, J.; Hao, J.; Chen, K., Preparation of high-flux PSF/GO loose nanofiltration hollow fiber membranes with dense-loose structure for treating textile wastewater. *Chem. Eng. J.* **2019**, *363*, 33-42.

150. Alvarez, P.J.J.; Chan, C.K.; Elimelech, M.; Halas, N.J.; Villagrán, D., Emerging opportunities for nanotechnology to enhance water security. *Nat. Nanotechnol.* **2018**, *13*, 634-641.

151. Mauter, M.S.; Zucker, I.; Perreault, F.; Werber, J.R.; Kim, J.-H.; Elimelech, M., The role of nanotechnology in tackling global water challenges. *Nat. Sustain.* **2018**, *1*, 166-175.

152. Hamedi, A.; Zarandi, M.B.; Nateghi, M.R., Highly efficient removal of dye pollutants by MIL-101(Fe) metal-organic framework loaded magnetic particles mediated by Poly L-Dopa. *J. Environ. Chem. Eng.* **2019**, *7*, 102882.

153. Jiang, N.; Shang, R.; Heijman, S.G.; Rietveld, L.C., High-silica zeolites for adsorption of organic micro-pollutants in water treatment: A review. *Water Res.* **2018**, *144*, 145-161.

154. Zhu, F.; Zheng, Y.-M.; Zhang, B.-G.; Dai, Y.-R., A critical review on the electrospun nanofibrous membranes for the adsorption of heavy metals in water treatment. *J. Hazard. Mater.* **2021**, *401*, 123608.

155. Zhao, C.; Zhou, J.; Yan, Y.; Yang, L.; Xing, G.; Li, H.; Wu, P.; Wang, M.; Zheng, H., Application of coagulation/flocculation in oily wastewater treatment: A review. *Sci. Total Environ.* **2021**, *765*, 142795.

156. Wei, H.; Gao, B.; Ren, J.; Li, A.; Yang, H., Coagulation/flocculation in dewatering of sludge: A review. *Water Res.* **2018**, *143*, 608-631.

157. Hube, S.; Eskafi, M.; Hrafnkelsdóttir, K.F.; Bjarnadóttir, B.; Bjarnadóttir, M.Á.; Axelsdóttir, S.; Wu, B., Direct membrane filtration for wastewater treatment and resource recovery: A review. *Sci. Total Environ.* **2020**, *710*, 136375.

158. Chen, L.-Y.; Gai, Y.-N.; Gai, X.-T.; Qin, J.; Wang, Z.-G.; Cui, L.-S.; Guo, H.; Jiang, M.-Y.; Zou, Q.; Zhou, T.; Gai, J.-G., Interfacial synthesized covalent organic framework nanofiltration membranes for precisely ultrafast sieving. *Chem. Eng. J.* **2022**, *430*, 133024.

159. Long, L.; Wu, C.; Yang, Z.; Tang, C.Y., Carbon nanotube interlayer enhances water permeance and antifouling performance of nanofiltration membranes: mechanisms and experimental evidence. *Environ. Sci. Technol.* **2022**, *56*, 2656-2664.

160. Wang, J.-J.; Yang, H.-C.; Wu, M.-B.; Zhang, X.; Xu, Z.-K., Nanofiltration membranes with cellulose nanocrystals as an interlayer for unprecedented performance. *J. Mater.Chem. A* **2017**, *5*, 16289-16295.

161. Khalil, A.M.E.; Memon, F.A.; Tabish, T.A.; Salmon, D.; Zhang, S.; Butler, D., Nanostructured porous graphene for efficient removal of emerging contaminants (pharmaceuticals) from water. *Chem. Eng. J.* **2020**, *398*, 125440.

162. Feng, X.; Peng, D.; Zhu, J.; Wang, Y.; Zhang, Y., Recent advances of loose nanofiltration membranes for dye/salt separation. *Sep. Purif. Technol* **2022**, *285*, 120228.

163. Hong, S.; Na, Y.S.; Choi, S.; Song, I.T.; Kim, W.Y.; Lee, H., Non-covalent self-assembly and covalent polymerization co-contribute to polydopamine formation. *Adv. Funct. Mater.* **2012**, *22*, 4711-4717.

164. Lim, C.; Huang, J.; Kim, S.; Lee, H.; Zeng, H.; Hwang, D.S., Nanomechanics of Poly (catecholamine) Coatings in Aqueous Solutions. *Angew. Chem. Int. Ed.* **2016**, *55*, 3342-3346.

165. Wang, J.; He, R.; Han, X.; Jiao, D.; Zhu, J.; Lai, F.; Liu, X.; Liu, J.; Zhang, Y.; Van Der Bruggen, B., High performance loose nanofiltration membranes obtained by a catechol-based route for efficient dye/salt separation. *Chem. Eng. J.* **2019**, *375*, 121982.

166. Cheng, X.Q.; Wang, Z.X.; Zhang, Y.; Zhang, Y.; Ma, J.; Shao, L., Bio-inspired loose nanofiltration membranes with optimized separation performance for antibiotics removals. *J. Membr. Sci.* **2018**, *554*, 385-394.

167. Yang, L.; Liu, X.; Zhang, X.; Chen, T.; Ye, Z.; Rahaman, M.S., High performance nanocomposite nanofiltration membranes with polydopamine-modified cellulose nanocrystals for efficient dye/salt separation. *Desalination* **2022**, *521*, 115385.

168. He, Y.; Chen, Q.; Zhang, Y.; Zhao, Y.; Chen, L., H_2O_2-triggered rapid deposition of poly(caffeic acid) coatings: a mechanism-based entry to versatile and high-efficient molecular separation. *ACS Appl. Mater. Interfaces* **2020**, *12*, 52104-52115.

169. Wang, J.; Zhu, J.; Tsehaye, M.T.; Li, J.; Dong, G.; Yuan, S.; Li, X.; Zhang, Y.; Liu, J.; Van der Bruggen, B., High flux electroneutral loose nanofiltration membranes based on rapid deposition of polydopamine/polyethyleneimine. *J. Mater.Chem. A* **2017**, *5*, 14847-14857.

170. Wei, Q.; Zhang, F.; Li, J.; Li, B.; Zhao, C., Oxidant-induced dopamine polymerization for multifunctional coatings. *Polym. Chem.* **2010**, *1*, 1430-1433.

171. Du, X.; Li, L.; Li, J.; Yang, C.; Frenkel, N.; Welle, A.; Heissler, S.; Nefedov, A.; Grunze, M.; Levkin, P.A., UV‑triggered dopamine polymerization: control of polymerization, surface coating, and photopatterning. *Adv. Mater.* **2014**, *26*, 8029-8033.

172. Kirschner, A.Y.; Chang, C.-C.; Kasemset, S.; Emrick, T.; Freeman, B.D., Fouling-resistant ultrafiltration membranes prepared via co-deposition of dopamine/zwitterion composite coatings. *J. Membr. Sci.* **2017**, *541*, 300-311.

173. Shahkaramipour, N.; Jafari, A.; Tran, T.; Stafford, C.M.; Cheng, C.; Lin, H., Maximizing the grafting of zwitterions onto the surface of ultrafiltration membranes to improve antifouling properties. *J. Membr. Sci.* **2020**, *601*, 117909.

174. Cheng, K.; Zhang, N.; Yang, N.; Hou, S.; Ma, J.; Zhang, L.; Sun, Y.; Jiang, B., Rapid and robust modification of PVDF ultrafiltration membranes with enhanced permselectivity, antifouling and antibacterial performance. *Sep. Purif. Technol* **2021**, *262*, 118316.

175. Mi, Y.-F.; Xu, G.; Guo, Y.-S.; Wu, B.; An, Q.-F., Development of antifouling nanofiltration membrane with zwitterionic functionalized monomer for efficient dye/salt selective separation. *J. Membr. Sci.* **2020**, *601*, 117795.

176. Ye, W.; Lin, J.; Borrego, R.; Chen, D.; Sotto, A.; Luis, P.; Liu, M.; Zhao, S.; Tang, C.Y.; Van der Bruggen, B., Advanced desalination of dye/NaCl mixtures by a loose nanofiltration membrane for digital ink-jet printing. *Sep. Purif. Technol* **2018**, *197*, 27-35.

177. Nadizadeh, Z.; Mahdavi, H., Grafting of zwitterion polymer on polyamide nanofiltration membranes via surface-initiated RAFT polymerization with improved antifouling properties as a new strategy. *Sep. Purif. Technol* **2021**, *254*, 117605.

178. Ye, W.; Liu, H.; Lin, F.; Lin, J.; Zhao, S.; Yang, S.; Hou, J.; Zhou, S.; Van der Bruggen, B., High-flux nanofiltration membranes tailored by bio-inspired co-deposition of hydrophilic g-C$_3$N$_4$ nanosheets for enhanced selectivity towards organics and salts. *Environ. Sci. Nano* **2019**, *6*, 2958-2967.

179. Ding, J.; Wu, H.; Wu, P., Development of nanofiltration membranes using mussel-inspired sulfonated dopamine for interfacial polymerization. *J. Membr. Sci.* **2020**, *598*, 117658.

180. Bai, L.; Ding, J.; Wang, H.; Ren, N.; Li, G.; Liang, H., High-performance nanofiltration membranes with a sandwiched layer and a surface layer for desalination and environmental pollutant removal. *Sci. Total Environ.* **2020**, *743*, 140766.

181. Cheng, X.Q.; Wang, Z.X.; Guo, J.; Ma, J.; Shao, L., Designing multifunctional coatings for cost-effectively sustainable water remediation. *ACS Sustain. Chem. Eng.* **2018**, *6*, 1881-1890.

182. Li, Y.; Xiong, S.; Tang, X.; Wu, H.; Han, C.; Yi, M.; Wang, Y., Loose nanofiltration membrane with highly-branched SPEI/PEI assembly for dye/salt textile wastewater treatment. *J. Environ. Chem. Eng.* **2021**, *9*, 106371.

183. Guo, Y.-S.; Ji, Y.-L.; Wu, B.; Wang, N.-X.; Yin, M.-J.; An, Q.-F.; Gao, C.-J., High-flux zwitterionic nanofiltration membrane constructed by in-situ introduction method for monovalent salt/antibiotics separation. *J. Membr. Sci.* **2020**, *593*, 117441.

184. Xu, R.; Wang, J.; Chen, D.; Liu, T.; Zheng, Z.; Yang, F.; Chen, J.; Kang, J.; Cao, Y.; Xiang, M., Preparation and performance of a charge-mosaic nanofiltration membrane with novel salt concentration sensitivity for the separation of salts and dyes. *J. Membr. Sci.* **2020**, *595*, 117472.

185. Werber, J.R.; Osuji, C.O.; Elimelech, M., Materials for next-generation desalination and water purification membranes. *Nat. Rev. Mater.* **2016**, *1*, 1-15.

186. Li, A.; Rao, Q.; Liang, F.; Song, L.; Zhan, X.; Chen, F.; Chen, J.; Zhang, Q., Polyhydroxy group functionalized zwitterion for a polyamide nanofiltration membrane with high water permeation and antifouling performance. *ACS Appl. Polym. Mater.* **2020**, *2*, 3850-3858.

187. Cheng, C.; Liu, B.; Liu, C.; Shen, J.; Nurlan, J.; Khan, M.F.S.; Huang, Z.; Qian, Y.; Shen, F.; Wu, J., Tracking variation of fluorescent dissolved organic matter during full-scale printing and dyeing wastewater treatment. *Chemosphere* **2020**, *252*, 126559.

188. Cui, M.-H.; Gao, L.; Lee, H.-S.; Wang, A.-J., Mixed dye wastewater treatment in a bioelectrochemical system-centered process. *Bioresour. Technol.* **2020**, *297*, 122420.

189. Yagub, M.T.; Sen, T.K.; Afroze, S.; Ang, H.M., Dye and its removal from aqueous solution by adsorption: A review. *Adv. Colloid Interface Sci.* **2014**, *209*, 172-184.

190. Zhang, G.; Zhang, X.; Meng, Y.; Pan, G.; Ni, Z.; Xia, S., Layered double hydroxides-based photocatalysts and visible-light driven photodegradation of organic pollutants: a review. *Chem. Eng. J.* **2020**, *392*, 123684.

191. Gao, Y.; Deng, S.-Q.; Jin, X.; Cai, S.-L.; Zheng, S.-R.; Zhang, W.-G., The construction of amorphous metal-organic cage-based solid for rapid dye adsorption and time-dependent dye separation from water. *Chem. Eng. J.* **2019**, *357*, 129-139.

192. Xu, H.-M.; Sun, X.-F.; Wang, S.-Y.; Song, C.; Wang, S.-G., Development of laccase/graphene oxide membrane for enhanced synthetic dyes separation and degradation. *Sep. Purif. Technol.* **2018**, *204*, 255-260.

193. Deng, L.; Li, S.; Qin, Y.; Zhang, L.; Chen, H.; Chang, Z.; Hu, Y., Fabrication of antifouling thin-film composite nanofiltration membrane via surface grafting of polyethyleneimine followed by zwitterionic modification. *J. Membr. Sci.* **2021**, *619*, 118564.

194. Ormanci-Acar, T.; Tas, C.E.; Keskin, B.; Ozbulut, E.B.S.; Turken, T.; Imer, D.; Tufekci, N.; Menceloglu, Y.Z.; Unal, S.; Koyuncu, I., Thin-film composite nanofiltration membranes with high flux and dye rejection fabricated from disulfonated diamine monomer. *J. Membr. Sci.* **2020**, *608*, 118172.

195. Li, X.; Wang, Z.; Han, X.; Liu, Y.; Wang, C.; Yan, F.; Wang, J., Regulating the interfacial polymerization process toward high-performance polyamide thin-film composite reverse osmosis and nanofiltration membranes: A review. *J. Membr. Sci.* **2021**, *640*, 119765.

196. Liu, Y.; Liu, J.; Jiang, Y.; Meng, M.; Ni, L.; Qiu, H.; Yang, R.; Liu, Z.; Liu, H., Synthesis of novel high flux thin-film nanocomposite nanofiltration membranes containing GO–SiO$_2$ via interfacial polymerization. *Ind. Eng. Chem. Res* **2019**, *58*, 22324-22333.

197. Lee, H.S.; Im, S.J.; Kim, J.H.; Kim, H.J.; Kim, J.P.; Min, B.R., Polyamide thin-film nanofiltration membranes containing TiO$_2$ nanoparticles. *Desalination* **2008**, *219*, 48-56.

198. Li, C.; Li, S.; Tian, L.; Zhang, J.; Su, B.; Hu, M.Z., Covalent organic frameworks (COFs)-incorporated thin film nanocomposite (TFN) membranes for high-flux organic solvent nanofiltration (OSN). *J. Membr. Sci.* **2019**, *572*, 520-531.

199. Liu, T.; Liu, X.; Graham, N.; Yu, W.; Sun, K., Two-dimensional MXene incorporated graphene oxide composite membrane with enhanced water purification performance. *J. Membr. Sci.* **2020**, *593*, 117431.

200. Wang, L.; Wang, N.; Li, J.; Li, J.; Bian, W.; Ji, S., Layer-by-layer self-assembly of polycation/GO nanofiltration membrane with enhanced stability and fouling resistance. *Sep. Purif. Technol.* **2016**, *160*, 123-131.

201. Ma, W.; Chen, T.; Nanni, S.; Yang, L.; Ye, Z.; Rahaman, M.S., Zwitterion-functionalized graphene oxide incorporated polyamide membranes with improved antifouling properties. *Langmuir* **2019**, *35*, 1513-1525.

202. Han, R.; Wu, P., High-performance graphene oxide nanofiltration membrane with continuous nanochannels prepared by the in situ oxidation of MXene. *J. Mater. Chem. A* **2019**, *7*, 6475-6481.

203. Ma, W.; Yang, L.; Chen, T.; Ye, Z.; Tufenkji, N.; Rahaman, M.S., Engineering polymer forest on membranes: tuning density, thickness, and architecture for biofouling control. *ACS Appl. Polym. Mater.* **2020**, *2*, 4592-4603.

204. Li, B.; Jain, P.; Ma, J.; Smith, J.K.; Yuan, Z.; Hung, H.-C.; He, Y.; Lin, X.; Wu, K.; Pfaendtner, J.; Jiang, S., Trimethylamine N-oxide–derived zwitterionic polymers: A new class of ultralow fouling bioinspired materials. *Sci. Adv.* **2019**, *5*, eaaw9562.

205. Li, M.; Hu, J.; Li, B.; Deng, S.; Zhang, X., Graphene oxide nanofiltration membrane with trimethylamine-N-oxide zwitterions for robust biofouling resistance. *J. Membr. Sci.* **2021**, *640*, 119855.

206. Getter, T.; Zaks, I.; Barhum, Y.; Ben-Zur, T.; Böselt, S.; Gregoire, S.; Viskind, O.; Shani, T.; Gottlieb, H.; Green, O.; Shubely, M.; Senderowitz, H.; Israelson, A.; Kwon, I.; Petri, S.; Offen, D.; Gruzman, A., A chemical chaperone-based drug candidate is effective in a mouse model of amyotrophic lateral sclerosis (ALS). *ChemMedChem* **2015**, *10*, 850-861.

207. Ciganek, E.; Read, J.M.; Calabrese, J.C., Reverse cope elimination reactions. 1. Mechanism and scope. *J. Org. Chem.* **1995**, *60*, 5795-5802.

208. O'Neil, I.A.; Cleator, E.; Elena Ramos, V.; Chorlton, A.P.; Tapolczay, D.J., The synthesis of chiral functionalised morpholine N-oxides using a tandem Cope elimination/reverse-Cope elimination protocol. *Tetrahedron Lett.* **2004**, *45*, 3655-3658.

209. Alkhouzaam, A.; Qiblawey, H., Novel polysulfone ultrafiltration membranes incorporating polydopamine functionalized graphene oxide with enhanced flux and fouling resistance. *J. Membr. Sci.* **2021**, *620*, 118900.

210. Li, Q.; Liao, Z.; Fang, X.; Xie, J.; Ni, L.; Wang, D.; Qi, J.; Sun, X.; Wang, L.; Li, J., Tannic acid assisted interfacial polymerization based loose thin-film composite NF membrane for dye/salt separation. *Desalination* **2020**, *479*, 114343.

211. Zhu, J.; Tian, M.; Zhang, Y.; Zhang, H.; Liu, J., Fabrication of a novel "loose" nanofiltration membrane by facile blending with Chitosan–Montmorillonite nanosheets for dyes purification. *Chem. Eng. J.* **2015**, *265*, 184-193.

212. Jin, P.; Zhu, J.; Yuan, S.; Zhang, G.; Volodine, A.; Tian, M.; Wang, J.; Luis, P.; Van der Bruggen, B., Erythritol-based polyester loose nanofiltration membrane with fast water transport for efficient dye/salt separation. *Chem. Eng. J.* **2021**, *406*, 126796.

213. Zhang, C.; Wei, K.; Zhang, W.; Bai, Y.; Sun, Y.; Gu, J., Graphene oxide quantum dots incorporated into a thin film nanocomposite membrane with high flux and antifouling properties for low-pressure nanofiltration. *ACS Appl. Mater. Interfaces* **2017**, *9*, 11082-11094.

214. Ye, C.-C.; Zhao, F.-Y.; Wu, J.-K.; Weng, X.-D.; Zheng, P.-Y.; Mi, Y.-F.; An, Q.-F.; Gao, C.-J., Sulfated polyelectrolyte complex nanoparticles structured nanoflitration membrane for dye desalination. *Chem. Eng. J.* **2017**, *307*, 526-536.

215. Jin, P.; Chergaoui, S.; Zheng, J.; Volodine, A.; Zhang, X.; Liu, Z.; Luis, P.; Van der Bruggen, B., Low-pressure highly permeable polyester loose nanofiltration membranes tailored by natural carbohydrates for effective dye/salt fractionation. *J. Hazard. Mater.* **2022**, *421*, 126716.

216. Li, P.; Wang, Z.; Yang, L.; Zhao, S.; Song, P.; Khan, B., A novel loose-NF membrane based on the phosphorylation and cross-linking of polyethyleneimine layer on porous PAN UF membranes. *J. Membr. Sci.* **2018**, *555*, 56-68.

217. Zhu, J.; Wang, J.; Uliana, A.A.; Tian, M.; Zhang, Y.; Zhang, Y.; Volodin, A.; Simoens, K.; Yuan, S.; Li, J., Mussel-inspired architecture of high-flux loose nanofiltration membrane functionalized with antibacterial reduced graphene oxide–copper nanocomposites. *ACS Appl. Mater. Interfaces* **2017**, *9*, 28990-29001.

218. Zhang, L.; Xu, L.; Yu, H.; Yao, P.; Zhang, M.; Guo, F.; Yu, L., Capsaicin mimic-polyethyleneimine crosslinked antifouling loose nanofiltration membrane for effective dye/salt wastewater treatment. *J. Membr. Sci.* **2022**, *641*, 119923.

219. Ang, M.B.M.Y.; Huang, G.-W.; Chu, M.-Y.; Millare, J.C.; Huang, S.-H.; Lee, K.-R., Use of aqueous polyol monomer for superior dye separation performance and high chlorine resistance of thin-film composite polyester nanofiltration membranes. *J. Water Process. Eng.* **2022**, *48*, 102843.

220. Ma, J.; Ma, Y.; Yu, F., A novel one-pot route for large-scale synthesis of novel magnetic CNTs/Fe@C hybrids and their applications for binary dye removal. *ACS Sustain. Chem. Eng.* **2018**, *6*, 8178-8191.

221. Danner, M.-C.; Robertson, A.; Behrends, V.; Reiss, J., Antibiotic pollution in surface fresh waters: Occurrence and effects. *Sci. Total Environ.* **2019**, *664*, 793-804.

222. Nsenga Kumwimba, M.; Meng, F., Roles of ammonia-oxidizing bacteria in improving metabolism and cometabolism of trace organic chemicals in biological wastewater treatment processes: A review. *Sci. Total Environ.* **2019**, *659*, 419-441.

223. Coha, M.; Farinelli, G.; Tiraferri, A.; Minella, M.; Vione, D., Advanced oxidation processes in the removal of organic substances from produced water: Potential, configurations, and research needs. *Chem. Eng. J.* **2021**, *414*, 128668.

224. Tanudjaja, H.J.; Hejase, C.A.; Tarabara, V.V.; Fane, A.G.; Chew, J.W., Membrane-based separation for oily wastewater: A practical perspective. *Water Res.* **2019**, *156*, 347-365.

225. Adham, S.; Hussain, A.; Minier-Matar, J.; Janson, A.; Sharma, R., Membrane applications and opportunities for water management in the oil & gas industry. *Desalination* **2018**, *440*, 2-17.

226. Ahmad, N.N.R.; Ang, W.L.; Teow, Y.H.; Mohammad, A.W.; Hilal, N., Nanofiltration membrane processes for water recycling, reuse and product recovery within various industries: A review. *J. Water Process. Eng.* **2022**, *45*, 102478.

227. Zhang, L.; Zhang, R.; Ji, M.; Lu, Y.; Zhu, Y.; Jin, J., Polyamide nanofiltration membrane with high mono/divalent salt selectivity via pre-diffusion interfacial polymerization. *J. Membr. Sci.* **2021**, *636*, 119478.

228. Lasisi, K.H.; Zhang, K., Polyamine-based thin-film composite nanofiltration membrane embedded with catalytic chemical additive for enhanced separation performance and acid stability. *J. Membr. Sci.* **2022**, *644*, 120155.

229. Li, P.; Lan, H.; Chen, K.; Ma, X.; Wei, B.; Wang, M.; Li, P.; Hou, Y.; Jason Niu, Q., Novel high-flux positively charged aliphatic polyamide nanofiltration membrane for selective removal of heavy metals. *Sep. Purif. Technol.* **2022**, *280*, 119949.

230. Wu, B.; Weng, X.-D.; Wang, N.; Yin, M.-J.; Zhang, L.; An, Q.-F., Chlorine-resistant positively charged polyamide nanofiltration membranes for heavy metal ions removal. *Sep. Purif. Technol.* **2021**, *275*, 119264.

231. An, Q.; Li, F.; Ji, Y.; Chen, H., Influence of polyvinyl alcohol on the surface morphology, separation and anti-fouling performance of the composite polyamide nanofiltration membranes. *J. Membr. Sci.* **2011**, *367*, 158-165.

232. Soyekwo, F.; Wen, H.; Liao, D.; Liu, C., Fouling-resistant ionic graft-polyamide nanofiltration membrane with improved permeance for lithium separation from MgCl$_2$/LiCl mixtures. *J. Membr. Sci.* **2022**, *659*, 120773.

233. Liu, C.; Lee, J.; Small, C.; Ma, J.; Elimelech, M., Comparison of organic fouling resistance of thin-film composite membranes modified by hydrophilic silica nanoparticles and zwitterionic polymer brushes. *J. Membr. Sci.* **2017**, *544*, 135-142.

234. Jung, K.H.; Kim, H.J.; Kim, M.H.; Seo, H.; Lee, J.-C., Superamphiphilic zwitterionic block copolymer surfactant-assisted fabrication of polyamide thin-film composite membrane with highly enhanced desalination performance. *J. Membr. Sci.* **2021**, *618*, 118677.

235. Cheng, Q.; Zheng, Y.; Yu, S.; Zhu, H.; Peng, X.; Liu, J.; Liu, J.; Liu, M.; Gao, C., Surface modification of a commercial thin-film composite polyamide reverse osmosis membrane through graft polymerization of N-isopropylacrylamide followed by acrylic acid. *J. Membr. Sci.* **2013**, *447*, 236-245.

236. Fan, K.; Liu, Y.; Wang, X.; Cheng, P.; Xia, S., Comparison of polyamide, polyesteramide and polyester nanofiltration membranes: properties and separation performance. *Sep. Purif. Technol.* **2022**, *297*, 121579.

237. Yan, F.; Chen, H.; Lü, Y.; Lü, Z.; Yu, S.; Liu, M.; Gao, C., Improving the water permeability and antifouling property of thin-film composite polyamide nanofiltration membrane by modifying the active layer with triethanolamine. *J. Membr. Sci.* **2016**, *513*, 108-116.

238. Tang, B.; Huo, Z.; Wu, P., Study on a novel polyester composite nanofiltration membrane by interfacial polymerization of triethanolamine (TEOA) and trimesoyl chloride (TMC): I. Preparation, characterization and nanofiltration properties test of membrane. *J. Membr. Sci.* **2008**, *320*, 198-205.

239. Mah, K.H.; Yussof, H.W.; Abu Seman, M.N.; Mohammad, A.W., Optimisation of interfacial polymerization factors in thin-film composite (TFC) polyester nanofiltration (NF) membrane for separation of xylose from glucose. *Sep. Purif. Technol.* **2019**, *209*, 211-222.

240. Cheng, J.; Shi, W.; Zhang, L.; Zhang, R., A novel polyester composite nanofiltration membrane formed by interfacial polymerization of pentaerythritol (PE) and trimesoyl chloride (TMC). *Appl. Surf. Sci.* **2017**, *416*, 152-159.

241. Li, J.; Gong, J.-L.; Zeng, G.-M.; Song, B.; Cao, W.-C.; Fang, S.-Y.; Tang, S.-Q.; Guan, Y.; Tan, Z.-K.; Chen, Z.-P.; Mao, X.-Q.; Zhu, R.-L., Thin-film composite polyester nanofiltration membrane with high flux and efficient dye/salts separation fabricated from precise molecular sieving structure of β-cyclodextrin. *Sep. Purif. Technol.* **2021**, *276*, 119352.

242. Cheng, J.; Li, Z.; Bao, X.; Zhang, R.; Yin, S.; Huang, W.; Sun, K.; Shi, W., A novel polyester-amide loose composite nanofiltration membrane for effective dye/salt separation: The effect of long molecule on the interfacial polymerization. *J. Membr. Sci.* **2022**, *657*, 120675.

243. Zheng, J.; Zhao, R.; Uliana, A.A.; Liu, Y.; de Donnea, D.; Zhang, X.; Xu, D.; Gao, Q.; Jin, P.; Liu, Y.; Volodine, A.; Zhu, J.; Van der Bruggen, B., Separation of textile wastewater using a highly permeable resveratrol-based loose nanofiltration membrane with excellent anti-fouling performance. *Chem. Eng. J.* **2022**, *434*, 134705.

244. Li, R.; Mai, Z.; Peng, D.; Xu, S.; Wang, J.; Zhu, J.; Zhang, Y., In situ formation of porous organic polymer-based thin polyester membranes for loose nanofiltration. *J. Membr. Sci.* **2022**, *644*, 120074.

245. Xia, D.; Zhang, M.; Tong, C.; Wang, Z.; Liu, H.; Zhu, L., In-situ incorporating zwitterionic nanocellulose into polyamide nanofiltration membrane towards excellent perm-selectivity and antifouling performances. *Desalination* **2022**, *521*, 115397.

246. Li, A.; Rao, Q.; Liang, F.; Song, L.; Zhan, X.; Chen, F.; Chen, J.; Zhang, Q., Polyhydroxy group functionalized zwitterion for a polyamide nanofiltration membrane with high water permeation and antifouling performance. *ACS Appl. Polym. Mater.* **2020**, *2*, 3850-3858.

247. Yao, Z.; Guo, H.; Yang, Z.; Qing, W.; Tang, C.Y., Preparation of nanocavity-contained thin film composite nanofiltration membranes with enhanced permeability and divalent to monovalent ion selectivity. *Desalination* **2018**, *445*, 115-122.

248. Wen, P.; Chen, Y.; Hu, X.; Cheng, B.; Liu, D.; Zhang, Y.; Nair, S., Polyamide thin film composite nanofiltration membrane modified with acyl chlorided graphene oxide. *J. Membr. Sci.* **2017**, *535*, 208-220.

249. Li, Y.; Su, Y.; Dong, Y.; Zhao, X.; Jiang, Z.; Zhang, R.; Zhao, J., Separation performance of thin-film composite nanofiltration membrane through interfacial polymerization using different amine monomers. *Desalination* **2014**, *333*, 59-65.

250. Tavangar, T.; Jalali, K.; Alaei Shahmirzadi, M.A.; Karimi, M., Toward real textile wastewater treatment: Membrane fouling control and effective fractionation of dyes/inorganic salts using a hybrid electrocoagulation – Nanofiltration process. *Sep. Purif. Technol.* **2019**, *216*, 115-125.

251. Huang, B.-Q.; Tang, Y.-J.; Zeng, Z.-X.; Xue, S.-M.; Li, S.-Q.; Wang, Y.-R.; Li, E.-C.; Tang, C.Y.; Xu, Z.-L., Enhancing nanofiltration performance for antibiotics/NaCl separation via water activation before microwave heating. *J. Membr. Sci.* **2021**, *629*, 119285.

252. Xue, J.; Jiao, Z.; Bi, R.; Zhang, R.; You, X.; Wang, F.; Zhou, L.; Su, Y.; Jiang, Z., Chlorine-resistant polyester thin film composite nanofiltration membranes prepared with β-cyclodextrin. *J. Membr. Sci.* **2019**, *584*, 282-289.

253. Wang, T.; Wu, H.; Zhao, S.; Zhang, W.; Tahir, M.; Wang, Z.; Wang, J., Interfacial polymerized and pore-variable covalent organic framework composite membrane for dye separation. *Chem. Eng. J.* **2020**, *384*, 123347.

254. Parakala, S.; Moulik, S.; Sridhar, S., Effective separation of methylene blue dye from aqueous solutions by integration of micellar enhanced ultrafiltration with vacuum membrane distillation. *Chem. Eng. J.* **2019**, *375*, 122015.

255. Liu, Y.; Wang, J.; Wang, Y.; Zhu, H.; Xu, X.; Liu, T.; Hu, Y., High-flux robust PSf-b-PEG nanofiltration membrane for the precise separation of dyes and salts. *Chem. Eng. J.* **2021**, *405*, 127051.

256. Fan, H.; Gu, J.; Meng, H.; Knebel, A.; Caro, J., High-Flux membranes based on the covalent organic framework COF-LZU1 for selective dye separation by nanofiltration. *Angew. Chem. Int. Ed.* **2018**, *57*, 4083-4087.

257. Zhu, J.; Uliana, A.; Wang, J.; Yuan, S.; Li, J.; Tian, M.; Simoens, K.; Volodin, A.; Lin, J.; Bernaerts, K.; Zhang, Y.; Van der Bruggen, B., Elevated salt transport of antimicrobial loose nanofiltration membranes enabled by copper nanoparticles via fast bioinspired deposition. *J. Mater. Chem. A* **2016**, *4*, 13211-13222.

258. Zhu, J.; Wang, J.; Uliana, A.A.; Tian, M.; Zhang, Y.; Zhang, Y.; Volodin, A.; Simoens, K.; Yuan, S.; Li, J.; Lin, J.; Bernaerts, K.; Van der Bruggen, B., Mussel-inspired architecture of high-flux loose nanofiltration membrane functionalized with antibacterial reduced graphene oxide–copper nanocomposites. *ACS Appl. Mater. Interfaces* **2017**, *9*, 28990-29001.

259. Jin, J.; Du, X.; Yu, J.; Qin, S.; He, M.; Zhang, K.; Chen, G., High performance nanofiltration membrane based on SMA-PEI cross-linked coating for dye/salt separation. *Journal of Membrane Science* **2020**, *611*, 118307.

260. Liu, L.; Yu, L.; Borjigin, B.; Liu, Q.; Zhao, C.; Hou, D., Fabrication of thin-film composite nanofiltration membranes with improved performance using β-cyclodextrin as monomer for efficient separation of dye/salt mixtures. *Appl. Surf. Sci.* **2021**, *539*, 148284.
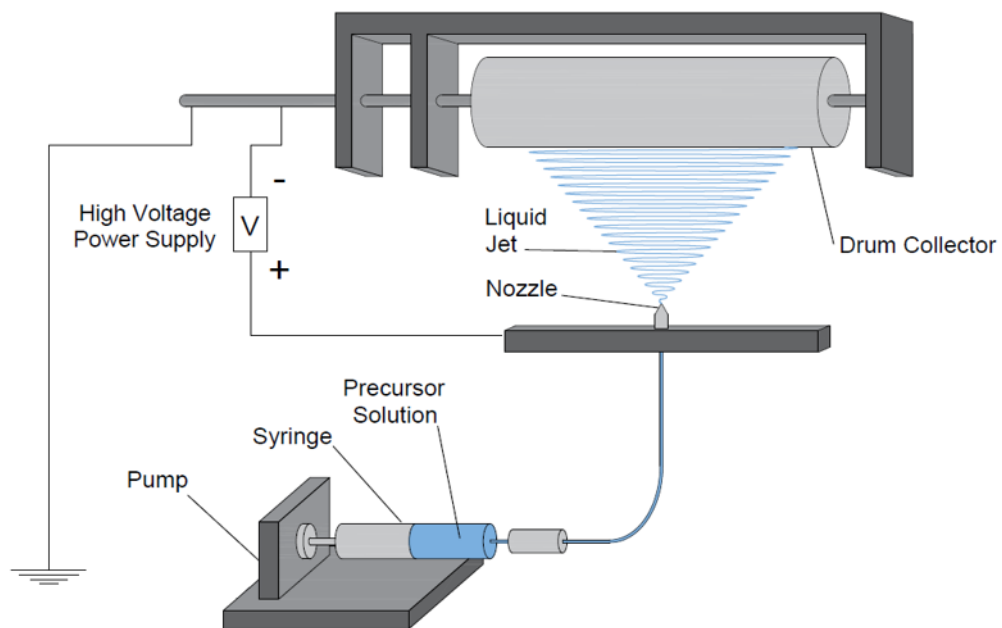
Appendix

Figure S3.1 Schematic illustration of electrospun nanofiber mats (ENMs) preparation.
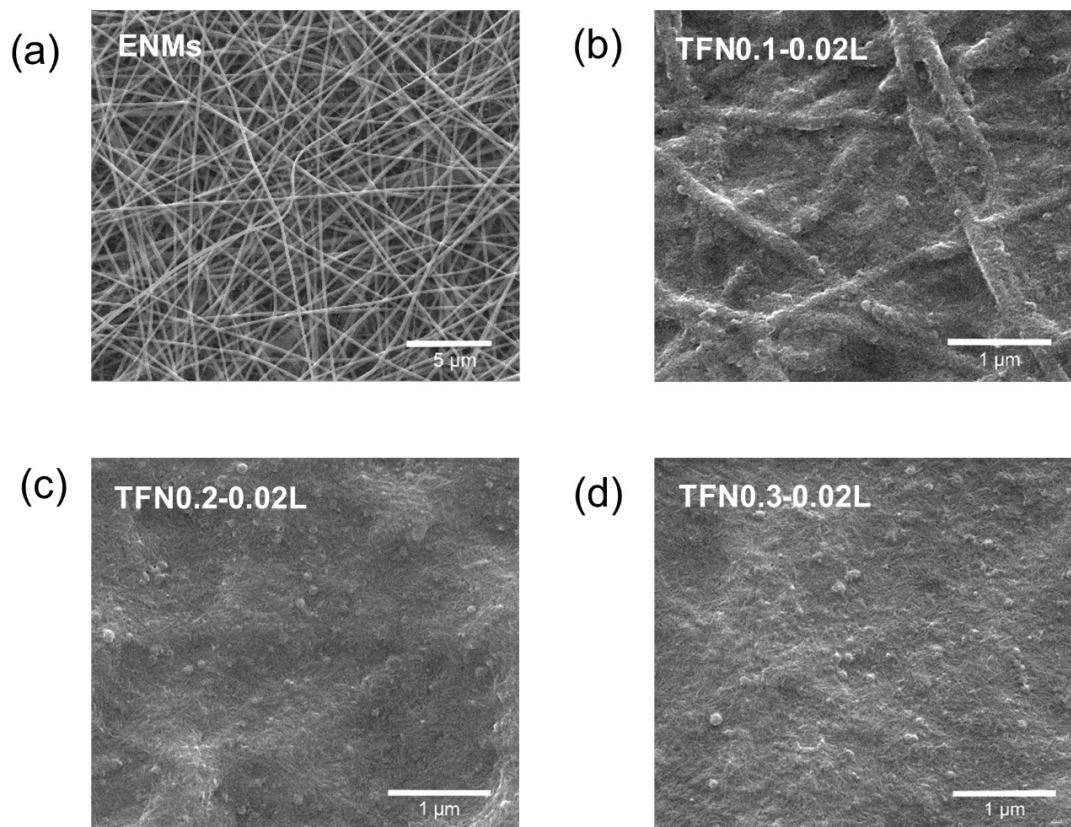
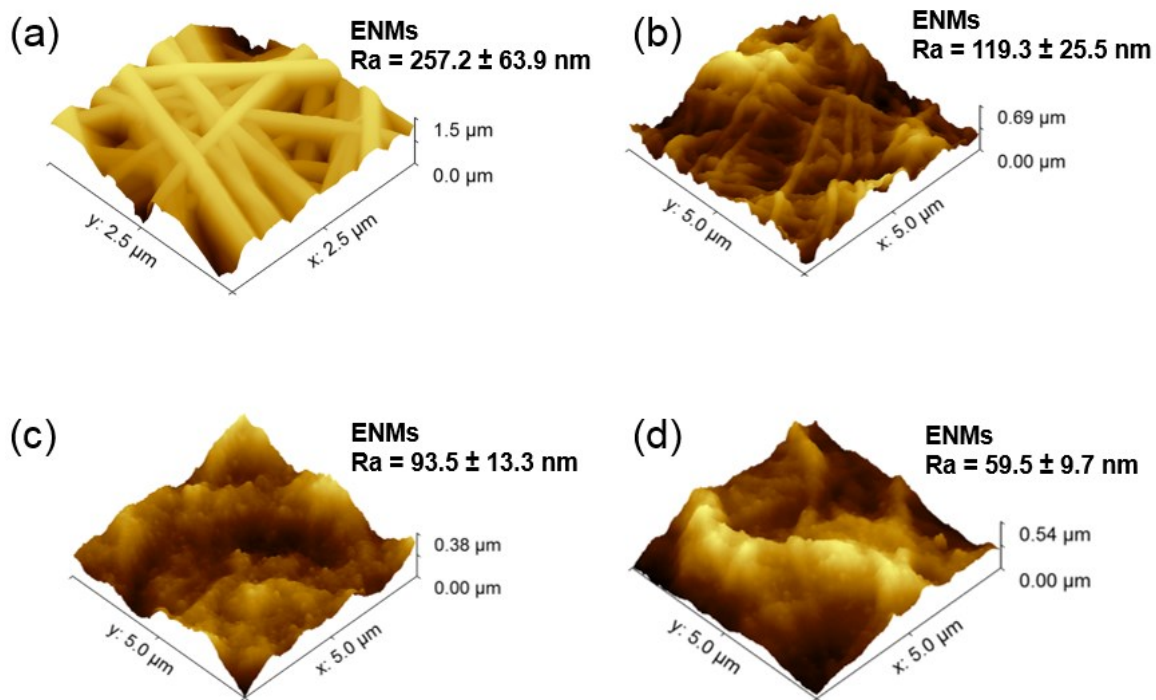**Figure S3.2** Top view SEM images: (a) ENMs, (b) TFN0.1-0.02L, (c) TFN0.2-0.02L, (d) TFN0.3-0.02L.

Figure S3.3 AFM images of TFN membranes: (a) ENMs, (b) TFN0.1-0.02L, (c) TFN0.2-0.02L, (d) TFN0.3-0.02L.
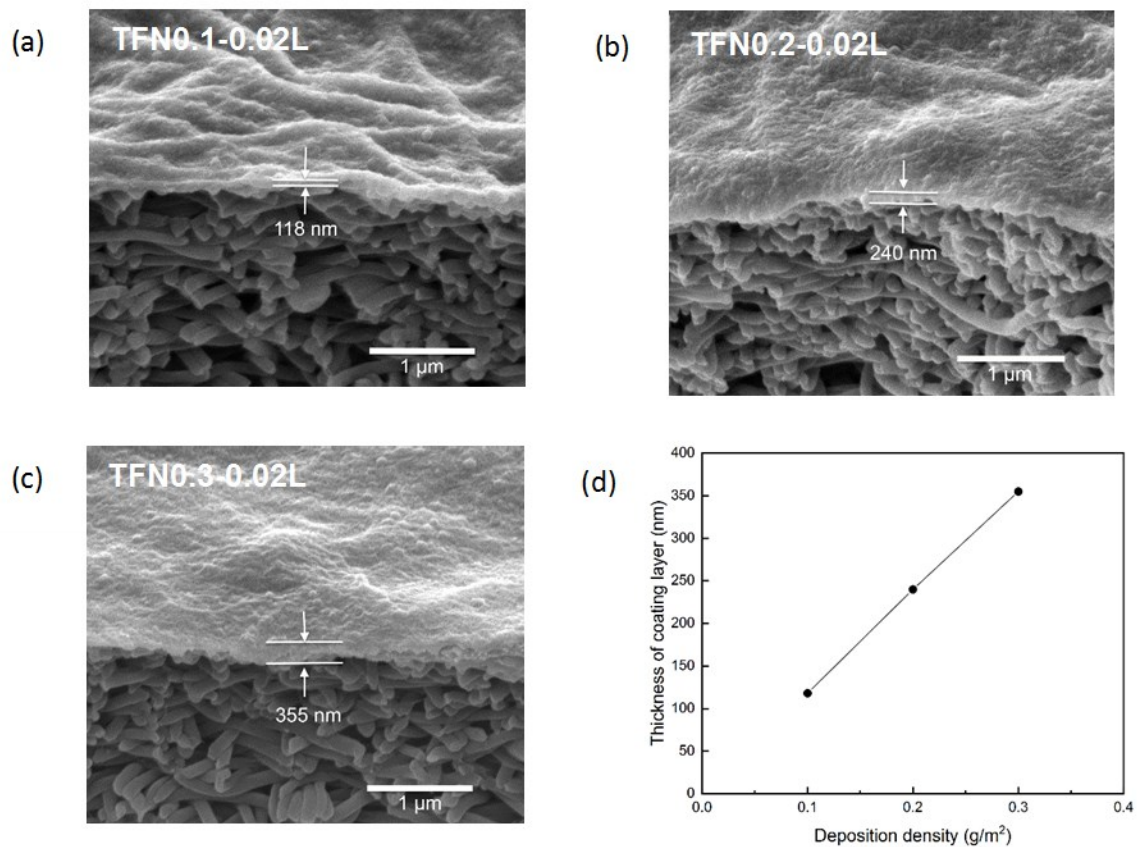
Figure S3.4 Cross-sectional view SEM images: (a) TFN0.1-0.02L, (b) TFN0.2-0.02L, (c) TFN0.1-0.02L, (d) thickness change depending on the deposition density of hybrid core-shell CNCs.

Table S3.1 Elemental composition of the TFN membranes by XPS.

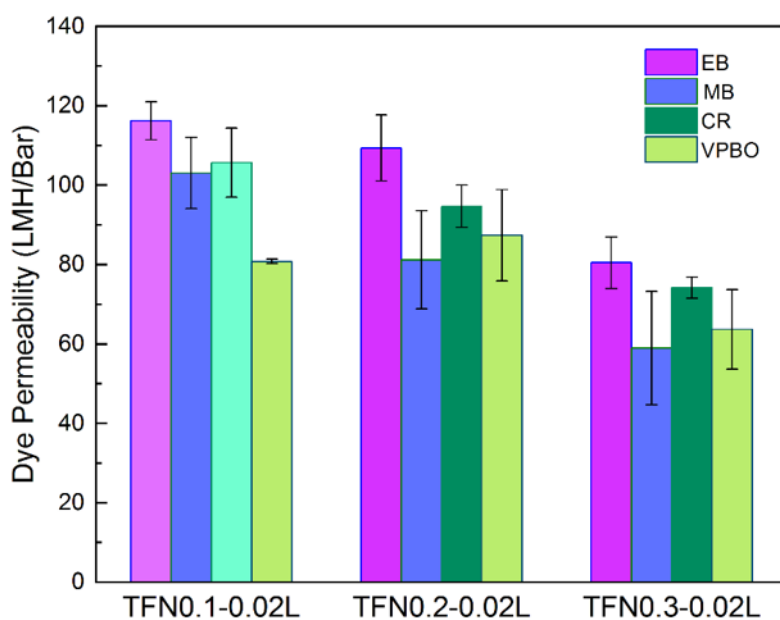| Membrane	Composition (%)			Atomic ratio
	C	O	N	N/O
TFN0.1-Control	58.38	39.51	1.63	0.04
TFN0.1-0.5H	58.31	33.41	7.61	0.23
TFN0.1-0.5L	58.50	35.29	5.58	0.16
TFN0.1-0.001L	57.73	36.78	4.46	0.12
TFN0.1-0.02L	59.12	34.88	5.02	0.14
TFN0.2-0.02L	58.64	36.67	4.08	0.11
TFN0.3-0.02L	60.42	35.46	3.58	0.10

Figure S3.5 Dye solution permeability for EB, MB, CR, and VPBO.

Table S3.2 Comparison of dye/salt separation performance reported in literatures and this study.

| Membrane	PWP (LMH/bar)	Dye	Rejection (%)			Ref.
			Dye	NaCl	Na$_2$SO$_4$	
PEI/Gallic acid	~40	Congo Red	97.1	~3	~3	[90]
PSf-b-PEG	49.3	Congo Red	98.3	0.02	0.03	[255]
E-MSTF (+) AAO	310	Congo Red	97.7	2.5	4	[52]
COF-LZU1	76	Congo Red	98.6	4	3	[256]
Oxidized CTF	64.5	Congo Red	97.9	4.8	8.5	[93]
TA/GOODs-1	23.3	Congo Red	99.8	17.2	66.7	[69]
ZDNMA	10.7	Congo Red	99.9	14.3	~90	[147]
PSF/GO	36.9	Congo Red	99.9	5	32	[149]
EIP (M30)	20.2	Congo Red	99.6	6.3	-	[53]
Co-NF-2	18.2	Congo Red	99.4	3.3	25.2	[257]
Fe-PEI/HPAN	10.96	Congo Red	99.53	7.46	5.89	[216]
PDA/rGOC3	22.8	Congo Red	98.9	~5	7.4	[258]
SMA-PEI/PES	23	Congo Red	99.4	2.5	-	[259]
PEI-TA/PES	42.6	Congo Red	99.4	8.4	6.0	[91]
LNFM-2	53.23	Congo Red	99.6	5.6	11.0	[212]
β-CD/TMC	103.9	Congo Red	99.0	10.6	-	[260]
CNCs-Dopamine/PEI (TFN0.2-0.02L)	128.4	Congo Red	99.91	1.14	1.05	This study
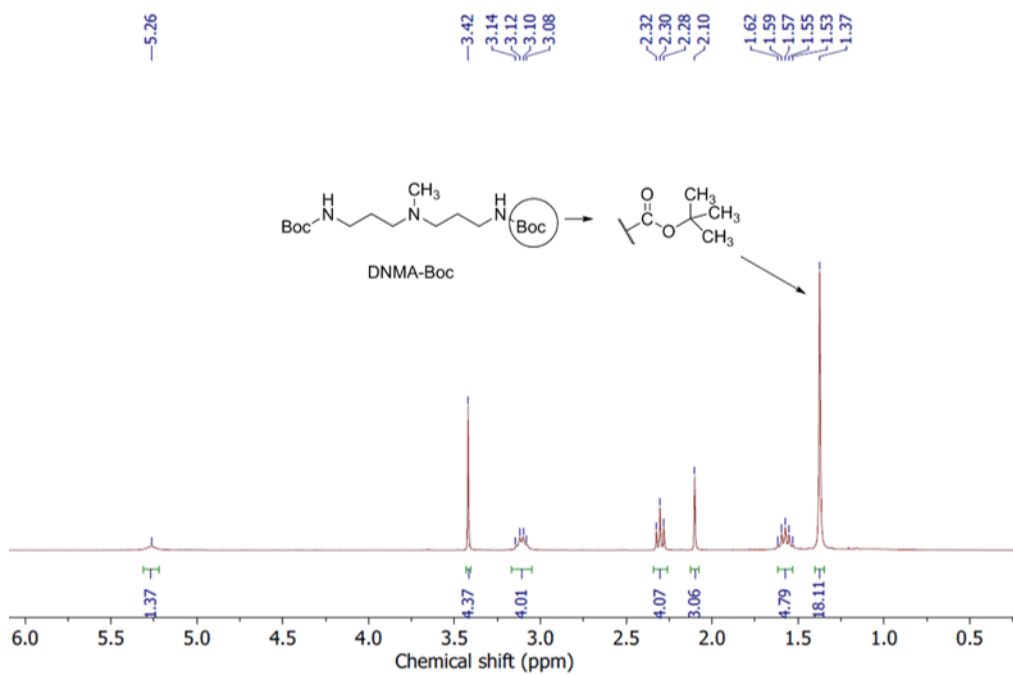
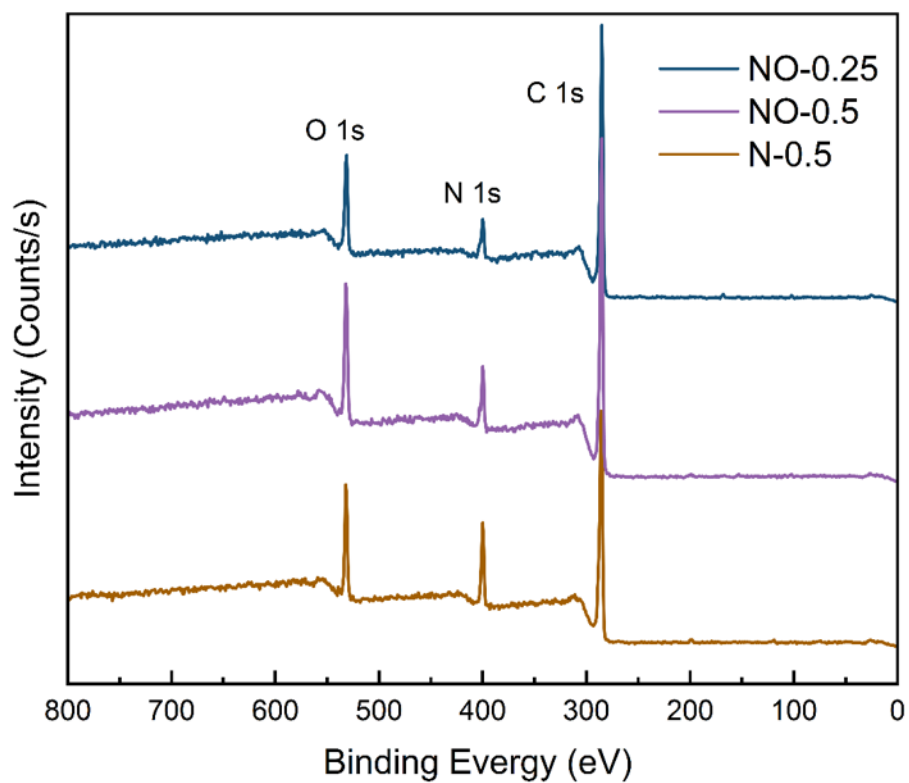**Figure S4.1** ^{1}H NMR spectrum of DNMA-Boc.

Figure S5.1 XPS spectra of polyamide TFC membranes (NO-0.25, NO-0.5 and N-0.5).

Table S5.1 Elemental compositions of membrane surfaces.

Membrane	Composition (%)	
	C	N
NO-0.25	78.5	9.2
NO-0.5	75.5	10.3
N-0.5	71.7	15.0

Table S5.2 CR concentrations during the four cycles of purification and recovery test.

Cycle	Initial concentration (ppm)	Terminal concentration (ppm)
Cycle 1	100.0	198.13
Cycle II	99.26	196.55
Cycle III	98.35	193.30
Cycle IV	96.65	187.57
End	94.82	-

Table S5.3 NaCl concentrations during the four cycles of purification and recovery test.

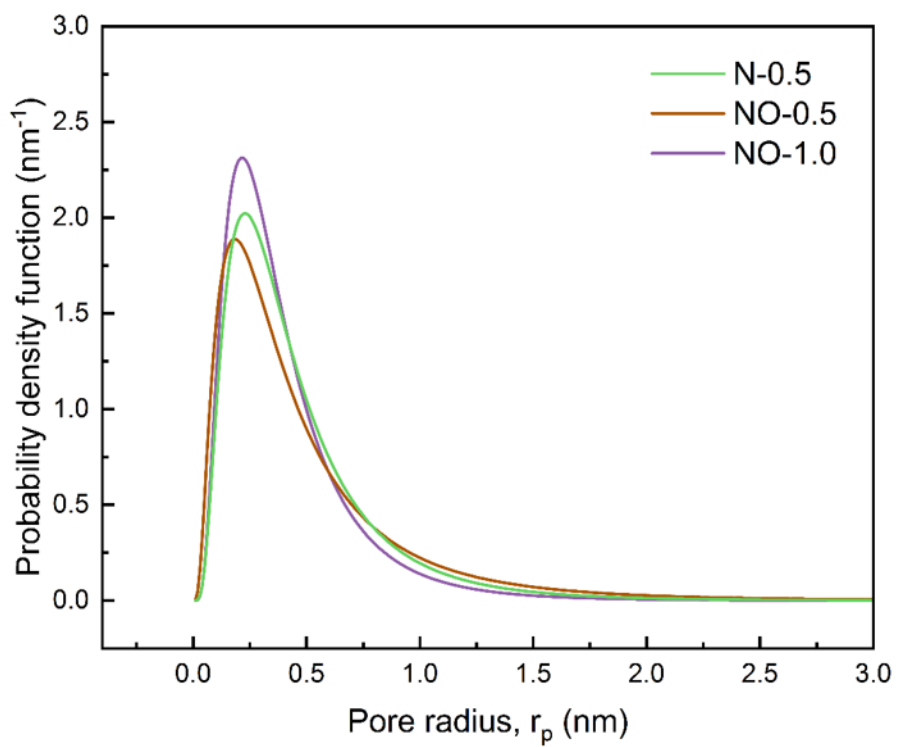| Cycle	Initial concentration $(g\ L^{-1})$	Terminal concentration $(g\ L^{-1})$
Cycle 1	1.0	1.074
Cycle II	0.599	0.661
Cycle III	0.366	0.395
Cycle IV	0.230	0.281
End	0.144	-

Figure S5.2 Pore size distribution of polyamide membranes (N-0.5, NO-0.5, and NO-1.0).
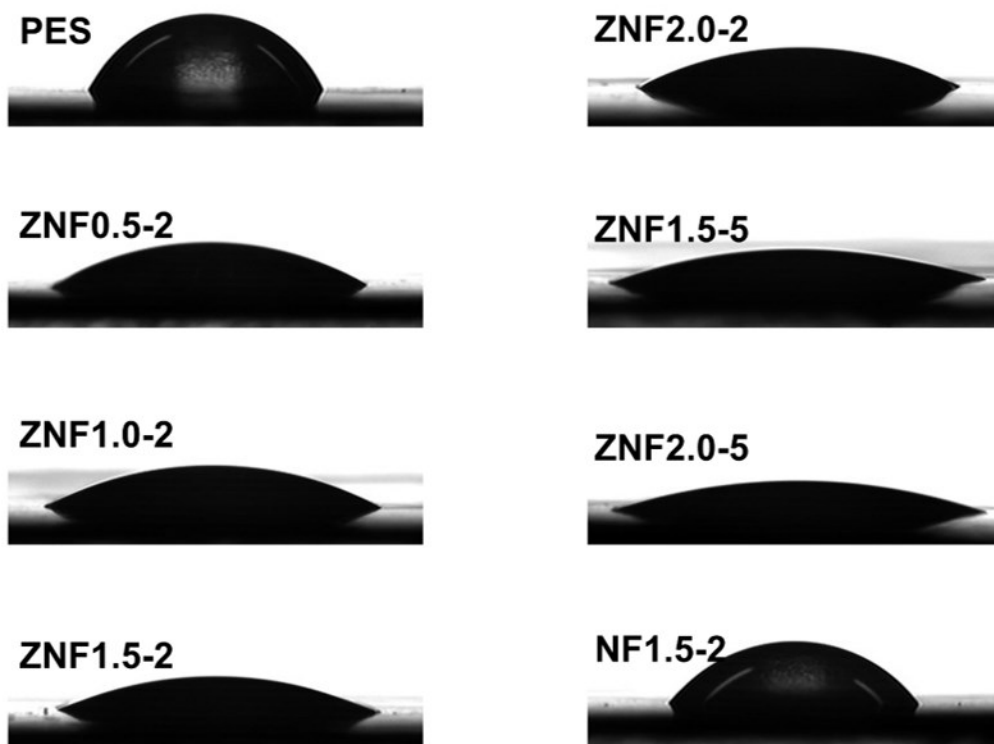
Figure S6.1 Water contact angle images of membranes (PES, ZNF2.0-2, ZNF0.5-2, ZNF1.0-2, ZNF1.5-2, ZNF2.0-2, ZNF1.5-5, ZNF2.0-5, and NF1.5-2)